Titre: Title:	Integrated Cannabinoid Extraction-Purification Process by Nonionic Surfactant
Auteur: Author:	Yu Xiang Song
Date:	2020
Type:	Mémoire ou thèse / Dissertation or Thesis
Référence: Citation:	Song, Y. X. (2020). Integrated Cannabinoid Extraction-Purification Process by Nonionic Surfactant [Mémoire de maîtrise, Polytechnique Montréal]. PolyPublie. https://publications.polymtl.ca/5274/

POLYTECHNIQUE MONTRÉAL
affiliée à l'Université de Montréal

Integrated Cannabinoid Extraction-Purification Process by Nonionic Surfactant

YU XIANG SONG
Département de génie chimique

Mémoire présenté en vue de l'obtention du diplôme de *Maîtrise ès sciences appliquées*
Génie chimique

Avril 2020

POLYTECHNIQUE MONTRÉAL
affiliée à l'Université de Montréal

Ce mémoire intitulé :

Integrated Cannabinoid Extraction-Purification Process by Nonionic Surfactant

présenté par **Yu Xiang SONG**
en vue de l'obtention du diplôme de *Maîtrise ès sciences appliquées*
a été dûment accepté par le jury d'examen constitué de :

Nick VIRGILIO, président
Gregory PATIENCE, membre et directeur de recherche
Géraldine MERLE, membre

DEDICATION

To the big homie Bobo...

ACKNOWLEDGEMENTS

First, I would like to express my gratitude to my research director Professor Gregory Patience. Your work ethic (or fanaticism?) inspired me to push myself on a daily basis. You emphasized on skills beyond simply the theoretical that are prioritized during undergraduate studies. Because of it, I've come realized that there is such a thing as personality in science and it made my time much more enjoyable. Half the success is in the presentation and you will be successful if you use the "active voice." Mostly, thank you for giving me the opportunity, resources and freedom to build a project of my own.

Dalma, Marco, Davide, Nooshin and Federico, I wouldn't have made it without you. To the interns who've worked with me, Matt "The Machine", Brendan "Mellow" and Mireya I am grateful that you've accepted to place your trust in me and I genuinely hope that you were able to gather some valuable skills and knowledge.

To everyone from room A-675 and A-685, Endy, Mina, Mahmoud, Hela, Jacopo, Ariane, Philipy, Tugce, Mario, Yanfa, Marlon, Insa, Gianluca, Roberto, Fiona, Olga, Adrien, Léa, Léa, Laurianne, Olivier, Moustapha, Zi Xuan, Jabber, He, Zhenni, Fernanda, Marius, Axel, Valentine, Alice, Nicolas, Mathilde and Theodore, Tim, Kieran, Andrew thank you for enduring me and for providing a pleasant work environment, although it might've felt like a daycare at times.

My thanks also go out to those that made it easier in the lab: Matthieu, Pablo, Martine and Sylvie. If I've forgotten your name that's because you are not important.

I'm kidding, of course. Apologies if I did forget.

These acknowledgments would be incomplete without the ones that brought me here. The ones who inspire me: Julie, Gary V., Andy, DD, Laetitia. Gianni and Dean, I miss you guys and our late-night talks on dreams of greatness and riches. Hope to see you soon. Finally, Mom and Dad, thank you for the constant support, even though sometimes my acts do not align with your morals and convictions.

RÉSUMÉ

D'ici 2025, l'industrie canadienne du cannabis générera jusqu'à la moitié de ses revenus sous forme de produits infusés. *Cannabis L. Sativa* produit deux molécules d'intérêt pharmacologiques: Δ^9-tétrahydrocannabinol (THC) et cannabidiol (CBD). Extraire ces cannabinoïdes de manière efficace et rentable est particulièrement pertinent sachant qu'ils représentent moins de 3 % du poids sec de la plante. Présentement, les extraits sont obtenus soit par CO_2 supercritique, une méthode à haute pression et coût élève, ou par macération à l'éthanol qui requière une purification intensive. Une alternative rentable et écologique consiste en l'utilisation de surfactants non ioniques en phase aqueuse. À température ambiante, les cannabinoïdes sont peu dans l'eau ($2.8\,\mathrm{g\,L^{-1}}$ pour le THC). Le tensioactif dissout les cannabinoïdes lipidiques présents en surface de la plante. De plus, ces surfactants possèdent une propriété unique, une température du point trouble (CPT). En atteignant le CPT, la solution se sépare en une fraction riche en eau et une fraction riche en surfactants. Ce dernier entraîne avec lui les composés hydrophobes et peut donc être exploité pour concentrer l'extrait.

Nos travaux détaillent le développement préliminaire d'un procédé constituer de deux unités en séries. Une première extraction augmentée par surfactants (SEE) et une deuxième séparation de l'extrait brut par points de trouble (CPS). Nos objectifs spécifiques sont de développer les méthodes analytiques pour l'analyse des extraits, d'étudier l'effet des paramètres d'opérations sur les rendements du SEE-CPS et, enfin, d'optimiser ce procédé.

Pour la première fois, les solutions de tensioactifs non ioniques (Trition X-100, Tween 20 et Tween 80) sont utilisées pour l'extraction-concentration simultanée d'inflorescences de cannabis afin d'en récupérer le THC et le CBD. Le procédé SEE produit un extrait de plus grande pureté comparé à l'éthanol. À 40 °C et une composition de 3.75 % massique, Triton X-100 cible sélectivement le cannabinoïde au lieu des cires cuticulaires de haute masse molaire. Au-dessus de son CPT à 65 °C, la température d'extraction corrèle négativement au rendement. Cela est attribuable à l'agrégation des monomères de surfactants, mi-extraction, et leurs fixations subséquentes sur la matrice végétale. La procédure CPS purifie l'extrait brut en éliminant l'eau et les hydrosolubles, tout en maintenant des rendement des rendements de 98 % et 96 % pour le THC et CBD respectivement. L'isolation des phases purifie l'extrait en éliminant les hydrosolubles. De plus, il concentre les cannabinoïdes par un facteur de 30 pour en produire une phase visqueuse contenant jusqu'à 2 % massique en THC. Toutefois, la méthode proposée reste limitée par de faibles rendements lors de l'extraction. Du fait

que la majorité des surfactants non ioniques sont non toxiques et comestibles, l'extrait est convenable pour une incorporation directe à des produits cosmétiques, de santé naturelle et alimentaire, et cela, en minimisant le traitement en aval.

ABSTRACT

Over the next five years, the 5-billion-dollar Canadian Cannabis industry is expected to generate up half of its revenues from cannabis infused products. *Cannabis L. Sativa*'s produces two molecules of interest: Δ^9- tetrahydrocannabinol (THC) and cannabidiol (CBD). A cost-effective extraction of these cannabinoids is of relevance considering that they account for less than 3 % of the plant's dry weight. Currently, extracts are derived from either supercritical CO_2 extraction, a high-pressure and high-cost process, or ethanolic maceration which is purification intensive. Aqueous mixtures of nonionic surfactants offer an alternative and more sustainable solvent. At ambient temperature, cannabinoids dissolve poorly in water ($2.8\,\mathrm{g\,L^{-1}}$ for THC). The surfactant helps solubilize these lipid present on the plant's surface. Moreover, it possesses a unique property: the cloud point temperature (CPT). Upon reaching this temperature, the solution segregates into two moieties: a water-rich and a surfactant-rich phase. The latter entrains hydrophobic compounds and can be exploited to substantially concentrate the cannabinoids.

Our work details the preliminary development of a surfactant enhanced extraction (SEE) and cloud point separation (CPS) process, based on the properties of nonionic surfactants. More specifically, our objectives were to develop the analytical methods to quantify extraction efficiency, to study the effect of processing parameters (time, temperature, particle size, solid to liquid ratio and surfactant concentration, electrolyte content) and finally to optimize the process.

For the first time, aqueous nonionic surfactant solutions were employed for the streamlined extraction and pre-concentration of THC and CBD from dried *Cannabis L. Sativa* inflorescence. Although ethanol yielded over twice the THC, SEE provides a higher purity extract. At up to 40 °C and 3.75 % weight in Triton X-100, the solvent selectively extracted the cannabinoid over cuticular waxes of the plant. Above, the surfactant's CPT of 65 °C, SEE yield negatively correlated with temperatures. This effect was attributed to the aggregation of surfactant on to the cannabis particles. In respect to CPS, THC and CBD recovery extended above 98 % and 96 %, respectively. The phase isolation removed water-soluble impurities and concentrated both cannabinoids by a factor of 30. The final extract contained up to 2 % by weight in actives. The proposed procedure remains limited by the extraction step's poor yieldswhat is it?. Nonetheless, given the non-toxic and compatible nature of a large number of nonionic surfactants, we believe the extract to be suitable for direct incorporation into cosmetics, natural health and food products and with minimal post-processing.

TABLE OF CONTENTS

LIST OF TABLES

LIST OF FIGURES

LIST OF SYMBOLS AND ACRONYMS

SYMBOLS

Symbol	Definition	Unit
A	Absorbance	AU
α_j	HPLC-UV slope coefficient for specie j	$\mathrm{mL\,AU^{-1}\,mg^{-1}}$
β_j	HPLC-UV intercept coefficient for specie j	AU
${\gamma_j}^i$	Mass concentration of specie j in phase i	$\mathrm{mg\,g^{-1}}$
D_p	Mean volumetric particle size	µm
E_{X100}	Surfactant efficiency	$\mathrm{g\,g^{-1}}$
F_c	Concentration factor	
Fmc_j	Mass concentration factor of specie j in the coacervate	
$k_{c,j}$	Mass transfer coefficient	$\mathrm{min^{-1}}$
k_{cpt}	CP temperature reduction constant	$\mathrm{°C^{-1}}$
m^i	Mass of phase i	g
m_{sol}	Mass of extract	g
m^{ext}	Mass of extract	g
m^{pm}	Mass of plant material	g
ϕ_m	CPS mass phase ratio	
m_j^i	Estimated mass of specie j in phase i	mg
$r_{THC/X100}^i$	THC to X100 concentration ratio in phase i	
R^2	Regression coefficient	
$R_{S/L}$	Solid to liquid weight ratio	
r_{CB}	THC to CBD mass fraction ratio during decarboxylation	
σ_p	Particle size standard distribution	µm
t_∞	Time at extraction equilibrium	min
t	Time	min
T	Temperature	°C
C_j^{ext}	Volume concentration of specie j in phase i	$\mathrm{mg\,mL^{-1}}$
w_j^i	Weight fraction of specie j in phase i	$\mathrm{mg\,g^{-1}}$
$w_{Na_2SO_4}^0$	Weight fraction of Na_2SO_4 in the extraction solvent	%
w_{X100}^0	Weight fraction of X100 in the extraction solvent	%
X_j	Recovery fraction of specie j in the coacervate	%
Y_{THC}	THC extraction yield	$\mathrm{mg\,g^{-1}}$
F_c	Concentration factor	

M	Molecular weight	$\mathrm{g\,mol^{-1}}$
n	Number of replicates	
g	Gravitational acceleration	$\mathrm{m^2\,min^{-1}}$

ABBREVIATIONS

AU	Absorbance units
CB	Cannabinoids (including THC, THCA, CBD, CBDA and CBN)
CBD	Cannabidiol
CBDA	Cannabidiolic acid
CBN	Cannabinol
CMC	Critical micellar concentration
CP	Cloud point
CPE	Cloud point extraction
CPS	Cloud point separation
CPT	Cloud point temperature
DF	Dilution factor
EO	Ethylene oxide
FC	Folin-Ciocalteu
FEG	Field emission gun
GA	Gallic acid
GAE	Gallic acid equivalent
HLB	Hydrophilic-lipophilic balance
HPLC	High performance liquid chromatography
IFT	Interfacial tension chromatography
KF	Karl-Fisher
MAE	Microwave assisted extraction
O/W	Oil in water
OSE	Organic solvent extraction
PEO	Polyethylene oxide
PIT	Phase inversion temperature
PM	Plant material
SCFE	Supercritical fluid extraction
SDS	Sodium dodecyl sulfate
SEM	Scanning electron microscopy
THC	Δ^9-tetrahydrocannabinol
THCA	Δ^9-tetrahydrocannabinolic acid

TPC	Total phenolic content
UAE	Ultrasound assisted extraction
UV	Ultra-violet
UV-vis	Ultraviolet and visible light
W/O	Water in oil
X100	Triton X-100

LIST OF APPENDICES

CHAPTER 1 INTRODUCTION

1.1 Context

Smoking of the dried inflorescence is the most common route of administration (ROA) for both medical and recreational cannabis. However, in addition to causing adverse respiratory symptoms as tobacco, it may also constitute the most inefficient method of consumption [1, 2]. A single gram of dried cannabis contains up to 240 mg of active molecules [3]. When smoked, four-fifths of these actives are lost to the flame through pyrolytic degradation and side stream smokes [4]. On the other hand, oral ingestion of only 20 mg of THC leads to the onset of its intoxication effect [3, 5]. As such, for cannabis producers, extracting the drugs and incorporating them in alternative ROAs is a more profitable option. Currently, cannabis concentrates are obtained through the following steps:

1. **Primary decarboxylation:** In live plants, cannabinoids are present as carboxylic acid, which exhibits low bioactivity. Decarboxylating, by heating the cannabis ground in an oven under vacuum or nitrogen environment between 100 °C to 150 °C, enables the pharmacological properties of the THC and CBD [6, 7].

2. **Extraction:** During extraction, cannabinoids are transfered in a solvent. Various organic solvent extractions (OSE) are employed including liquified hydrocarbons and dimethyl ether [8, 9]. Commercial process prominently employ ethanol and supercritical fluid carbon dioxide (SCFE)[10, 11].

3. **Winterization:** Winterization is an initial purification step aimed removing the high molar mass waxes and lipids by precipitating them in ethanol at −20 °C to −80 °C for periods of up to 48 h. Under those conditions, cannabinoids remain soluble and the waxes can be removed by filtration. Following winterization, an evaporator removes excess solvent and the extract may undergo secondary decarboxylation [12, 13].

4. **Purification:** This multi-step procedure concentrates and isolates the cannabinoids for its end use. It employs a sequential series of units, e.i. distillation, diafiltration, size-exclusion chromatography and affinity chromatography [14]. It aims to yield a cannabinoid concentrate conform to government regulation by removal of residual solvent, pesticides and microbial contaminants [15].

Health risks and costs must be taken into accounts during the production of drug substances destined for public consumption. In that regard, the two main extraction methods currently

employed suffers several drawbacks. OSE is a low-cost extractive process but leaves residual solvents such as methanol, ethanol and cyclohexane and offers poor selectivity. These solvents dissolve lipid cuticular waxes, chlorophylls and other metabolites of the plants, leading to stringent purification schemes [16, 17]. In addition, they are often toxic, offer low biocompatibility and poor environmental performance. Processes employing them are bound to strict regulation to prevent solvent leaks and explosions [18]. SCFE of cannabis inflorescence selectively extracts cannabinoids in a nontoxic and recyclable CO_2, but suffer from long processing time, high capital investment and energy consumption due to the elevated operative pressure surpassing 8 MPa [13]. Their operation requires extensive technical knowledge and is most suitable for the pharmaceutical industry.

In this work, we propose a new extraction procedure for cannabis, which may offer a better balance between safety, cost and performance with respect to traditional extraction methods. The envisioned process is sequential and is enabled by two properties of aqueous nonionic surfactant solutions: their detergency and their cloud point temperature. In a first surfactant enhance extraction (SEE) step, the surfactant recovers cannabinoids from the plant's surface and dissolves them in water. In the second cloud point separation (CPS) step, the crude extract is mildly heated to induce clouding, causing the separation of a large fraction water and substantially concentrating the extract. This integrated SEE-CPS process uses a solvent mixture consisting of water and biodegradable nonionic surfactants and is potentially less expensive and of lower environmental impact than conventional extraction.

1.2 Problem statement

Both *Cannabis L. Sativa* and solid-liquid surfactant enhanced extraction represent relatively novel themes within the scientific literature. As a source of bimolecular compounds for extraction, the former is the subject of few studies, owing to the strict regulatory schemes regarding its accessibility as an illicit drug. Prior to this decade, scientific publication which incorporated extraction procedures were mostly constrained to forensic sciences [19, 20]. In respect to SEE, a handful articles have applied surfactant solutions to extract biocomponents from plant matrices, but cannabis has not been one of them. In addition, these publications remain exploratory without considerations for economic viability and prospective scale-up. Liquid-liquid cloud point extraction (CPE) has previously been employed for the isolation of non-polar compounds from aqueous media, namely to pre-concentrate trace compounds in polluted water prior to chemical or for the recovery of lipophilic proteins following cell lysis [21]. Although, extensive literature data and thermodynamic models exist on CPE in a variety of complex liquid matrices, to the best of our knowledge, no publication has

applied this method to both THC and CBD. The previous work of Ameur et al. [22] on the cloud point extraction of THC focuses solely on the liquid-liquid separation of pre-solubilized cannabis resin.

1.3 Research objectives

This project aims to assess the applicability SEE-CPE for the extraction of the cannabinoids THC and CBD from *Cannabis L. Sativa* and to establish preliminary boundaries for the design of such a process. To do so, we define the following specific objectives:

- Development of analytical methods for in-lab characterization of aqueous surfactant extracts containing cannabinoids.
- Identification and study of the main process parameters affecting THC and CBD extraction performance during SEE and CPE.
- Optimization of the SEE-CPS.

1.4 Thesis outlines

Chapter 2 presents *Cannabis L Sativa*, its morphology and pharmaceutical properties. Chapter 3 provides an overview of surfactants in binary aqueous systems and in emulsions. Chapter 4, details the experimental protocol and analytical methods applied in this thesis. In chapter 5, we present and analyze our experimental results for the SEE-CPE process. Chapter 6 is devoted to the secondary results, that is, non-conclusive or less relevant data. Chapter 7 presents a general discussion on the main results of our work and highlights its limitations. The conclusion of chapter 8 summarizes the present work and proposes some suggestions for future developments of SEE-CPS.

CHAPTER 2 CANNABIS L. SATIVA

2.1 History and regulations

(a)

(b)

Figure 2.1 (a) Industrial hemp type *Cannabis L. Sativa* containing low amounts of THC. Historically, the plant has been used for diverse applications including as: textiles, paper and insulation material in buildings [23]. **(b)** Hemp inflorescence during germination. Cannabis seed also provided food in the form of nutrient rich oils (Images courtesy of Access CBD)

Cannabis has provided a multitude of raw materials for human civilizations throughout the centuries. Its seed were pressed to produce cooking oil, its fibers were sown into cloths and the cannabinoids it contained was a source of medical remedies [19]. The use of drug-type cannabis extends back to antiquity, with evidence found in *Shen Nung Pen Ts'ao Ching*, the first known Chinese pharmacopoeia [24]. The plant was introduced to western culture during the 18th century, where cannabis tinctures treated a range of conditions including: cholera, tetanus, rheumatism, and infantile convulsions [25]. Starting in the 1900s, amid increasing criticism for its potential for abuse, strict policies were implemented by the United States and other governing agencies. In 1961, the United Nations classified cannabis as a Schedule 1 narcotic. By 1970, the use of marijuanna was criminally punishable in most countries [26].

At the turn of the millennium, new evidence of the plant's lifesaving potential against chronic illnesses renewed scientific interest (figure 2.2). In Canada, the specific case of Terrance Parker, an epilepsy patient who successfully treated his ailments through use of marijuana, lead to the overruling of cannabis prohibition laws by the Supreme Court. As a results, in 2001, the Canadian government was the first in the world to establish a state-run medical

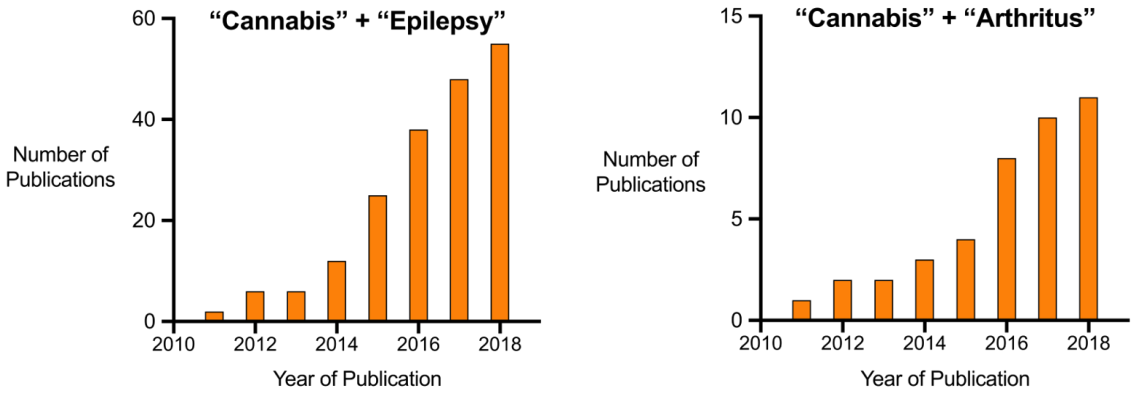

Figure 2.2 Web of Science trends for some medical applications of cannabis

marijuana program [27, 28, 29].

2.2 Morphology of drug type cannabis

Cannabis L. Sativa is an annual herbaceous plants of the *Cannabaceae* family, closely related to hops (*Humulus Lupulus*). They grow up to 5 meters tall and are in majority dioecious, meaning that male and female parts develop on separate plants. Drug type cannabis are harvested exclusively from female plants which produces the active cannabinoids in its unpollinated inflorescences. Inflorescences, shown in figure 2.4, are the flower bearing branches of the plants. They are present at the apex of the branches and at theirs internodes, appearing as dense assembly of flowers (figure 2.3).

2.3 Trichomes

The pharmaceutically active molecules produced by cannabis, Δ^9- tetrahydrocannabinol (THC) and cannabidiol (CBD), originates in its trichomes. Trichomes are microscopy follicles located on the surface of most plants serving as defense mechanisms against external stress. In marijuana, they are either glandular or non-glandular.

Glandular trichomes produces a variety of secondary metabolites as chemical repellents against predators. Three variety of glandular trichomes are found in cannabis: capitate-stalked, capitate-sessile and bulbous. The capitate-stalked variety of trichomes is composed of a of 50 µm to 70 µm spherical head and a stalk measuring up to 200 µm, whereas the capitate-sessile trichomes possess an identical head-structure, albeit 20 µm smaller in diame-

Figure 2.3 Morphology of drug type cannabis: Pistillate (female) plant **(A)** 22 days and **(B)** 28 days (near harvest) after the beginning of it's flowering stage. **(C)**. Representative cannabis branch 22 days into the flowering cycle. Adapted from [30]. Copyright (2019) Spitzer-Rimon, Duchin, Bernstein and Kamenetsky.

Figure 2.4 Female unpollinated inflorescence of *Cannabis L. Sativa* at maturity. Adapted from [31].

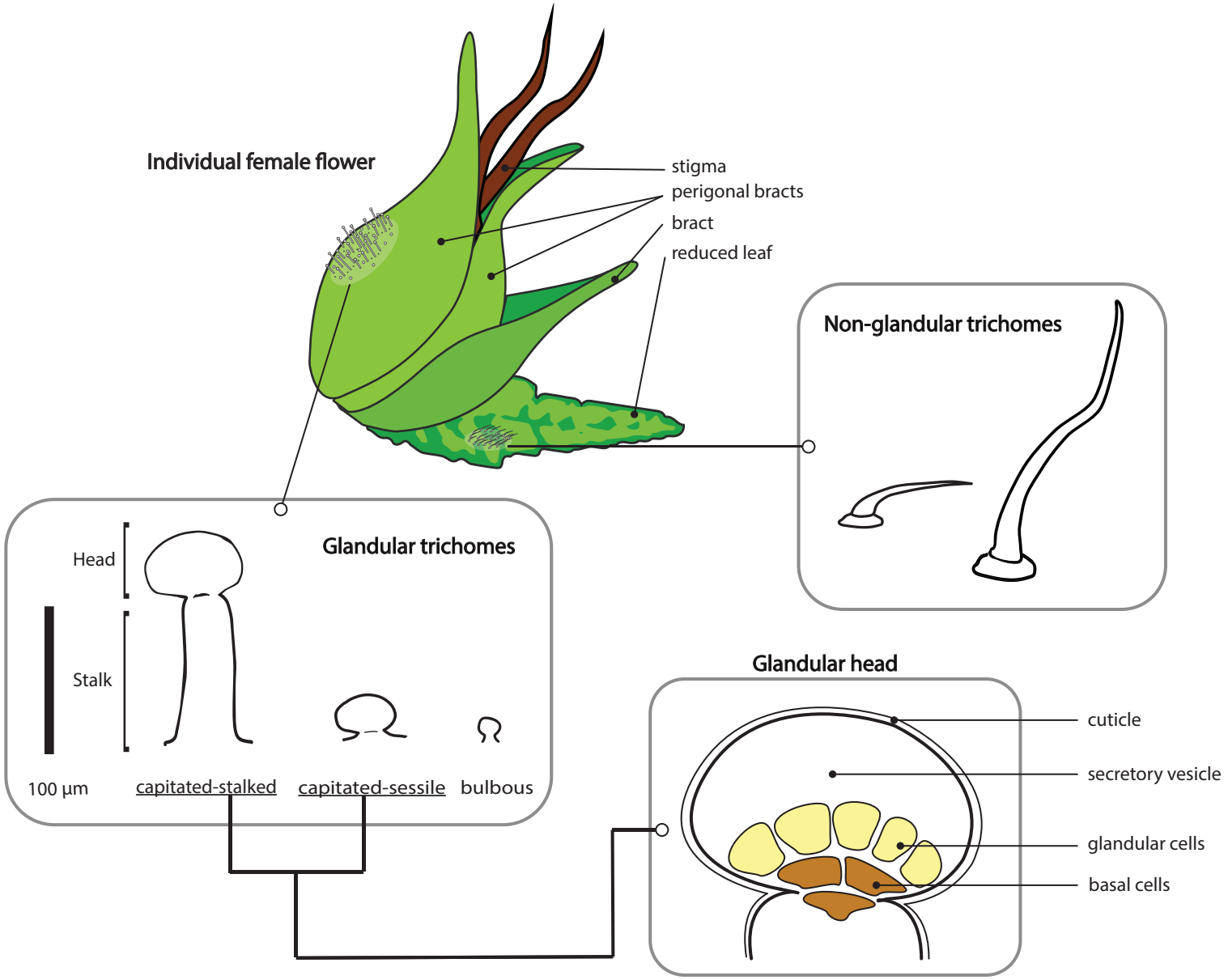

Figure 2.5 Schematic representation of an individual pistillate (female) flower and various types of cannabis trichomes.

ter on average, but lack the cylindrical base. Bulbous trichomes are much smaller, composed of two or four cells, and measure between 10 µm to 20 µm in diameter. Capitate trichomes are responsible for the synthesis of the pharmaceutical active cannabinoids THC and CBD. Specialized cells present within secrete and store the chemicals [32, 33]. The latter is protected by a waxy cuticle extending from and identical to the one found on the epidermis of the underlying leaves [34].

Non-glandular trichomes do not participate in cannabinoid synthesis, rather, their robustness provides a physical barrier against small arthropods and meteorological stress [35]. They slightly larger then glandular trichomes, ranging from 50 µm to 270 µm in length.

The quantity and the variety of trichomes depends on the organs on which they are grow. For instance, in a single leaves, non-glandular and glandular trichomes distributions can greatly differ between the abaxial and adaxial surfaces [36]. The potency of the female inflorescence is explained by the abundance of cannabinoid-rich capitate trichomes on it's perigonal bracts which averages 400 units per mm^2 [37].

2.4 Cannabinoids

Cannabis is a chemically complex species, containing over 500 different bioconstituents including terpenes, flavonoids and alkaloids [38]. Amongst those, over one hundred and twenty different cannabinoids have been indexed. THC and CBD are the two most abundant and have thus far been the primary focus of medical studies [39]. THC is well known for its psychomimetic properties typically associated with feelings of mild euphoria, relaxation and heightened sensory activity. It is also an appetite stimulant and has been formulated in anti-nausea medications. Contrarily, CBD is non-psychoactive. It does not affect human sense, but is a proven anti-convulsant and anti-inflammatory and is approved by the United States' Food and Drug Administration for the treatment of childhood epilepsy [40, 41].

Combined, THC and CBD account for up to half the weight of individual trichomes and between 4 % to 26 % the weight of dried inflorescence [42, 43]. At room temperature, pure CBD is solid crystalline and THC is a viscous liquid with color and consistency similar to that of honey [44]. The solubility of pure THC in water has been estimated at $2.8\,\mathrm{g\,L^{-1}}$ [45]. Some properties of pure THC and CBD are presented in table 2.1.

(a) (b)

Figure 2.6 Microscope imaging of *Cannabis L. Sativa*. **(a)** Lateral view of an individual capitate-stalked trichome at the leave's surface. **(b)** Trichome populated floral bract.

Table 2.1 Physico-chemical properties of cannabinoids

	Chemical formula	M_w, $\mathrm{g\,mol^{-1}}$	T_f, K
THC	$C_{21}H_{30}O_2$	314.5	<298
CBD	$C_{21}H_{30}O_2$	314.5	340

M_w, molecular weight; T_f, melting point.
Source: [46, 45]

2.5 Decarboxylation of natural cannabinoids

In live plants, up to 95 % of all cannabinoids are present as carboxylic acids; tetrahydrocannabinolic acid (THCA) and cannabidiolic acid (CBDA) [47]. Acidic cannabinoids are less biologically active. For instance, THCA possess 62 times lower affinity towards neuroreceptors than its neutral counterpart THC [48]. For the drug to take effect, THCA and CBDA must undergo decarboxylation to generates the active forms, THC and CBD (figure 2.8). The reaction is most prominent when cannabis is smoked in a cigarette, accelerated by the heat of the flame. However, direct burning destroys between 63 % to 80 % of the active cannabinoids. For industrial processing, decarboxylation is commonly performed by controlled heating, during which the cannabis or it's extract is placed at 100 °C to 140 °C for up to 2 h. The reaction ideally occurs under vacuum or nitrogen atmosphere to prevent oxidative degradation. [49, 6, 50].

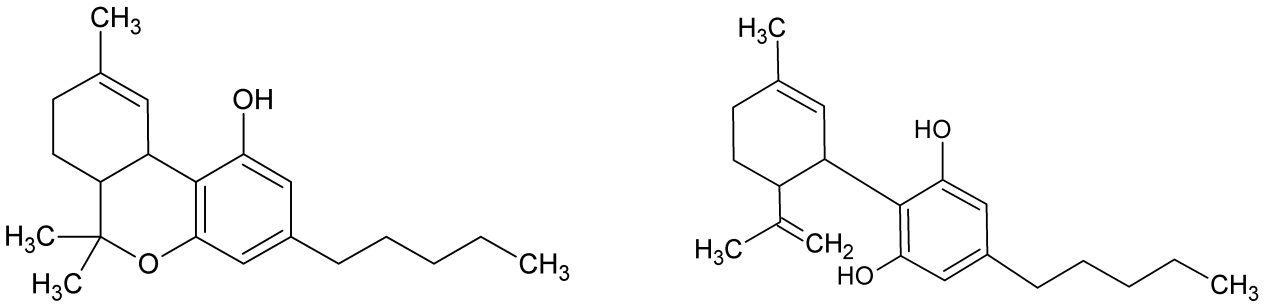

Figure 2.7 Major phytocannabinoids. **(a)** Δ^9-tetrahydrocannabinol and **(b)** cannabidiol. Both THC and CBD comprises of a main phenolic ring to which are attached a saturated C_5 alkyl chain and a cycloalkene substituent. For THC the substituent is a heterocyclic ether while for CBD it is a hydroxide group.

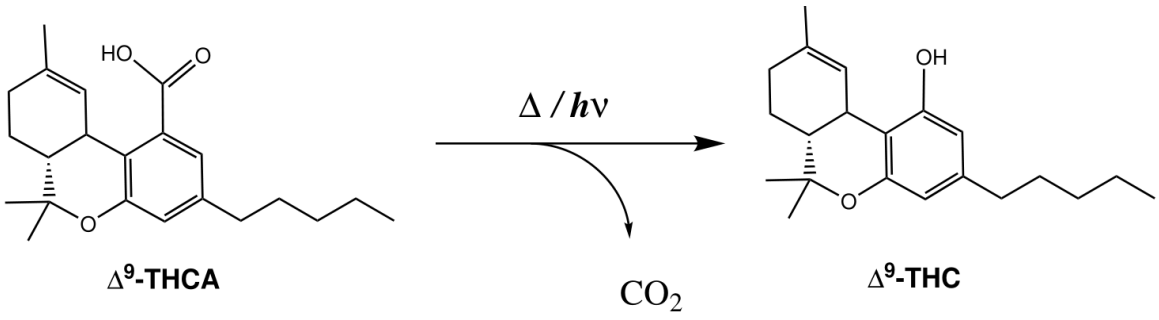

Figure 2.8 Decarboxylation of tetrahydrocannabinolic acid (THCA) toward pharmaceutically active neutral tetrahydrocannabinol (THC).

2.5.1 Kinetic of decarboxylation

During decarboxylation, the carboxylic group of the cannabinoid's benzene ring gives off to an alchohol, generating carbone dioxide (figure 2.8). The reaction is endothermic, promoted by light and heat. Kinetic for both THCA and CBDA can be fitted a pseudo-first order (equation (2.1)) with activation energies ranging from $85\,\mathrm{kJ\,mol^{-1}}$ to $87\,\mathrm{kJ\,mol^{-1}}$ and $90\,\mathrm{kJ\,mol^{-1}}$ to $112\,\mathrm{kJ\,mol^{-1}}$, respectively [51, 52, 53]. The first order kinetic representative of decarboxylation is modeled by the following equation:

$$w_j = w_j^0 e^{-kt} \tag{2.1}$$

Where w_j is the weight fraction of cannabinoids j (THCA or CBDA) at time t, w_j^0 is the

initial weight fraction in acidic cannabinoid and k is the rate coefficient in s^{-1} from the Arrhenius equation:

$$ln(k) = ln(k_0) - \frac{E_{A,j}}{RT} \tag{2.2}$$

Where k_0 is the pre-exponential constant in s^{-1}, $E_{A,j}$ is the activation energy, R is the ideal gas constant and T is the temperature in Kelvin.

CHAPTER 3 LITERATURE REVIEW: SURFACTANTS

3.1 Properties of surfactants

Surfactants, a contraction of the terms "surface active agents", are a class of compounds composed of two distinct regions, a hydrophilic head and a hydrophobic tail. They are either nonionic, anionic, cationic or zwetterionic (figure 3.1). Currently, there are a number of biocompatible and biodegradable surfactants commercially available which are found in over-the-counter products such as foods, cosmetics, pharmaceuticals and detergents. For instance, polyoxyethylene sorbitan (Tween 20) is employed in topical cremes to dissolves essential oils and mixes of glyceride, sorbitan and polyoxyethylene sorbitan stabilizes bread shortenings. In laundry, surfactants remove soil from textiles, keeping particles and oils in suspension and preventing their redeposition [54].

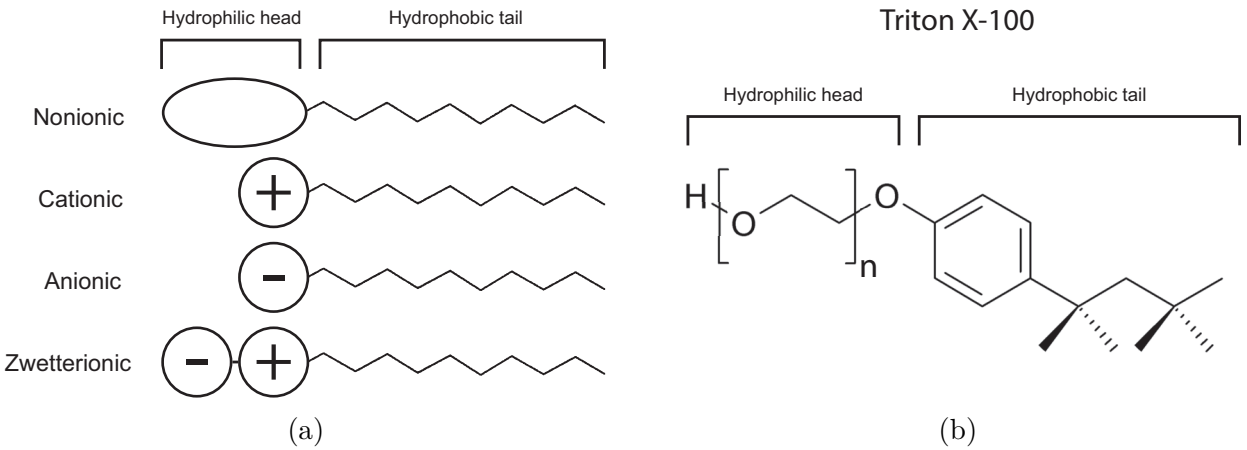

Figure 3.1 Surfactant structures and types. **(a)** Nonionic, anionic, cationic or zwetterionic types of surfactants. **(b)** Molecular structure of Triton X-100 (X100) a common detergent used in laboratories. In X100, the hydrophobic section is a 4-(1,1,3,3-tetramethylbutyl)-phenyl hydrocarbon group, whereas the hydrophilic head is formed by a polyethylene oxide (POE) chain with an average length of n = 9.5 ethylene oxide units. X100 is classified as nonionic as its ethylene oxide head does not ionize in aqueous phase. Contrarily, the hydrophilic heads of anionic and cationic surfactants assume negative and positive charges respectively. Zwitterionic surfactants display cationic or anionic behaviors depending on the pH of its environment [55, 56].

Definitions

Interface: contact region of finite width between two adjacent phases.

Surface tension: represents the the work per unit area required to form a new surface and is dependent on system temperature and pressure. Liquids with high surface tension tends to assume spherical shape to reduce their surface area. The surface tension between water and air at 20 °C is $73\,\mathrm{mN\,m^{-1}}$

Interfacial tension (IFT): surface tension equivalent between any two phases (i.e. liquid-liquid, solid-liquid).

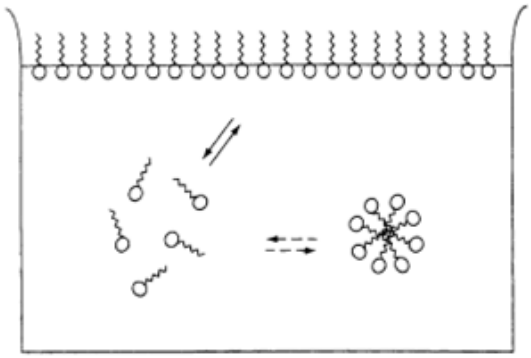

Figure 3.2 In aqueous surfactant solutions, monomers are either individually dispersed, layered at the interface or aggregated as micelles.

3.1.1 Accumulation at the interfaces

When a small quantity of surfactant is mixed in water, a portions of its monomers disperses while the other spontaneously reorganize. The strong attractive forces between water molecules pushes the surfactant's apolar (hydrophobic) tail towards the liquid's interface. This causes the surfactant monomers to accumulate in a mono-layer such that their hydrophilic component remains in water while their tail protrudes into the other phase. Such configuration disrupts the water-water cohesive forces at the interface and reduces the interfacial tension (IFT) proportionally to the surfactant's concentration. This trend continues until the interface is completely saturated with surfactant molecules at which point the IFT remains constant [57].

3.1.2 Micelles formation

Saturation of the interface occurs when the total concentration of surfactant in solution surpasses the critical micelle concentration (CMC). Above this concentration, it becomes thermodynamically favorable for surfactants to form micelles, dispersed spherical aggregates with sizes ranging from 2 nm to 20 nm in diameter. Within an individual micelles, surfactant monomers are oriented with their heads pointing towards water phase and their tails shielded from water pointing towards the micelle's core (figure 3.2). Repulsive forces at their surface cause them to remain dispersed within the solution. Under ambient conditions, CMC of nonionic surfactants range from 10^{-4} mM to 10^{-3} mM whereas those of ionic surfactants are between 10^{-3} mM to 10^{-2} mM. The CMC increases with temperature as the monomers become more hydro-soluble. System pressure and the presence of additives also alter the CMC [58, 59, 60, 55].

3.1.3 Aggregation structures

Dilute surfactant solutions produces small spherical micelles. Conditions which favors micelle-micelle interactions, such as an in increase temperature or monomer concentrations, causes the micelles rearrange and form highly ordered and complex structures known as mesophases. (figure 3.3). Some mesophases possess properties of both solid and liquid states, while also exhibiting properties that are not found in neither solids or liquids. Those are characterized as liquid crystals as they possess crystal-like characteristics such as birefringence [61, 62]. In water-surfactant systems, binary phase diagrams, such as the one presented in They possess properties of both solid and liquid states while also exhibiting properties that are not found in neither solids or liquids, are used to delimit the presence micellar solution from mesophases at higher surfactant concentrations.

3.1.4 Cloud point

On the macroscopic scale, the cloud point (CP) temperature marks the transition from a translucent water-surfactant solution to a turbid suspension (figure 3.5). If the mixture is allowed to settle undisturbed, two distinct liquids in equilibrium eventually appears: a surfactant-rich phase and a water-rich phase. This property results from an aggregation behavior unique to low concentration solutions of nonionic surfactants. When the system's temperature is increased above the CP, their micelles aggregates to form a second liquid phase. In contrast, micelles in aqueous ionic surfactant systems do not phase out and remain dispersed.

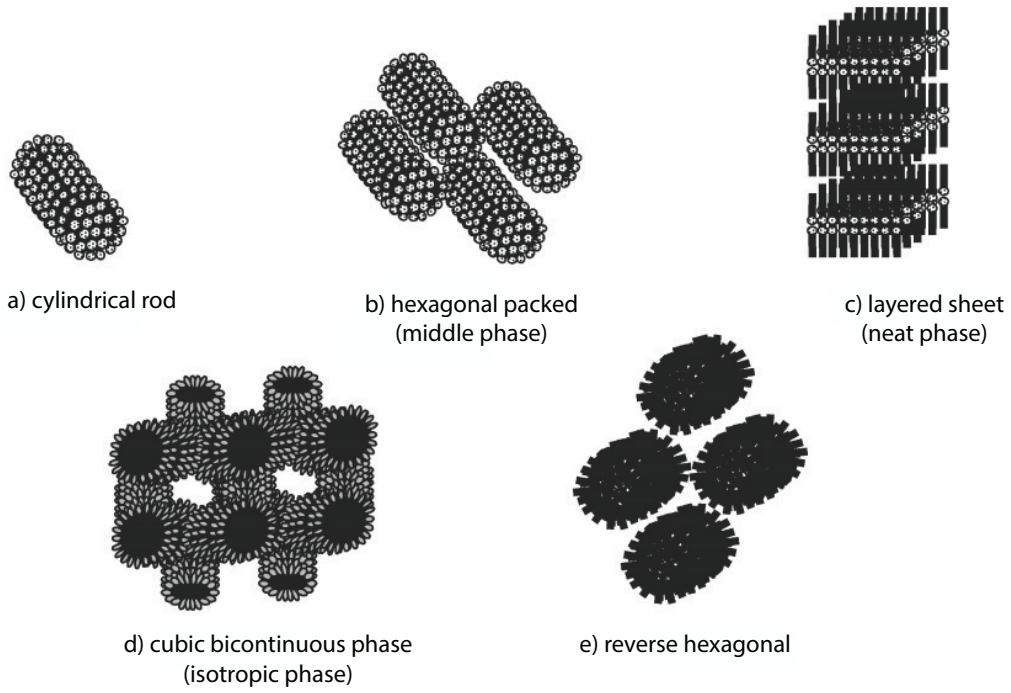

Figure 3.3 Schematic structures of surfactant mesophase structures. Adapted from from [62]. Copyright (2005), with permission John Wiley & Sons, Inc.

Clouding is characteristic of nonionic surfactants containing a polyoxyethylene (POE) head group. Below the CPT, the polar head group comes under a hydrated state as it combines with surrounding water through hydrogen bonds. The resulting structures are relatively large and sterical hinderance keeps the micelles from coming together. However, increase in temperature reduces polar interactions between the ethylene oxide (EO) head group and water, which, in turns, diminish inter-micelle repulsion, causing them to aggregate. The mechanism is entropic and micelle-micelle adhesion strengthens at higher temperature. The onset of turbidity during clouding is explained by an increasing in size of the micelle agglomerations which become sufficiently large to scatter visible light.

In a binary phase diagram, then clouding corresponds to the up-left region (figure 3.4). This region is isotropic as, upon reducing the temperature or increasing the surfactant concentration, the micelles separate. The biphasic liquid is hence reversed into a single homogeneous solution. Above the CP, micelles of the surfactant rich-phase become densely packed, either into a cubic bicontinuous phase or as cylindrical rod. The surfactant-rich phase inherently contains a fraction of bonded water. The water-rich phase however, is devoid of micelles. Instead, dissolved surfactant monomers are present at their CMC [57, 64] .

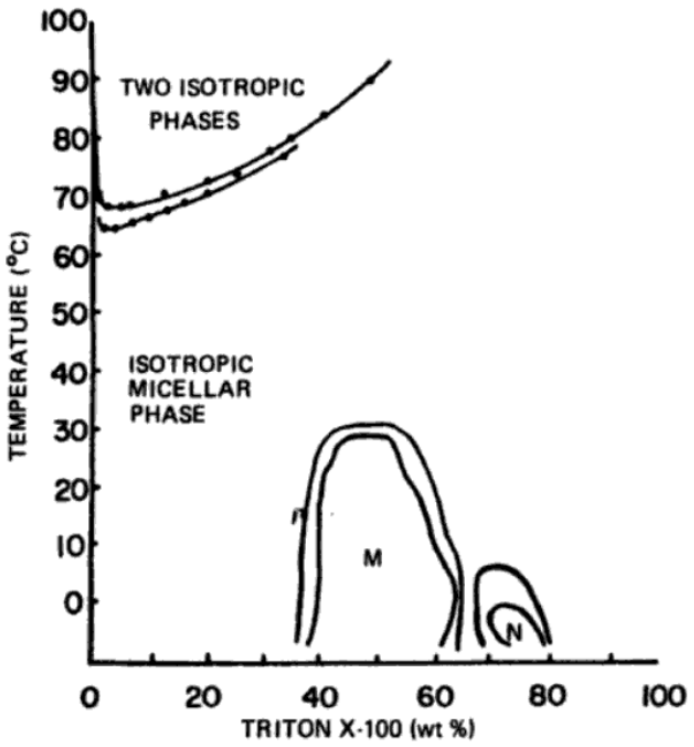

Figure 3.4 Binary phase diagram of Triton X-100 and water system. The two set of lines represent different commercial preparations of X100 with average molecular weights of 624 $g\,mol^{-1}$ and 680 $g\,mol^{-1}$. "M" is the hexagonal packed middle phase and "N" is the neat phase. The region labelled "two isotropic phase" indicates the clouded state. For a surfactant solurftion of given concentration above its CP, the composition of both water-phases and surfactant-rich phases is obtained by tracing isothermal tie-lines and observing the intersects. Reprinted from [63]. Copyright (1987), with permission Taylor & Francis Group LLC - Books.

Effect of ionic strength on the cloud point

Cloud point temperature of surfactants diminishes with increasing ionic strength of the aqueous solution. Small, highly-polar ions such as $SO_4{}^{2-}$ and Cl^- exhibit a preference to stay in the water bulk over the micellar core. There, they favor water-water cohesion over interactions between the surfactant's head group and water [65]. As such, an increase in the concentration of these ions corresponds to a proportional decrease in solubility of micelles, leading to a reduction in CPT. For a system already above its CPT, better cohesion in the aqueous phase dehydrates the surfactant-rich phase and reduces its water content [66, 67].

(a) (b)

Figure 3.5 Clouding of nonionic surfactant IGEPAL CA-620. A 1 % weight of surfactant solution was stirred on a heating plate. The pictures show both **(a)** before and **(b)** after the solution has reached it cloud point at 72 °C.

Effect of surfactant structure on the cloud point

Cloud point characteristics are function of the surfactant structure. For unbranched alkyl ethoxylated surfactants, the CPT increases with higher ethoxylation number and decreases with carbon chain length. Increasing the number of oxyethylene groups raises the cloud point due to the greater number of stabilizing interactions with surrounding water molecules. Conversely, increasing hydrocarbon tail length exerts a opposing effect and decreases the CP [68, 69]. Tani et al. [70] empirically the cloud point temperature of unbranched alkyl ethoxylated surfactants to their chemical structure: equation (3.1).

$$CPT = 220 log N_E - 5.5 log N_C - 55 \tag{3.1}$$

Where N_E is the number of ethylene oxide and N_C is the number of carbons in the surfactant's tail.

3.1.5 Emulsions

An emulsion consist two immiscible liquids dispersed as droplets one within the other. The liquid composing the droplets is referred to as the dispersed phase, while the other is the continuous phase. In most cases, one phase is aqueous while the other is a hydrocarbon (oil) which emulsified together by shear mixing. Emulsions obtained in such manner are not thermodynamically stable as the droplets will tend to coalesce in order to reduce their surface

area (figure 3.6). A surfactant added to such binary system will place itself in between the dispersed droplets and the continuous phase to form a barrier which prevents coalescence. This configuration lowers the IFT andi thermodynamically favors the presence of smaller drops ([71]).

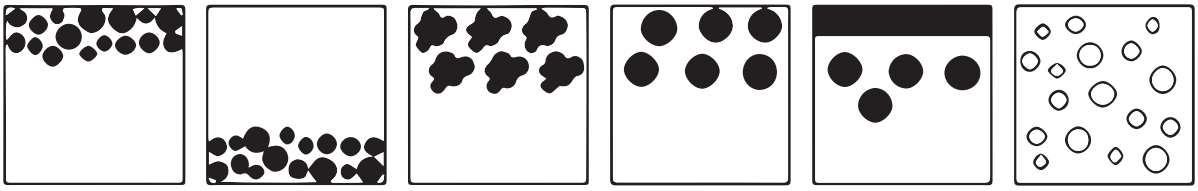

Figure 3.6 Mechanisms of emulsion destabilization. The term stability refers to the lifetime of an emulsion. High interfacial energy must be overcome to obtain a stable emulsion. If not, the mixture may be distabilized trough a number of mechanisms. These includes (from left to right): creaming, sedimentation, flocculation, Ostwald ripening, coalescence and phase inversion [72]. Image adapted from [73].

Surfactant stabilized emulsions are three phase systems composed of water, oil and surfactant. It is practical to represent them in ternary phase diagrams such as the one presented in figure 3.7. These diagrams display some of the same aggregations structures as in water-surfactant systems (i.e. lamella and hexagonal), but also indicates behaviors unique to emulsions, such as the presence of 3 phase region or the phase inversion compositions [74, 71].

3.1.6 Hydrophilic-lipophilic balance

The hydrophilic-lipophilic balance (HLB) classify the affinity of surfactants toward aqueous or lipophilic phase [76]. It ranges from 0 to 20, with a value of less than 10 corresponding to an oil-soluble surfactant and those above 10 describing a water-soluble surfactant [77]. This concept is critical when deciding on a surfactant for a specific application (figure 3.8). For instance, amphiphilic molecules with an HLB between 0 and 9 more readily form O/W emulsions, whereas those with an HLB above 11 form W/O emulsions. Multiple equations have been proposed for estimating HLB. The most common one is the Griffin's equation:

$$HLB = 20 \times \frac{M_{hydro}}{M_{total}} \tag{3.2}$$

where M_{hydro} is the molecular weight of the hydrophilic section and M_{total} is the total molecular weight.

In mixtures of emulsifier pairs a and b with matching ramification (e.g. SPAN 20 and Tween 20), HLB of the resulting mixed micelles are obtained by multiplying the mass fraction of

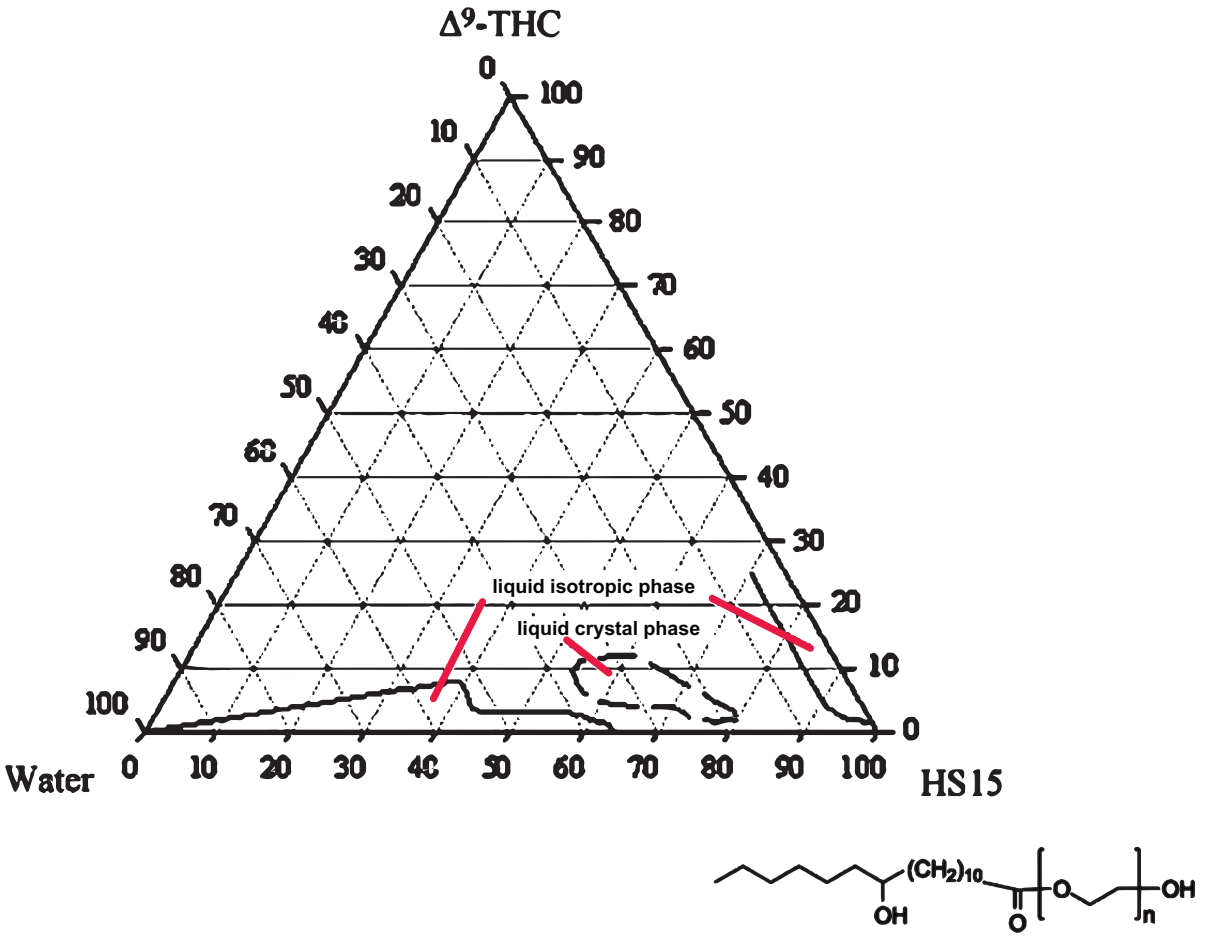

Figure 3.7 Partial ternary phase diagram of THC/H2O/nonionic Solutol HS15 system at 25 °C. The diagram show the phase behavior of systems containing up to 30 % THC by weight. Adapted from [44]. Copyright (2010), with permission from Elsevier.

each surfactant by their respective HLB [54].

$$HLB_{mix} = HLB_a \times w_a + HLB_b \times w_b \tag{3.3}$$

3.2 Detergency and the cleaning mechanisms of surfactants

Detergency studies the interaction between a substrate and soil accumulated at the substrate's surface. The addition of surfactant aids the removal of liquids oils through two mechanisms: roll-up and solubilization.

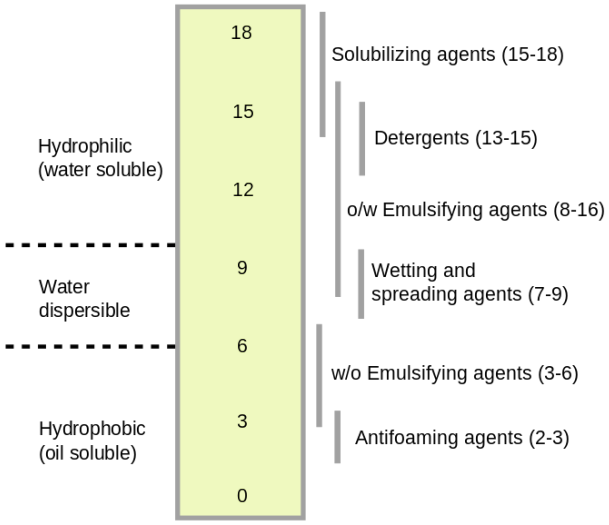

Figure 3.8 Hydrophilic-lipophilic balance scale. This value provides an indication of it's applications. Reprinted from [75].

3.2.1 Roll-up mechanism

The roll-up mechanism arises from the interface properties of surfactants. The system is represented by three phases containing water, oil and a substrate (figure 3.9). Oil attaches itself to the substrate through physical interactions, namely adsorption and electrostatic forces. The work maintaining liquid oil to it's substrate is named work of adhesion (W_{ad}) and represents the quantity of energy required to separate the oil from it's substrate while simultaneously creating new oil-water and substrate-water interfaces. It can be expressed as a summation of IFTs:

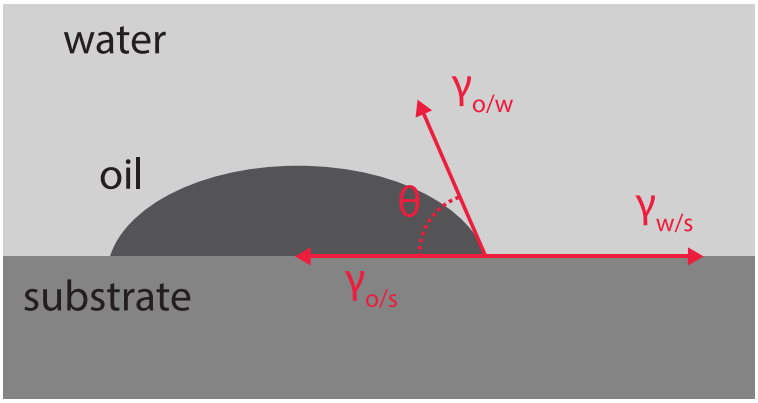

Figure 3.9 Schematic representation of liquid soil droplet attached to a surface immersed in water.

$$W_{ad} = \gamma_{o/w} + \gamma_{s/w} - \gamma_{o/s} \tag{3.4}$$

Where $\gamma_{a/b}$ is the IFT between phases a and b. The Young's equation describes the equilibrium force balance between the three phases based on the system's contact angle (θ).

$$\gamma_{o/w} \times cos(\theta) = \gamma_{o/s} + \gamma_{w/s} \tag{3.5}$$

The combination of the previous two equations yields the Young-Dupre equation which allows for the calculation of the W_{ad} on a liquid on solid surface based on contact angle measurements.

$$W_{ad} = \gamma_{oil/water} \times (1 + cos(\theta)) \tag{3.6}$$

When surfactants are added to such system, they adsorb at both the oil-water and substrate-water interfaces, reducing their IFTs. This in turns decreases the W_{ad} and therefore increases the contact angle. Detachment of the soils can then occur in several ways as shown in figure 3.10. If the surfactant nulls the cohesive forces at the surface ($W_{ad} = 0$), the contact angle is capped at 180° and the droplet spontaneously lifts up. If the contact angle is smaller then 180°, complete or partial separation may occurs but requires additional mechanical work such as stirring.

Detergency by roll-up plateaus near the CMC where IFTs in the water-oil-substrate system stabilizes at it's minimum. As such, it is best achieved by ionic surfactants due to their higher CMC (figure 3.11). Higher temperature improves this mechanism, by increasing the CMC. In emulsified systems formed with nonionic surfactant, roll-up is optimal at the phase inversion temperature where IFT reaches its lowest [79, 80].

3.2.2 Direct solubilization-emulsification mechanism

Solubilization is the second mechanism of detergency in which micelle formation drives the oil removal process. In contrast to roll-up, it occurs above the CMC and is improved by high surfactant concentrations. To visualize this mechanism, the core of the micelle can be represented as a nanoenvironment dispersed in the bulk of the water. Due to their apolar nature, they consistitute, a secondary phase toward which partioning of lipophilic compounds is favored. Several mechanism have been proposed to explain solubilization. Those include the capture of dissolved oils by lone micelles and the dissociation of interface-

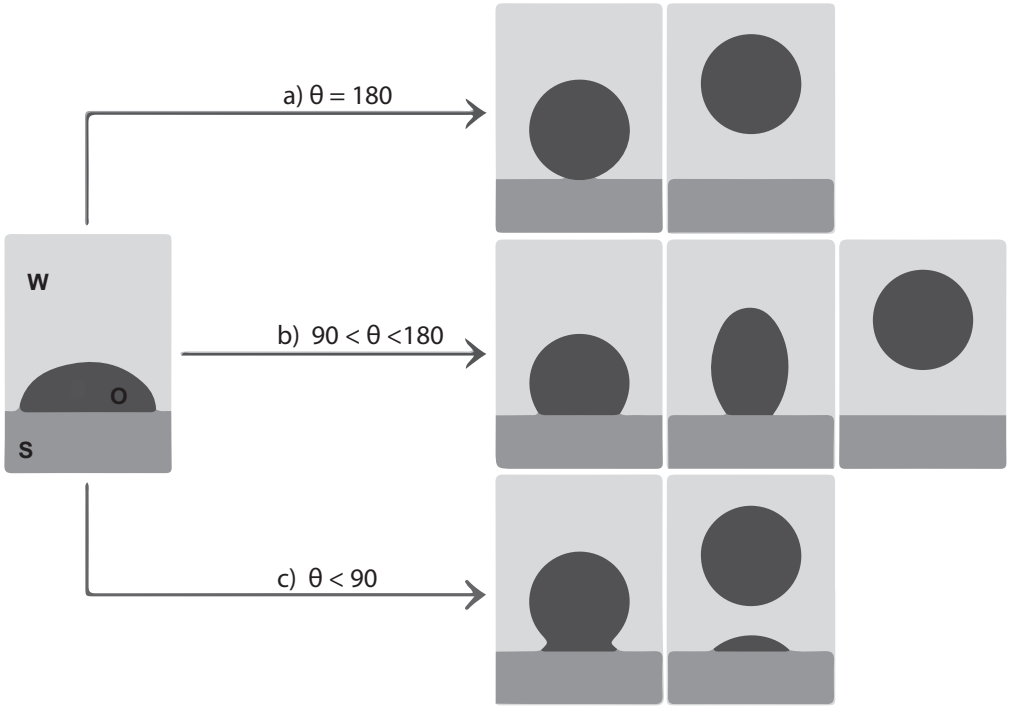

Figure 3.10 Roll-up mechanism of detergency illustrating how surfactants reshapes the liquid soil droplets. **(a)** Spontaneous separation. **(b)** Contact angle following the addition of surfactant ranges from 90° to 180°. Complete separation may be achieved by addition of mechanical energy to the system. **(c)** The cohesive forces between oil and substrate are maintained and the contact angle remains below 90°. External work may remove a portion of the droplet but complete separation cannot be achieved as some oil remain attached to the surface. Adapted from [78]. Copyright (2006), with permission from American Chemical Society.

adsorbed surfactants (figure 3.12).

3.2.3 Solubilization by mesophase

A third mechanism of liquid soil removal involves the formation of a mesophase within the washing bath. The aggregated phase either grows at the interface due to interactions between the oil and the adsorbed surfactants, or are initially present in the washing solution (such as in a surfactant solution above it's cloud point temperature). Superficial oils in contact with this phase are directly solubilized by the hydrophobic tails and spontaneously emulsify. Subsequently, this phase can be broken off by agitation and dispersed into the liquid. As such, the performance of these systems is reliant on the phase behavior of the surfactant. Whereas the phase equilibrium of ternary emulsions depends on the polarity of the solute, the temperature and the surfactant's structure and concentration, mesophase formation in

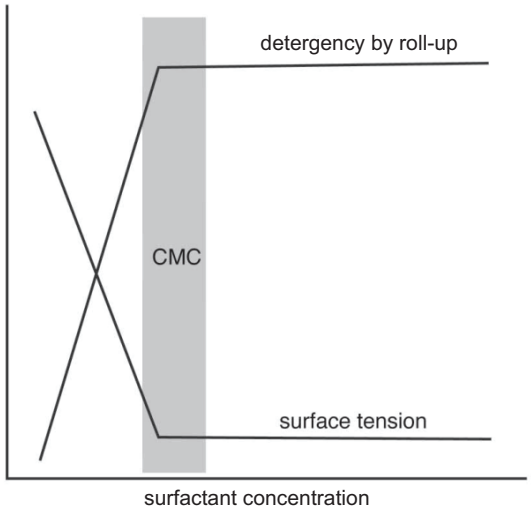

Figure 3.11 Effect of surfactant concentration on surface tension and roll-up. Adapted with permission from [78]. Copyright (2006) American Chemical Society.

detergency systems is also affected by the hydrophobicity of the surface on which the oils are attached [82, 83].

3.3 Cloud point extraction

3.3.1 Procedure and operating principle

CPE is a liquid-liquid extraction method predominantly applied in analytical chemistry for chromatographic quantification. It utilizes the cloud point properties of nonionic surfactants to recover hydrophobic compounds from water (detailed in section 3.3.1). A diagram of CPE steps is highlighted by figure 3.13.

In the standard procedure, low concentration of nonionic surfactants (i.e. 0.025 % to 0.3 % by volume) and inorganic salts are homogenized in an aqueous sample containing trace amounts of the molecule of interest. The surfactant encapsulates the compound and the solution is then brought above the CPT for phase segregation. This is achieved by gravitational settling (decantation or centrifugation) of the heated the solution. During separation, the surfactant micelles clusters, entraining the compounds contained within its core into the surfactant-rich phase. Once separate, the water phase can be removed while the surfactant phase may be diluted into a suitable solvent for analysis [84]. The result is significant increase in concentration of the analyte relative to the initial extract. Provided solutes are suitably hydrophobic (and hence poorly soluble in water), a complete partition into the coacervate is

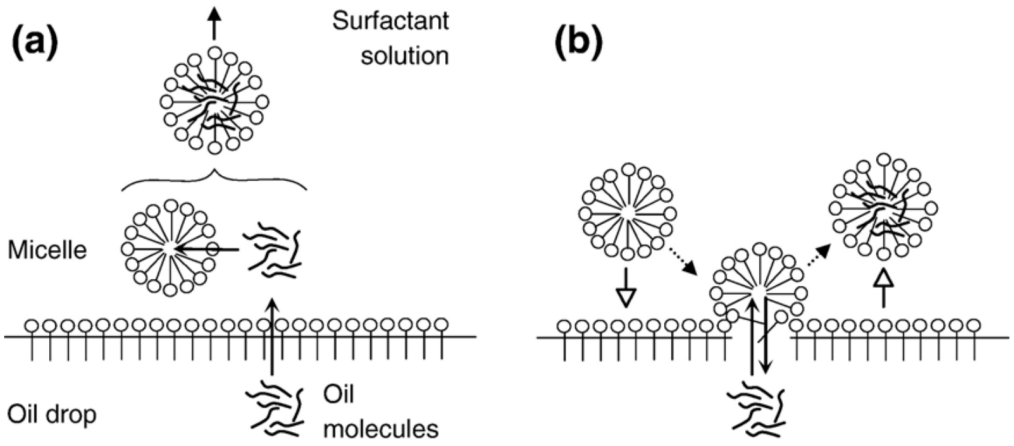

Figure 3.12 Plausible mechanisms for the solubilization of oil in aqueous micellar solutions. **(a)** Diffusion mechanism. Oil molecules dissolve and diffuse into the water phase and are subsequently encapsulated by micelles. This mechanism is most prevalent for ionic surfactant where micelles and oil drop exert repulsive forces on each other as a result of the orientation of the surfactant's head charge. **(b)** Micelle detachment mechanism. The micelle partially adsorbs/coalesces with droplet. Oil molecules are then entrained by it's apolar tail as the micelle detaches. This mechanism is observed for nonionic surfactant and water unsoluble oils. Reprinted from [81]. Copyright (2006), with permission from Elsevier.

obtained. Phase behavior during CPE can be model using several thermodynamic packages [85].

The relative concentration increase is commonly express as the pre-concentration factor (F_C), and is calculated using equation (3.7), where C_{surf} is the concentration of analyte in the surfactant-rich coacervate phase, and C_0 is the analyte concentration in the crude extract prior to phase separation.

$$F_C = \frac{C_{surf}}{C_0} \tag{3.7}$$

A second variable useful to CPE is the phase volume ratio (ϕ_V). As shown in equation (3.8), ir describes the relative reduction in volume obtained after phase separation. It is expressed as the volume ratio between surfactant-rich phase (V_{surf}) and the aqueous-phase (V_{aq}) after separation.

$$\phi_V = \frac{V_{surf}}{V_{aq}} \tag{3.8}$$

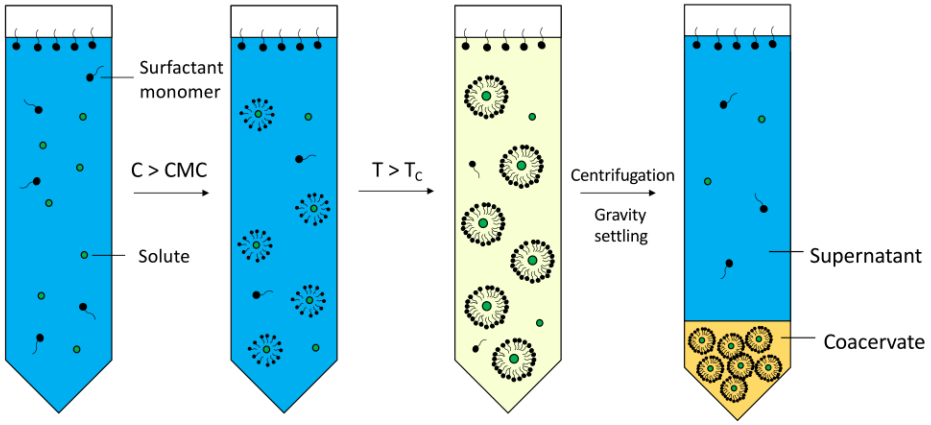

Figure 3.13 Schematic of cloud point extraction (CPE) process

3.3.2 Applications

Watanabe et al. [86] first exploited the phase separation behaviour of non-ionic surfactant systems for the isolation and analysis of hydrophobic zinc (II) complexes from municipal water sources. Subsequently, CPE has been extensively applied as a separation and pre-concentration technique for the analysis of trace metal ions and organics pollutants in aqueous media. The method has also extended towards more industrial applications, with studies oriented towards the separation and purification of proteins, and the recovery of bioactive compounds from liquid food waste. [21, 87, 88].

3.3.3 Variables affecting cloud point extraction

Recovery of a given compounds in the surfactant-rich phase is dependent on temperature, time, surfactant structure, ionic strength and pH.

Effect of temperature and equilibration time

Increasing the temperature above the cloud poin, or extending the equilibration period dehydrates the surfactant phase, reduces it water content and therefore increases the pre-concentration factor. The temperature's influence on separation yield can, however, be application-specific as certain systems will benefit from reduced viscosity at higher temperatures, whereas thermolabile molecules become susceptible to degradation [64, 68, 87].

Effect of surfactant structure

Cloud point temperatures are highly dependent on the surfactant's structure. For instance, solutions containing 1 % of non-ionic surfactants $C_{12}E_8$ and $C_{12}E_4$ undergo clouding at 80 °C and 10 °C, respectively. At a given temperature, the equilibrium water composition, aggregation number and phase partition of these surfactants differ, which influences both the concentration factor and recovery achieved [89].

Effect of inorganic salt

Inorganic salts are often added to aqueous solutions to improve CPE performance. Once in water, they dissociate into anions and cations, which and increase the solution's ionic strength. As discussed in section 3.1.4, the presence of electrolytes reduces water content of the surfactant-rich phase. This property is exploited to increase CPE concentration factor and is particularly useful when the analyte of interest are present only in minute concentrations. In addition, ionic species depresses the CPT and hence represent a route to preserve thermolabile compounds during extraction [64]. Fang et al. [90] observed an increased recovery in hydrophilic gensinosides from 70 % to 100 % with the addition of 0.5 % (w/v) of Na_2SO_4.

Effect of pH

Organic species containing phenolic or amine functional groups constitute a large portion of biomolecules present in plants. Under suitable pH, they ionize. The resulting electric charge benefits their affinity towards the water rather then the micellar phase, leading to a reduced CPS recovery. As such, CPS is optimally performed at pH for which the molecule of interest is present in their neutral form [64].

3.4 Description of a SEE-CPS process

The unique detergency and cloud point properties prime nonionic surfactants for use in cannabis extraction. The process draws parallels with both the laundry washing and the CPE method, which were reviewed in section 3.2 and section 3.3.1 respectively. These similarities are highlighted in figure 3.14. It is nevertheless useful to distinguish the particularities of the proposed SEE-CPS from traditional surfactant applications.

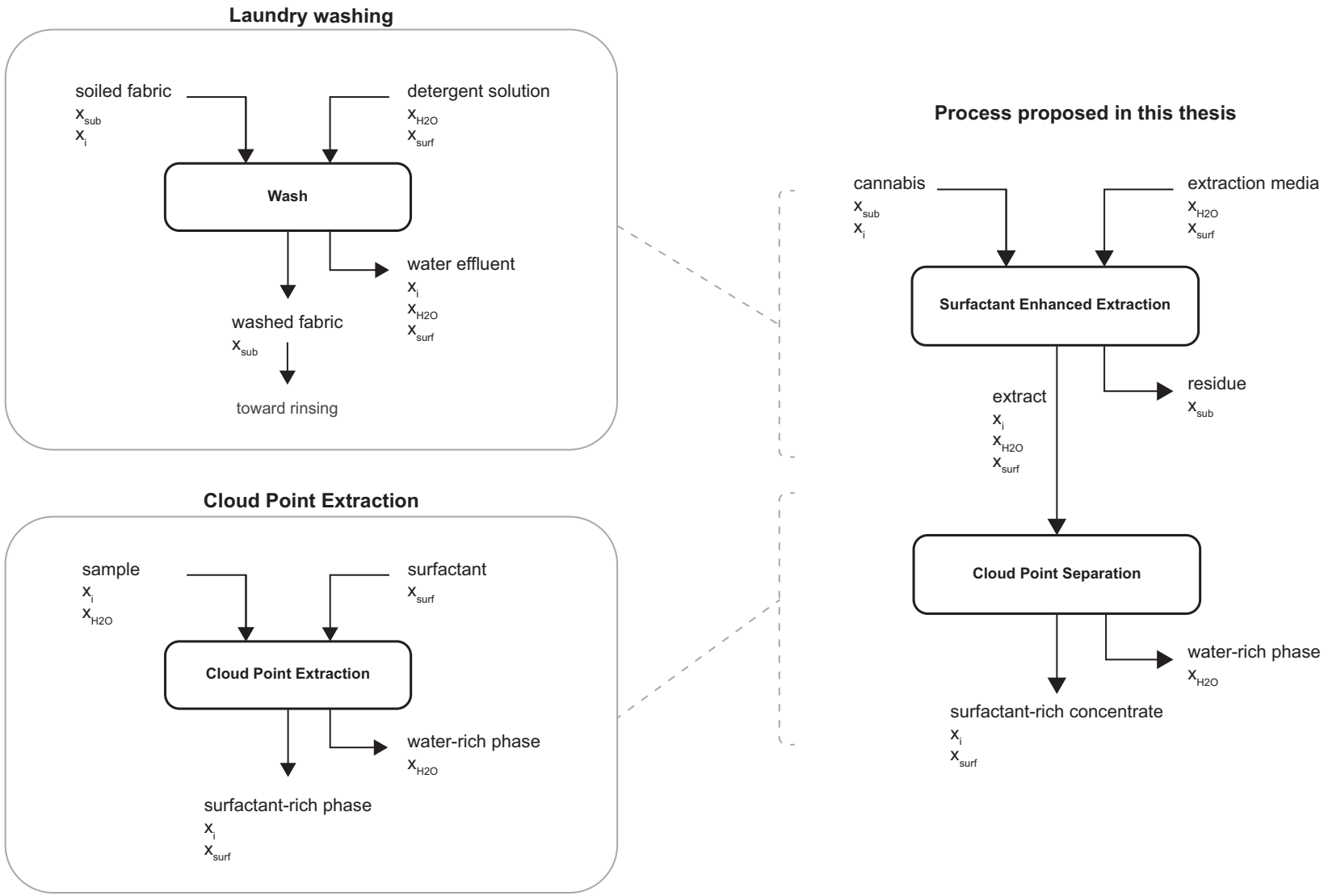

Figure 3.14 Diagram comparing laundry washing, cloud point extraction (CPE) and SEE-CPS. The "x"s the flow of major components in subscript. sub, solid substrate; i, hydrophobic compound of interest; H2O, water; surf, surfactant.

3.4.1 Surfactant enhanced extraction

SEE is a solid-liquid extraction. Milled plant matter is extracted in a solvent composed of nonionic surfactants and water. The surfactants monomers lift the cannabinoids from the leaves' surface while simultaneously dissolving them into the liquid-bulk. Following extraction, the slurry is filtered or centrifuged to remove the solid plant particles, yielding a raw extract. The latter then undergoes a procedure similar to CPE, where the cannabinoids are concentrated by phase separation.

For water-immiscible compounds, the extraction mechanism is best described by detergency and is therefore function of the properties of the surfactants (CMC, HLB) and that of the extraction systems (temperature, surfactant concentration). Contrary to a laundry systems however, the ideal SEE does not dissolve the entirety of oils present on the substrate. Instead, it aims target the molecules of interest (e.i. THC and CBD) over unwanted lipids to achieve a selective extraction, thus reducing the need for their removal in subsequent operations.

3.4.2 Cloud point separation

CPS is a aqueous-two-phase liquid-liquid separation. The raw extract, an O/W emulsion, undergoes the identical procedure as in CPE. The extract is equilibrated above its CPT and centrifugated to yield a micelle phase concentrated in cannabinoid and a water-rich phase. CPE must be differentiated from CPS. The former aims to recover presolubilized compounds from aqueous sample by incorporating nonionic surfactants, whereas, in the latter, both surfactants and the compound of interest are already present in the solution.

3.4.3 Examples in the literature

Previous studies applied SEE-CPS to a variety of solid plant matrices including to spinach leaves, ginseng roots and chili powder. These publications are summarized in table 3.1.

Leite et al. [76] identified the HLB of surfactant to be a variable of interest. During SEE of chlorophyll from spinach leaves, an optimal yield of $0.63\,\mathrm{mg\,g^{-1}}$ was achieved with nonionic surfactant mixtures with an HLB values between 10 and 13. Subsequently during CPS, the concentration of the extract was enhanced by a factor of 9. Surfactants with higher CMC were observed to better extraction of Labdane diterpenoids, a water-insoluble drug found in herbal medicines used against respiratory infections [91]. Of relevance to the present research, is the study by Ameur et al. [22] who employed SEE-CPS to seized cannabis resins (trichomes). Aqueous solution 1 % of *Dowfax 201B102* by weight optimally extracted of 81 % of THC at T= 318 K.

Table 3.1 Application of SEE and CPE to plant matrices

Matrix	Molecules of interest	Solvent	Method*	Ref.
Crotalaria L. Sessiliaflora	Vitexin, isovitexin and monocrotaline	Triton X-100	Microwave-assisted-SEE and CPS	[92]
Ardisia Japonica	Bergenin	Triton X-114	SEE-CPS	[93]
Spinach leaves	Chloropyll *a* and *b*	Brij 30, Brij98, Triton X-100, Triton X-114, $C_9-C_{11}EO_7$, $C_{12}-C_{15}EO_7$, $C_{11}-C_{13}EO_9$, Tween 20 and Tween 80	SEE-CPS	[76]
Chilli powder	Sudan Dye I, II, III and IV	Triton X-100	Ultrasound-assisted-SEE and CPS	[94]
Ginsen roots	Ginsennosides: Rg1, Re, Rb1, Rc, Rb2 and Rd	Triton X-100 and Triton X-114	Micellar extraction in X-100 and X-114 and cloud point concentration using X-100	[90]
Olive leaves	Polyphenols	Tween 80	SEE-CPS	[95]
Bidens tripartita	Various polyphenols	Tego Care CG 90, Sucrose Stearate, Triton X-100 and Rokanol B2	Ultrasound-assisted-SEE	[96]
Licorice root	Glycyrrhizic acid	Triton X-100	Ultrasound-assisted-SEE and CPS	[97]
Cortex fraxini	Aesculin and aesculetin	Genapol X-080	Ultrasound-assisted-SEE and CPS	[98]
Andrographis paniculata	Labdane diterpenoids	Triton X-100, Triton X-114 and Genapol X-080	Ultrasound/microwave-assisted-SEE and CPS	[91]
Cannabis resin	Δ^9-tetrahydrocannabinol	Dowfax 20B102	CPE	[22]

* SEE is often paired with ultrasound or microwave as means to enhance extraction yield. Ultrasound-assisted-extraction (UAE) and microwave-assisted-extraction (MAE) have been widely employed to recover bioactive compounds in organic solvents. They are labelled as "green" methods as they improves both the energy performance and solvent consumption of maceration.

A note on the terminologies of SEE-CPS

Herein, the terms "surfactant enhanced extraction" and "cloud point separation" are attributed to the solid-liquid extraction and the liquid-liquid separation steps respectively. Although sequential SEE-CPS has previously been performed on a variety of plant matrices, the current nomenclature is ambiguous as multiple terms are used to describe the method (figure 3.15). In addition, many of the authors reviewed in table 3.1 merge the extraction and separation into a single procedure, reporting a single yield. This emphasis on terminology is necessary as, from a process design perspective, SEE and CPS are two distinct operations which requires independent optimization.

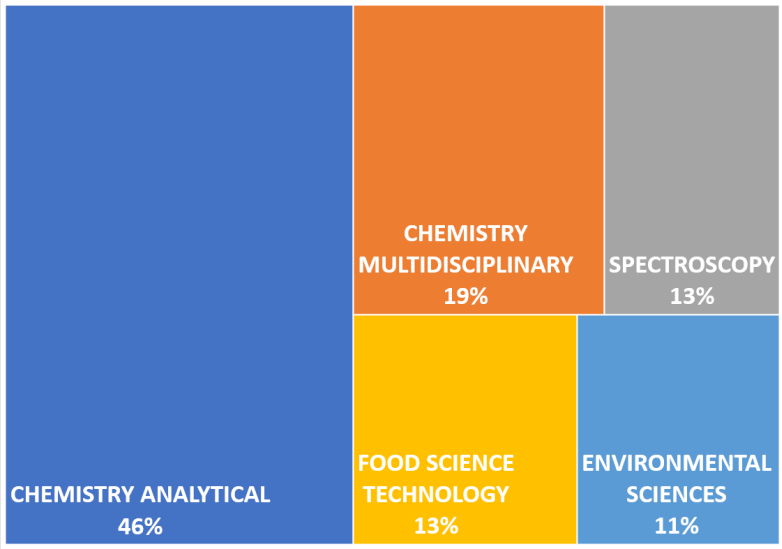

Figure 3.15 Treemap showing the Web of Science trends for cloud point extraction. The record distribution was obtained with the following search string: "micelle enhanced extraction" OR "micelle mediated extraction" OR "cloud point extraction" OR "cloud point concentration". In over 70 % of the publications, these terms are employed in fields relating to analytical chemistry or environmental sciences. In those instances, they refer to the CPE laboratory protocol described in section 3.3.1.

3.5 Analytical methods for cannabis extract

3.5.1 Reverse phase HPLC-UV

High performance liquid chromatography (HPLC) is a technique for the separation and quantification of individual species in liquid mixtures. The separation is achieved through affinity difference of each compounds towards a mobile and a stationnary phase. Samples injected

along with the mobile phase (eluant) are pumped through the stationary column consisting of packed solid adsorbents. The analytes interact by physical adsorption with the solid, causing them to exit the column at varying retention time. When the sample concentration is low, the adsorbed fraction proportionally correlates with the increase in concentration. Reverse phase columns, such as C18 columns, are composed of a non-polar stationary phase and through which flows a polar eluant. The retention time of each compound is in part affected by column temperature, pressure and flow rate [99].

Compounds exiting the columns are identified by a detector to generate explicit datam which generates a chromatograph . Several types of detectors exist, namely thermal conductivity detectors, flame ionization detectors and ultra-violet or visible light detectors. Peaks appear on the chromatograph ss the eluted compounds passes through the detector. The area under each peak and is proportional to the concentration of analyte within the sample. UV detectors, such as the one we employed, are the most common and practical detector available, with most organic substances adsorbing UV light between 200 nm to 350 nm [100].

The adsorption relies on the Beer-Lambert principle in which concentration (C) of a given compound is proportionally correlated with it's light absorbance (A) at a given wavelength, provided that the molar absorptivity of the specie (ϵ) and the optical path length (l) remain constant [101].

$$A = \epsilon l C \tag{3.9}$$

3.5.2 Folin-Ciocalteu assay

The Folin-Ciocalteu (FC) assay measures the polyphenolics composition of a mixtures and regularly performed on biological and food products for quality control in the food industry. Phenolics represent the main antioxidant agents in plant extracts. During the assay, they reduce the FC reagent which produces blue pigments proportional to the extract's reducing capacity [102, 103].

The assay is initiated by thoroughly mixing and homogenizing the FC reagent, a mixture of phosphomolybdic and phosphotungstic acids, with the sample. Concentrated aqueous sodium carbonate (Na_2CO_3) then bring the pH of the solution to 10. This initiate the electron transfer reaction causing the sample adopt a blue coloration over a period of up to 2 h. The color intensity, measured at 760 nm, is proportional to the concentration of phenolic antioxidants present in solution [104, 105]. Although the precise nature of the reaction is unknown, it is believed that in alkaline environments the phenol transitions to a phenolate

ion. It is then this anion which reduces the FC reagent [106].

3.5.3 Karl-Fisher assay

The Karl-Fisher (KF) assay measures water content in liquid and solid powder samples. The reagent comprises of a mixture of iodine, sulfate dioxide and pyridine (or another weak organic base) dissolved in methanol [107, 76]. In the presence of water, the reagent forms an intermediate alkyl sulfite salt which oxidizes iodine and consumes it at equal molar ratio with H_2O [107, 108].

$$I_2 + SO_2 + 3B + H_2O \longrightarrow 2(B, H^+, I^-) + BSO_3^-$$

This is followed by a Bunsen reaction which produces an alkyl sulfate salt and ionizable iodide.

$$BSO_3^- + ROH \longrightarrow (BH)SO_4R$$

The complete reaction mechanism hence becomes:

$$ROH + I_2 + SO_2 + 3B + H_2O \longrightarrow (BH)SO_4R + 2(B, H^+, I^-)$$

In this thesis, we employed an automated bipotentialmetric titrator. A pair of electrodes measured the the voltage in solution by maintaining a constant current while the reagent was precisely titrated by an inboard pump. As iodine is highly conductive, sudden drop in voltage indicated the present of excess iodine at which point the titration equivalence is reacged. A second pair of electrodes electrochemically converted the iodide ions back to iodine:

$$2I^- \longrightarrow I_2 + 2e$$

Iodide produced by 1 mg of H_2O require 10.173 C [109]. The water content can therefore be calculated from the current applied at the electrode.

CHAPTER 4 MATERIALS AND METHODS

4.1 Materials

4.1.1 Chemicals

Polyethylene oxide-type surfactants Tween 20, Tween 80 and Triton X-100 (>99 %) were purchased from Sigma-Aldrich and stored at 4 °C. Polytechnique Montreal's water system provided the deionized water. 1 mg mL^{-1} cannabinoid analytical standards (Sigma Aldrich) for δ_9-tetrahydrocannabinol (THC), cannabidiol (CBD) and cannabinol (CBN) were stored at −20 °C. Acetic acid (>99 %), HPLC grade methanol (Honeywell, >99 %), sodium dodecyl sulfate (ACS, >99 %) were also supplied by Sigma-Aldrich. A Milli-Q purification system (Millipore, Bedford, MA) provided ultra-pure water. Anhydrous Sodium sulfate, sodium carbonate sodium chloride (certified ACS) and Folin-Ciocalteu phenol reagent were obtained from Fisher Scientific (United States). HYDRANAL Composite 5 titrating agent (Honey-Well) and dry methanol used in the Karl-Fischer analysis were obtained from Sigma-Aldrich.

4.1.2 Cannabis

Cannabis L. sativa flowers buds were purchased from Société Québecoise du Cannabis dispensaries (Montreal, Canada). Per federal regulations, we were allowed to carry a maximum of 30 g of cannabis at a time. Hence, the cannabis material employed in the experiments were divided in multiple batches. Prior to experiments, each lot was decarboxylated, milled and characterized for THC and CBD content as well as particle size. THC and CBD contents are defined as the mass of cannabinoid per mass of dried cannabis. The preprocessing method is detailed below. Table 4.1 summarizes the properties of each batch of cannabis.

Table 4.1 Cannabis lots

Sample	Concentration, mg g^{-1}		Particle diameter, µm
	THC	CBD	
PM01	85 ± 2	n.d.	700
PM02	96 ± 6	45 ± 3	700
PM03	105 ± 1	63.5 ± 0.3	700
PM04	87 ± 4	13.4 ± 8	N/A

Additional information and calculations are shown in appendix F.
n.d, not detected; N/A, not available.

Figure 4.1 Cannabis preparation procedure

Decarboxylation

Whole cannabis inflorescence were placed in a hermetically sealed glass vessel and heated at 140 °C for 105 min. In a preliminary test, we demonstrated that acidic THCA and CBDA undergo complete decarboxylation under these conditions. Decarboxylation experiments, showing the evolution of neutral cannabinoid content in PM02, are presented section 6.1.

Milling

A commercial coffee grinder (SmartGrind, Black & Decker) ground the decarboxylated plant matter into a resinous powder with mean diameter between 300 and 900 mm. When specific diameters were desired, the cannabis was subjected to multiple milling cycles and measurements were performed between each cycle until the appropriate size was obtained.

Quantification initial of cannabinoid content

THC and CBD concentrations were obtained by three subsequent methanol extractions of the milled cannabis at room temperature. Following the first two extractions, the solid plant residues were recovered, dried and extracted anew in fresh methanol. Cannabinoid content of all three extracts were summed and divided by the weight of starting material to provide its normalized cannabinoid content.

Particle size measurement

A laser diffractometer (LA-950, Horiba) measured the powder's mean diameter in distilled water. The Mie algorithm refractive indexes were set at 1.4 and 1.333 for the cannabis material and water, respectively (appendix F).

4.2 SEE screening tests

Prior to the single factor of SEE, we performed screening test in order to identify a suitable surfactant. Extraction experiments were conducted with three nonionic surfactants: Tween 20, Tween 80 and Triton X-100. Their properties are summarized in table 4.2. These surfactants are commercially available and have been previously employed for SEE-CPS in the literature [76, 91, 95]. We prepared 40 g solutions containing 1 % (w/w) of each surfactant in a 50 mL Erlenmeyer flask. 0.4 g of cannabis was then directly added to the flask and mixed with a magnetic stirrer at 900 rpm. Extraction occured at room temperature for 40 min. In addition to the surfactant solution, cannabis was also extracted in distilled water and 95 % (v/v) ethanol-water. Table 4.3 outlines the screening conditions. Concentration of THC and total phenolic content were obtained by HPLC and FC assay, respectively.

Table 4.2 Properties of nonionic surfactant employed in the screening tests

Surfactant	M, g/mol	CPT, °C	HLB	w_{H_2O}, wt.%	CMC, mM	CMC, wt %
Tween 20	1227	93.0 ± 0.1	16.7	2.61 ± 0.02	0.059	0.0007
Tween 80	1310	85.3 ± 0.1	15	2.69 ± 0.01	0.012	0.0015
Triton X-100	647	65.15 ± 0.07	13.5	0.17 ± 0.02	0.22	0.014

We followed ASTM method D2024 [110] to characterize CPT of surfactants ($n = 2$). Karl-Fisher titration quantified water content (w_{H_2O}, $n = 2$). Molecular weight (M), hydrophilic-lipophilic balance (HLB) and critical micellar concentrations (CMC) were obtained from the manufacturer's data sheets.

Table 4.3 Screening parameters

Solvents	Concentration	m_{sol}, g	m_{pm}, g	T, °C	t, min	Stir rate, rpm
Tween 20 Tween 80 Triton X100	1 % w/w in H_2O	40	0.4*	21	40	900
EtOH	95 % v/v in H_2O					
H_2O	-					

* Solid to liquid ratio ($R_{S/L}$) of 1:100

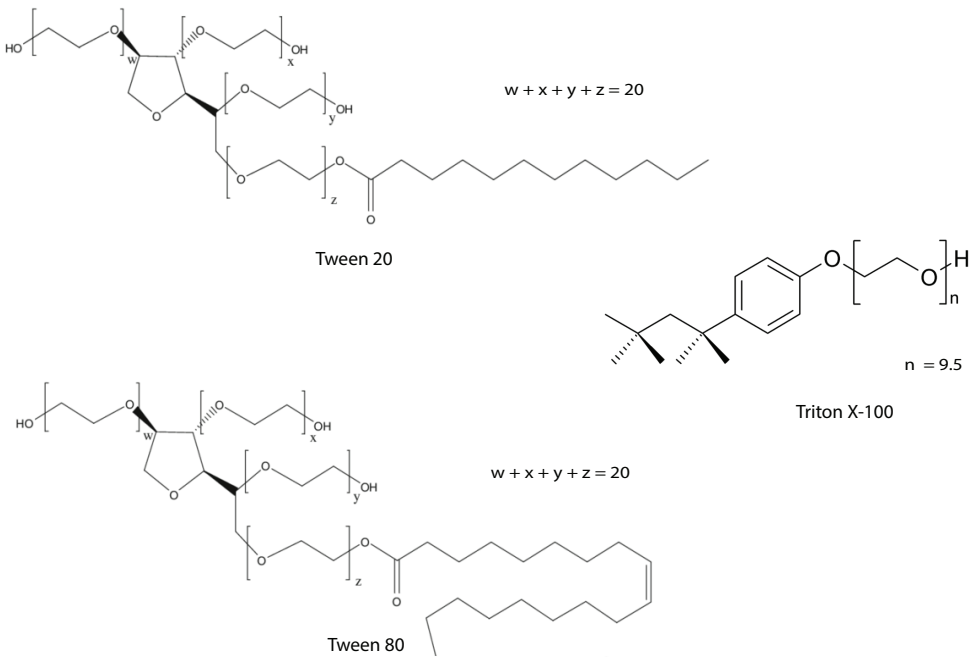

Figure 4.2 Molecular structure of the nonionic surfactants used in this work

4.3 Single variable optimization of surfactant enhanced extraction

4.3.1 Choice of surfactant

We selected Triton X-100 for single factor optimization based on the higher extraction yield obtained during screening. In addition, its CPT of 65 °C enabled easy laboratory manipulations.

4.3.2 Surfactant enhanced extraction protocol

The detailed SEE procedure is presented in figure 4.3. Our extraction protocol employed 30 g of water-surfactant solution to extract 0.3 g of milled cannabis. We gravimetrically prepared the solvent by accurately weighing (within 1×10^{-4} g) the appropriate amounts of Triton X-100 and deionized water in a 50 mL Erlenmyer flask. The flask simultaneously served as the extraction vessel. Its content was temperature equilibrated in a thermostatic bath (B-491, Buchi) for 30 min prior to incorporating the cannabis. During experiments, an Orion stirrer probe (ThermoFisher), homogenized the mixture. The stirrer was placed slightly above the bottom of the flask. Its rotation was set at the lowest speed of 1 (on a scale of 5). The stirrer was equipped with a hollowed rubber stopper to prevent evaporation at higher temperatures.

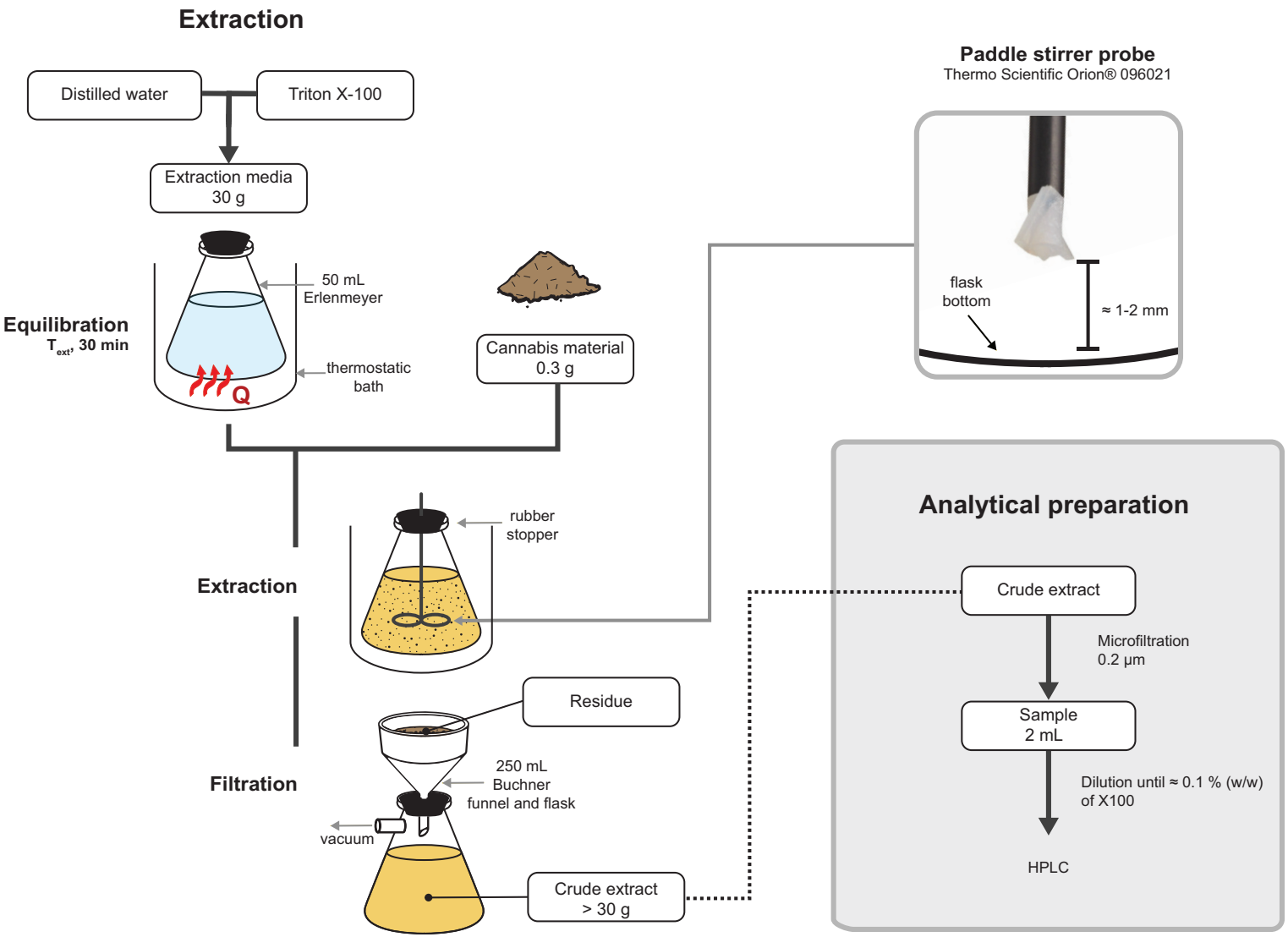

Figure 4.3 Laboratory flowchart for surfactant enhanced extraction

Following extraction, the cannabis residues were removed by vaccum filtration over Grade 1 qualitative filter paper (11 µm pore size; Whatman). A 2 mL portion of the crude extract was then further purified through a sterile, 0.2 µm, polyethylene sulfone syringe filter (Corning). The resulting solution was stored at 4 °C prior to analysis.

4.3.3 Operating conditions

Table 4.4 provides an overview of the experimental design. We studied the following independent SEE variables: time, surfactant concentration, temperature, solid to liquid ratio and particle size. Cannabis lots were assigned to each variable according to the number of expected experiments. To offset the variation in THC within each lot and to provide a basis for comparison between sets of experiments, control conditions were defined. For each variable, a duplicate extraction performed under those conditions. With the exception of the studied variables, all other variables were maintained at their control value.

Table 4.4 Single factor experimental summary

Independent variable	Range	Control values	Cannabis lot
Time (t)	0 up to 105 min	40 min[a]	PM01 and PM03
X100 concentration (w_{x100})	0 to 3.75 %	1 %[b]	PM02
Temperature (T)	25 to 85 °C	21 °C	PM02
Particle size (D_p)	300 to 700 µm	700 µm	PM01
Solid to liquid ratio ($R_{S/L}$)	1:75 to 1:370	1:370 [b]	PM01

4.3.4 Result analysis

Following extraction, the THC, CBD and X100 concentrations were obtained by the HPLC method presented in section 4.5. The extraction yield was determined for THC (and when available for CBD). Yields were calculated according to the total mass of cannabinoid present in the extract divided by the mass of biomass:

$$\text{Yield} = \frac{\text{mass of cannabinoid in the extract}}{\text{mass of cannabis}} \tag{4.1}$$

Yield is converted in percentage by dividing with the cannabinoid content of the initial biomass (table F.1).

$$\text{Percentage yield} = \frac{\text{yield}}{\text{cannabinoid concentration of the lot}} * 100\% \tag{4.2}$$

Example of calculation are presented in appendix B.

Kinetic regression

Kinetic models are useful tools in process design and provide a quantitative measurement of performance. Hence, the time variable was also studied by regression of the data to a kinetic mass transfer model. For solid-liquid extractions, mass transfer is limited by diffusion rate at the interface [111] and can be represented by the following first-degree model:

$$Y_j = Y_j^{eq} * (1 - e^{-k_{c,j}\, t}) \tag{4.3}$$

Where, Y_j is the concentration yield of compound j (either THC or CBD) in the liquid phase at time t, $k_{c,j}$ is the mass transfer coefficient, and Y_j^{eq} equilibrium concentration of j at equilibrium time t_∞. SigmaPlot 14 software (Systat Sofware Inc., United States) computed the model parameters $k_{c,j}$ and Y_j^{eq} from non-linear regression of the data.

4.4 Cloud point separation

4.4.1 Choice of operating conditions

Inorganic salt content of the extract was studied during CPS experiments. Given the instruments available and the limited quantities of samples, it was the only quantitative variable which could be reproduced accurately. For CPS, the ionic specie selected is sodium sulphate (Na_2SO_4) which was incorporated to the SEE extracts. Na_2SO_4 has been widely applied to liquid-liquid CPE experiments in the literature. The compound is generally regarded as safe and used as additive in food dye [112].

4.4.2 Protocol

CPS was performed at Na_2SO_4 concentrations ranging from 0 % to 4 % with a 1 % between levels. For each level, we prepared 14 g solutions by accurately measuring the required weights of Na_2SO_4 and extract in a 15 mL centrifuge tube. The solution were then homogenized by vortex and brought above their cloud point temperature in a thermostatic bath. The tubes were submerged in the bath for 15 min where clouding occurred at 95 °C. We then removed the samples from the bath and rapidly introduced them into the centrifuge. A Sigma 2-7

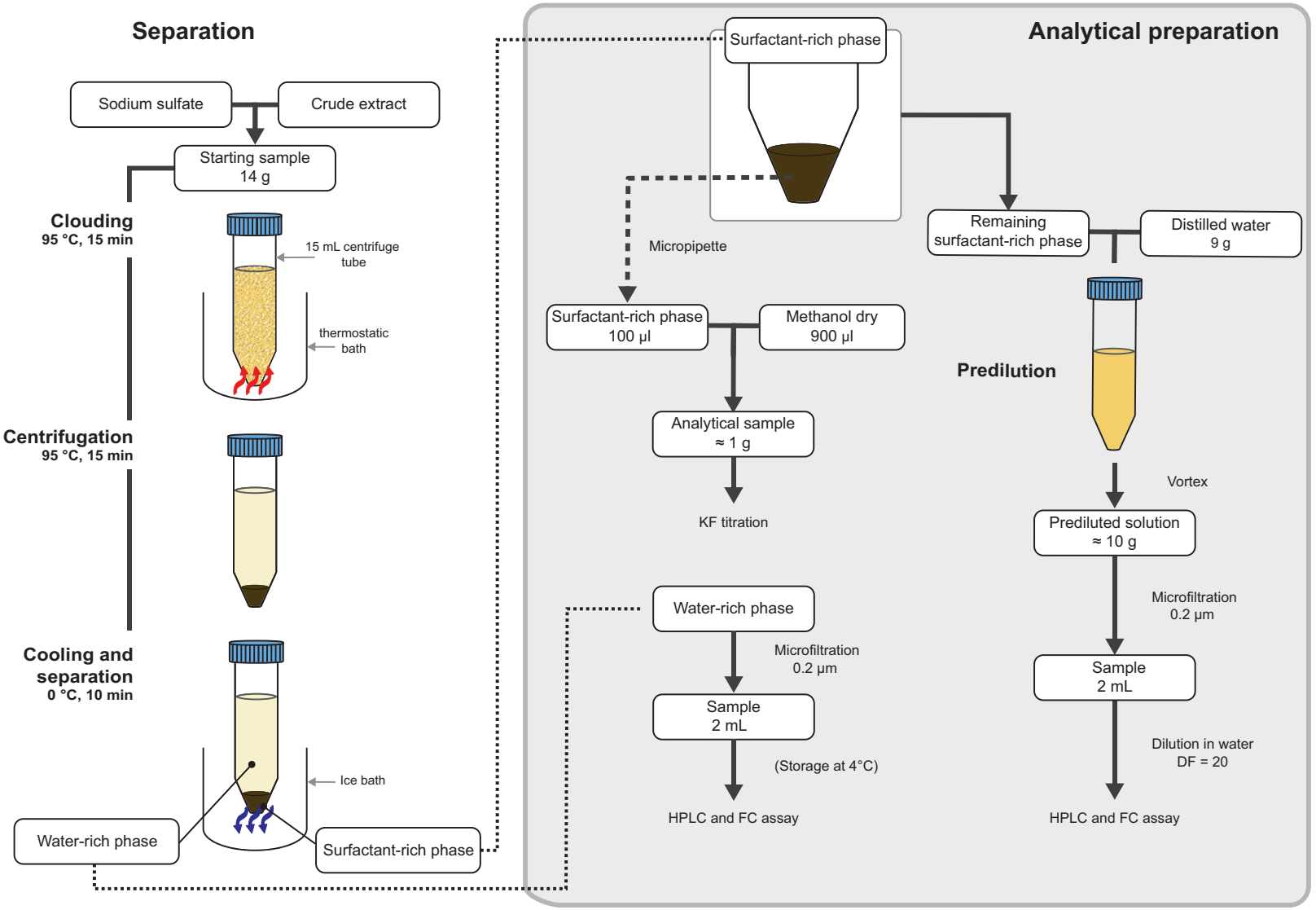

Figure 4.4 Laboratory flowchart for cloud point separation

centrifuge (Sigma, Germany) equipped with swinging bucket rotors separated the aqueous phase from the surfactant-rich phase at 4000 rpm (2540 x g) for 1 min. Following centrifugation, the tubes were placed in an ice bath for 10 min and cooled to approximately 5 °C. This procedure reduced the surfactant's viscosity, thereby facilitating physical separation of the two phases. The top water phase was then removed from the tube by careful pouring, taking particular care not to induce remixing of the phases. The water-rich was immediately filtered in a 0.2 µm syringe filtered and both phases stored at 4 °C prior to analysis. Figure 4.3 details the complete CPS procedure.

4.4.3 Result analysis

Following the clouding procedure, concentrations of THC, CBD, TPC and X100 in the surfactant-rich phases were obtained by HPLC and FC assay. We then computed the weight fractions in both phases through mass balance. The calculation method is detailed in appendix E. Water weight fraction of the surfactant-coacervate was obtained by Karl-Fisher titration described in section 4.5.4.

The results were discussed by analyzing trends in concentration factor(Fmc_j) and recovery (X_j). The concentration factor is defined as the weight fraction of each specie j (THC, CBD, TPC and X100) in the coacervate divided by their weight fraction within the crude extract:

$$\text{Concentration factor} = \frac{\text{weight fraction of } j \text{ in the surfactant-rich phase}}{\text{weight fraction of } j \text{ in the crude extract}} \tag{4.4}$$

The recovery is defined as the percentage of specie j remaining in coacervate relative to its total initial mass within the crude extract.

$$\text{Recovery} = \frac{\text{mass of } j \text{ in the surfactant-rich phase}}{\text{mass of } j \text{ in the crude extract}} \times 100\,\% \tag{4.5}$$

Experiments were duplicated and the results are presented as their means along with their standard deviation (±SD). Each compound were also quantified in the water-rich phase to check for mass balance. Mass balance for all of our samples closed within 1 % error, indicating good reproducibility.

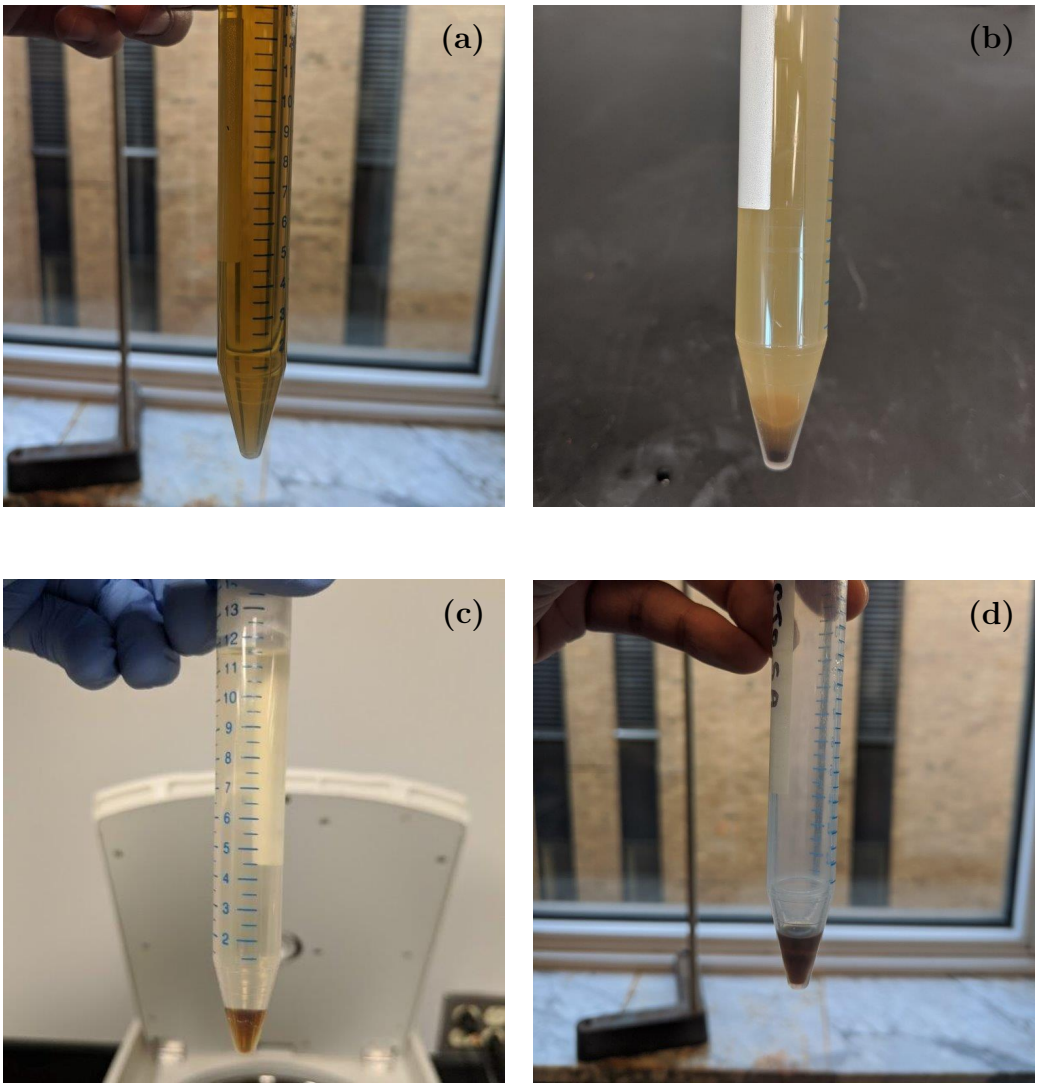

Figure 4.5 Cloud point separation steps. **(a)** Initial sample. **(b)** Samples after 15 min equilibration at 95 °C. Separation occurs by sedimentation. The coacervate transitions from turbid (top) to translucent (bottom) corresponding to a suspended and a continuous surfactant phase, respectively. **(c)** Samples after centrifugation. The increased hydrostatic pressure causes the surfactant phase to coalesce, resulting in a defined separation line. **(d)** Sample after removal of the aqueous phase.

4.5 Analytical methods

4.5.1 High performance liquid chromatography-ultraviolet

HPLC-UV obtained the content of THC, CBD and X100 within samples. The method, developed internally, was able to quantify the concentration all three compounds in a single

injection (some details on method development are presented in appendix B).

System and elution parameters

The HPLC-UV system (Prostar series, Varian, United States) consisted of an auto sampler (model 410), a piston pump module (model 215), a column oven and a single diode UV detector (model 325) . It was coupled with a Microsorb MV 100-4 C18 column (250 mm x 4.6 mm, Agilent Technologies, US).

The mobile phase consisted of CH3OH:H2O:CH3COOH (volume ratio of 85:14.2:0.8) and was isocratically eluted at a column temperature of 28 °C. 20 µL of analytical samples were injected at a flow rate of 0.8 mL min^{-1} and a detection wavelengths of 235 µm. The Varian ProStar 6.41 Workstation software performed data acquisition, chromatogram generation and peak area integration.

Sample preparation

Prior to injection, we diluted each sample in ultra-pure Milli-Q water to obtain a solution containing approximately 1 mg mL^{-1} of X100. For SEE samples, the appropriate dilution factor (DF) was determined base on the concentration of the pure X100 solution. In standard experiments, the extraction media contained 1 % (w/w) in surfactant and therefore was diluted by a factor of 10 ($\rho_{X100} \approx \rho_{H_2O}$). For CPS, the more concentrated surfactant phase was first thinned down by adding 9 g of Milli-Q water to the centrifuge tube. Prior to HPLC injection, the samples were filtered and diluted a second time to meet the instrument's detection range. The dilution factor (DF) is defined by the following equation.

$$C_{ext} = DF \times C_{dil} \tag{4.6}$$

Where DF is the dilution factor. C_{ext} and C_{dil} are the concentrations of the initial and the diluted samples, respectively. The analytical preparation procedure for SEE and CPS are also presented by the flowcharts in figure 4.3 and in figure 4.4.

Data processing

Prior to each set of analysis, we injected standard solutions of known concentrations in THC, CBD and X100. Calibration lines, correlating concentration to UV absorbance, were then traced. The calibration is described by :

$$A = \alpha\, C + \beta \tag{4.7}$$

Where α and β are the linear regression coefficient corresponding to the slope and the mathematical intercept, respectively. A is the absorbance of the sample, corresponding to the area under the curve of the chromatograph, in absorbance unit (AU). In equation (4.7), C is the concentration in the diluted extract. The concentration of the extract is obtained with the dilution factor of equation (4.6). Therefore:

$$C_{ext} = \frac{A - \beta}{\alpha} \times DF \tag{4.8}$$

Examples of calibration curves and calculations are presented in appendix B.

4.5.2 Scanning electron microscopy

A Hitachi S4100 field emission gun scanning electron microscope (FEG-SEM) captured the morphology of the cannabis leaves prior and post extraction at an acceleration voltage of 5.0 kV. A plasma sputter first gold coated the samples to increase electrical conductivity and provide images with enhanced contrast.

4.5.3 Total polyhenolic quantification

Total polyphenolic content (TPC) of fruits and vegetables is strongly correlated with their health benefits and antioxidant activity. As such, it has been systematically measured on a variety of biomass extract as an indicator of extraction performance. The anti-oxidant activity of these mixtures may be traced to a wide range of polyphenolics including flavonoids, anthocyanin and catechin which are co-extracted with the cannabinoids during SEE [104, 113, 114]. Pertaining to SEE in the present study, TPC quantifies the co-extraction's extend and provides a basis for solvent performance comparison. During CPS, TPC provides an indicator of cannabinoid partitioning of relative to the co-extracted biocompounds.

We applied the Folin-Ciocalteu (FC) assay for total polyphenolic content (TPC) quantification. The assay employed 2.5 µL aliquots of extract samples which were first mixed with 50 µL of sodium dodecyl sulfate (SDS) in a well micro-plate. The mixture then equilibrated for 2 min with 12.5 µL of Folin-Ciocalteu reagent. 50 µL of aqueous sodium carbonate 10 % weight then brought the pH to 10. Distilled water corrected the final within each well volume to 200 µL. The solution was shielded from light for 1 h for color development and it absorbance measured at 760 nm. We opted for Gallic acid as calibration standard to provide

numerical comparison.

FC method was adapted from Bindes et al. [104] Direct application of standard method to a surfactant extract was not possible as it resulted in the formation of precipitate. This likely occurred due to the salting-out of the surfactant bsodium carbonate at high concentrations. Herein, the procedure was modified by incorporating anionic SDS to counter precipitation. Details and validations are presented in (appendix C).

4.5.4 Water content quantification

We employed Karl-Fisher (KF) titration to determine water weight fractions in our samples. This procedure was only applied to the surfactant-rich phase obtained by CPS. A portion of was sampled from the centrifuge tube and mixed to dry methanol with known water mass fraction. We combined 900 mg of the alchohol with 100 mg of surfactant-rich phase. An automated V20S volumetric KF titrator (Mettler Todelo, United States) then determined water content of the mixture and H_2O mass fraction in the coacervate were computed by mass balance. For each extract, the analysis was performed in duplicate and the results reported as the average with the standard deviation ($\pm$ SD).

CHAPTER 5 RESULTS AND DISCUSSION

5.1 Screening tests

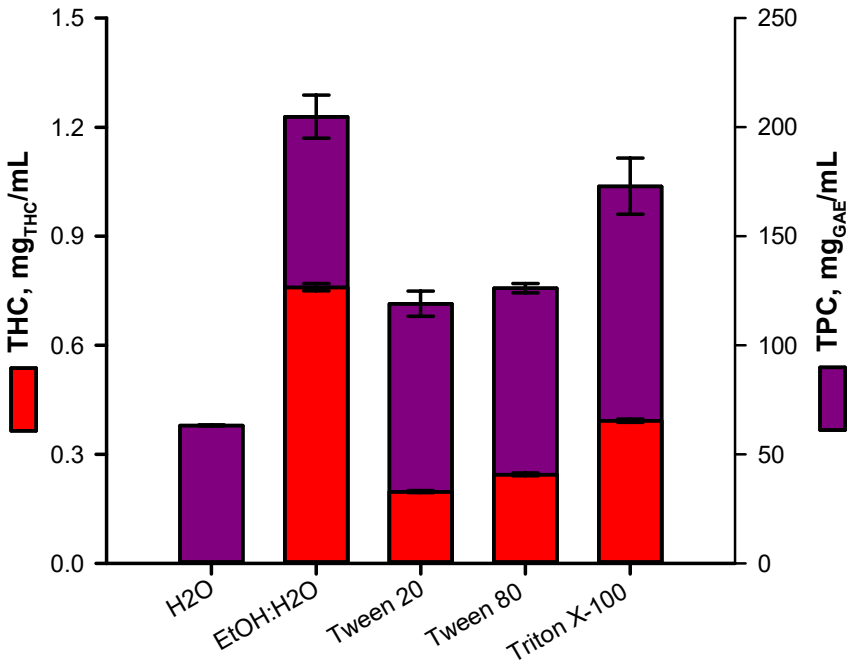

Figure 5.1 THC and TPC concentrations in *Cannabis L. Sativa* extracts obtained from water, ethanol and aqueous solutions of 1 % weight in Tween 20, Tween 80 and Triton X-100 (PM02; $R_{S/L}$ 1:100 ; 40 mL of solvent; t = 40 min; T = 21 °C; 900 rpm).

The highest concentration in THC was obtained with the ethanolic solvent. At 0.76 ± 0.01 mg mL^{-1}, ethanol yielded an extract at least twice as concentrated as the surfactant solutions. Of the three nonionic surfactants tested, X100 achieved the highest THC concentration of 0.3922 ± 0.0004 mg mL^{-1} whereas Tween 20 and Tween 80 extracted 0.197 ± 0.003 mg mL^{-1} and 0.245 ± 0.004 mg mL^{-1}, respectively. Detergents featuring an HLB value between 13 and 15, a balance which organic matter are best removed from surfaces. At 13.5, X100 exhibits the lowest HLB. Comparatively, Tween 20 and 80's HLBs respectively rank at 16.7 and 15. This correlation between surfactant hydrophobicity and SEE yield is in agreement with

studies on SEE of spinach where non-ionic surfactants with HLB values between 12 and 14 significantly out performed those outside that range during chlorophyll extraction [76].

Concerning the TPC, the solvent with the highest THC extraction ability also recovered the highest amount of polyphenolics. In our experiments, THC was not detected in the water extract. However, some polyphenolics compounds were present in the solution, which can be associated to the extraction of water-soluble plants metabolites. This demonstrates that the presence of surfactants and, more specifically, the presence of micelles is necessary for recovery of cannabinoids, as they otherwise do not dissolve in water alone.

5.2 Single factor experiments

5.2.1 Effect of time on the extraction of THC and CBD

Time experiments were performed from 0 min to 60 min on a cannabis strain containing a 2:1 ratio in THC to CBD (lot PM03). The results regressed to a first order diffusion kinetic and results are presented in table 5.1.

The model match our experimental data with $R^2 > 0.979$. Here, the diffusion rate coefficient, $k_{c,j}$, reflects the affinity of the surfactant solvent towards the target molecules: the cannabinoid with the highest coefficient is extracted faster. The identical rates obtained for THC and CBD ($k_{c,THC} \approx k_{c,CBD} \approx 0.09$) indicate that the X100 solution equally extracts both compounds. In fact, with respect to the predicted equilibrium yield (Y_j^{eq}), THC:CBD ratio within the extract is identical to that in PM03. This comes in contrast with previous studies, which reported targeted extraction of CBD over THC in formulations of ionic surfactants [115]. In subsequent tests, SEE yields did not deviate from this behavior, even when temperature or surfactant concentration were increased. Hence, for the sake of brevity THC yields are exclusively reported in the subsequent sections.

With respect to the predicted THC yield of $30 \pm 1\,\mathrm{mg\,g^{-1}}$, it accounts for less then 30 % of the starting material's total content and indicates an incomplete extraction for periods under 60 min. Hence, range of the time variable was extended in further experiments.

Table 5.1 THC and CBD regression parameters

	$Y_j^{eq}, \mathrm{mg\,mL^{-1}}$	$k_{c,j}, \mathrm{min^{-1}}$	R^2
THC	30 ± 1	0.09 ± 0.01	0.979
CBD	15.6 ± 0.6	0.088 ± 0.009	0.982

Errors represent the standard errors of the estimate

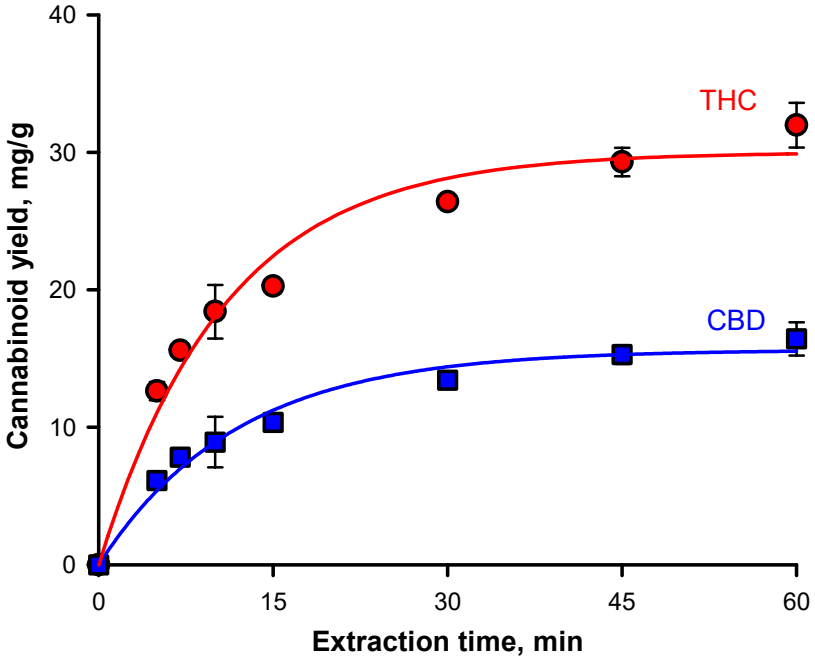

Figure 5.2 SEE kinetic of cannabis containing both THC and CBD. The solid lines represent the regression models. (PM03; 1051 mg g^{-1} in THC; 1 % weight X-100; $R_{S/L}$ = 1:100; t = 0 min to 60 min; T = 21 °C; $n = 2$).

Extraction by Triton X-100 and ethanol

SEE was further studied from 0 min to 105 min with starting cannabis PM02 (96 ± 6 mg g^{-1} in THC). To compare the performance of the proposed surfactant enhanced process with traditional organic solvent extractions (OSE), ethanol was chosen as benchmark solvent (figure 5.3).

Extraction behavior of the two solvent significantly differed. With respect to the regression constants (presented in table 5.2), ethanol exhibited a better fitting to a first order kinetic model and exhibited a rate constant ($k_{c,j}$) four times that of SEE. THC extraction in ethanol was nearly complete and yields increased exponentially in the first 30 min, reaching a maximum of 77.6 ± 0.5 mg g^{-1}. The latter represents an 80 % recovery with respect to PM02, after which no significant variations were observed ($p<0.05$).

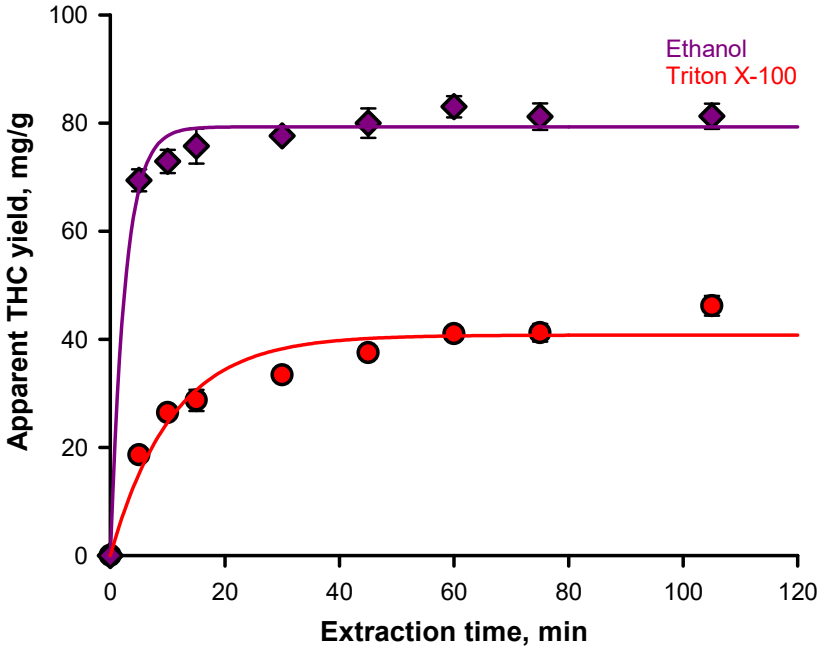

Figure 5.3 Effect of time on extraction yield (PM01; 852 mg g^{-1} in THC; 1 % weight X-100; $R_{S/L} = 0.01$; t = 0 min to 105 min; T = 25 °C; $n = 2$).

In contrast, SEE kinetics appeared to be governed by two compounded rates. The surfactant media produces an initial uptake in THC up to 30 min, where the yield is 33.4 ± 0.5 mg g^{-1}. Beyond, although rates are reduced, extraction continues, linearly increasing with time. Towards, 60 min, the experimental data points intersect with the horizontal regression line. By the end of the experiment, SEE appears not to have reach equilibrium and yielded 46 ± 2 mg g^{-1} of THC.

The reduced yield and the apparent two-stepped extraction results from the seclusion of cannabinoids within the trichomes. In the following section, to demonstrate the role of trichomes during processing, we closely examine the surface morphology of cannabis residues.

Table 5.2 Ethanol and SEE regression parameters for THC

Solvent	Y^{eq}_{THC}, mg mL^{-1}	$k_{c,j}$, min^{-1}	R^2
Ethanol 95 %(v/v)	79 ± 1	0.39 ± 0.05	0.989
Triton X-100 1 %(w/w)	41 ± 2	0.09 ± 0.02	0.951

Scanning electron microscopy of cannabis residues

Scanning electron microscopy (SEM) provides an interesting perspective into the mechanism of action of ethanol and X100 on the ground cannabis. Figure 5.4a is representative of the untreated cannabis material prior to decarboxylation and milling. The characteristic bulb and stem structures of the trichomes can be observed. Relative to the ligno-cellulosic leaves on which they erect, glandular trichomes possess little resistance to mechanical stress. Their brittleness is exploited in the preparation of cannabis resin, where plant matter are vigorously sieved. The glands detach due to impact between leaves particles and are separated by the mesh [116]. The effect of mechanical procedures on glandular trichomes has also been reported in hemp fiber processes, where contact with ruptured vesicles causes the accumulation of THC and CBD on non-cannabinoid producing plant organs [7, 117]. The preparation methods we employed, milling in particular, causes the trichomes to break. As a results, the starting material employed for extraction exhibits uneven and rough surfaces (shown in figure 5.4b). Following, extraction, the residues obtained by ethanol maceration displays smooth surfaces (figure 5.4c), whereas SEE extracted cannabis, in figure 5.4d retains the rugosity of the starting material. In fact, intact trichomes structures can be identified.

These images provide basis to SEE's relatively poor yield and two-stepped kinetic behavior. Ethanol's high solvent power readily dissolve the trichomial waxes. However, cannabinoids available for SEE is split into two fraction: a surface fraction, either spread across the plant particles or present within ruptured trichomes, and a more difficult to access trichome-contained fraction.

With respect to the results presented in figure 5.3, upon introducing the cannabis in the liquid, X100 captures and emulsifies the surface oil fraction, causing an initial yield spike. Extraction rate then diminishes as the peripheral oils depletes. The more gradual yield increase observed above 30 min in figure 5.3 may be linked to the disintegration of the trichomes or to the extraction of remaining surface cannabinoid fraction: cannabinoids not immediately present at the water-oil interface, which only becomes available after the surrounding oil layers are dissolved.

5.2.2 Effect of surfactant concentration and solid to liquid ratio

When mass fraction of Triton X-100 was increased, yield improvement was most important between 0.1 % and 0.3 %. Although relatively low, these concentrations and represents 10 and 20 times that of the X100's CMC, respectively and indicates that the presence of micelles are required for extraction to occur. With regards to the mechanisms of detergency, our results

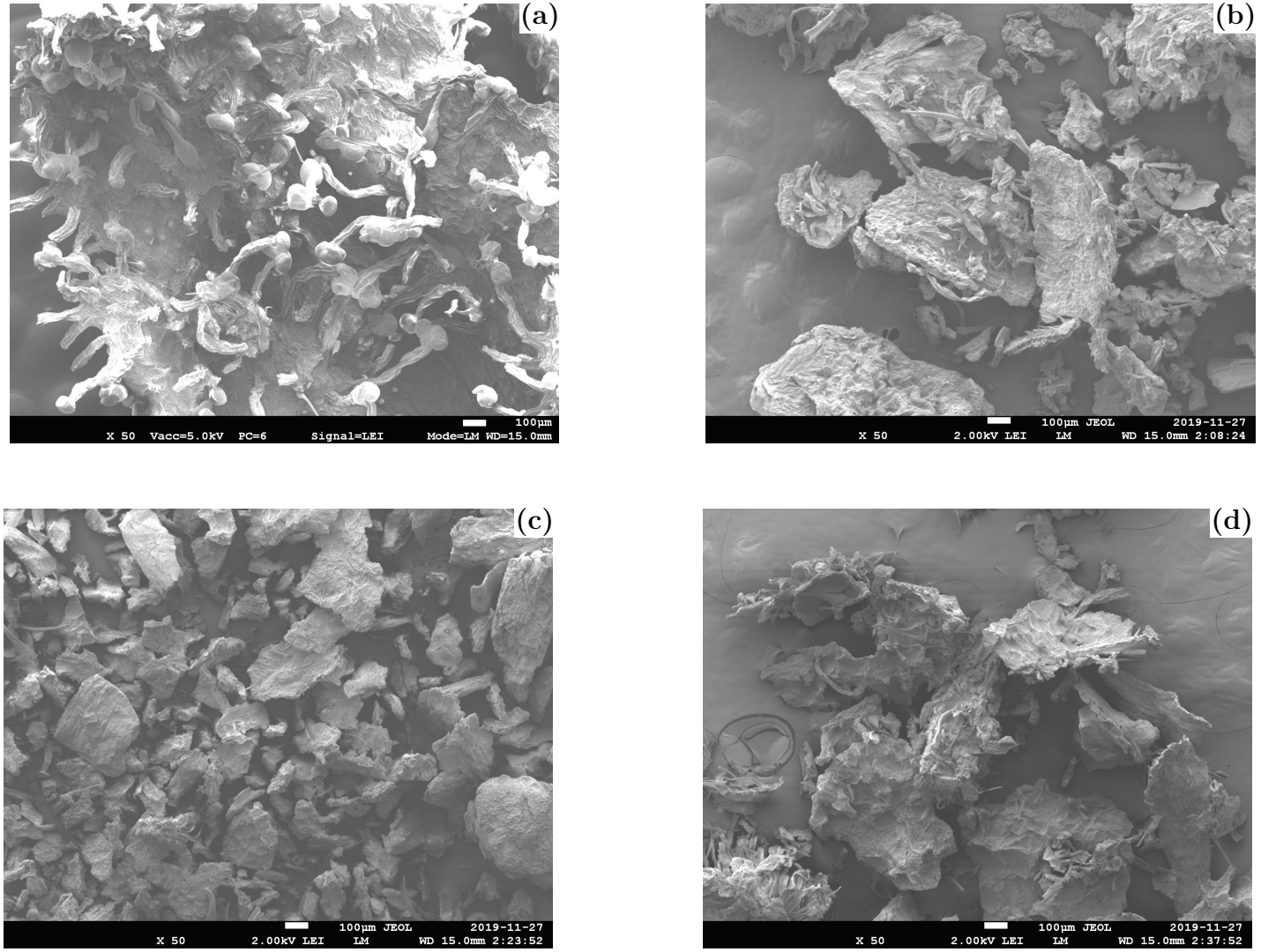

Figure 5.4 Scanning electron micrographs of various cannabis sample. **(a)**, leaves surface of the initial material obtained from the SQDC dispensary. **(b)**, particles following decarboxylation and milling. **(c)**, residue of ethanolic maceration. **(d)**, residues of SEE in 2.6 % X100 by weight ($R_{S/L}$ = 1:100; t = 68 min; T = 45 °C).

indicates that THC extraction occurs through micelle solubilization. Unlike roll-up, for which detergency is dictated by the interfacial tensions between the leaves' surface, oils and water, solubilization is directly proportional to the amount of micelles available to encapsulate the lipids.

With respect to our hypothesis on the mechanical rupture of the trichomes, it appears that, even at high X100 concentrations, extraction remains limited to the superficial fraction of cannabinoids, as additional surfactants do not provide improved detersive action towards breaking down the trichomes. The maximum yield obtained at 3.75 % is $48 \pm 2\,\mathrm{mg\,g^{-1}}$ and, again, represents 50 % of PM02's total THC content. Microscope analysis of the residues obtained with 1 % and 2.6 % in X100 did not show structural differences. Cuticular waxes surrounding the trichomes are composed of $C_{32}{}^{+}$ straight aliphatic chains. They possess reduced solubility in micelles and difficultly incorporates into surfactant films [82]. Although this limits SEE yields, it indicates that nonionic surfactants selectively target cannabinoids over the hydrocarbon chains.

5.2.3 Effect of Temperature

Temperatures from 25 °C to 45 °C corresponded to a linear increase in THC yield. Optimal recovery of $49 \pm 4\,\mathrm{mg\,g^{-1}}$ arises at 65 °C, the cloud point pure Triton X-100 (CPT = 65 °C). Beyond this point, temperature negatively affects the yield and a temperature of 85 °C extracted only $25 \pm 5\,\mathrm{mg\,g^{-1}}$ in THC. This result is counterintuitive, as in standard extractive processes heat improves the diffusion rate leading to superior yields. Despite being true for the SEE process, this only applies for conditions up CPT. Such effect has not been reported in previous SEE of plant matter and was further investigated by analyzing residual X100 content in the extract.

5.2.4 Analysis of residual surfactant content

We improved of our initial HPLC-UV method to include the quantification of residual X100 concentration (C_{X100}^{ext}). The final method has already been presented in the analytical part of section 4.5. The samples were reanalyzed and the residual X100 concentrations are presented as yellow triangles in figure 5.6. Examples of chromatograms can be found in appendix B.

Temperature experiments were conducted with an extraction media containing 1 % (w/w) in X100 or approximately $10\,\mathrm{mg\,mL^{-1}}$%. A reduction in residual surfactant (C_{X100}^{ext}) is expected due to adsorption. This is observed From 25 °C to 55 °C, where C_{X100}^{ext} remains constant and averages $8.1\,\mathrm{mg\,mL^{-1}}$. However, from 65 °C to 75 °C, X100 content of the extract drops

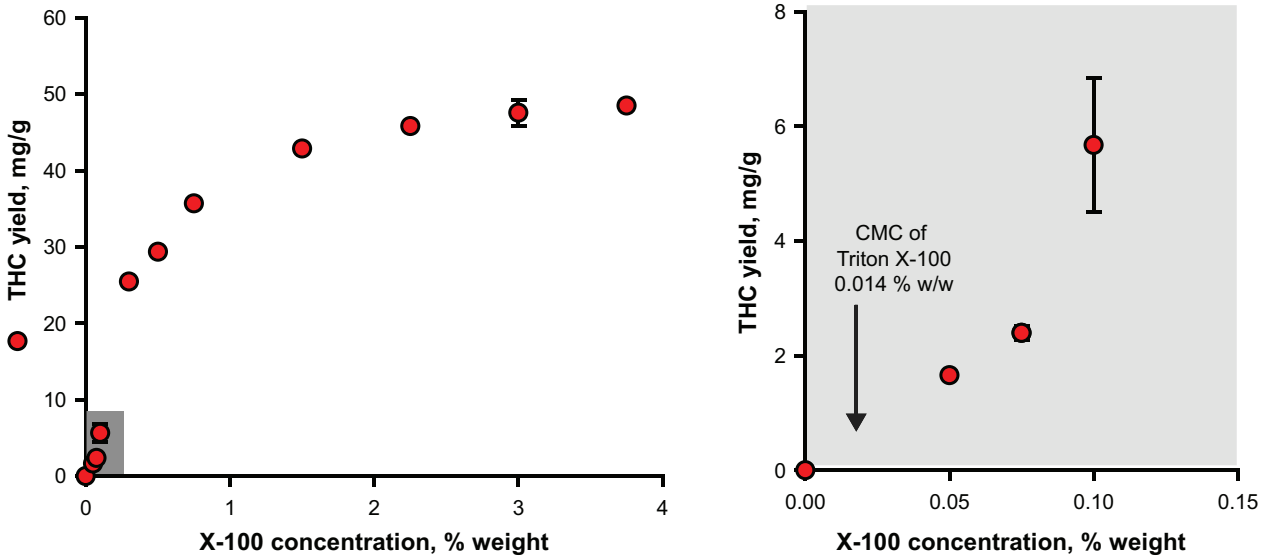

Figure 5.5 Effect of surfactant concentration on extraction yield. The figure on the right represents an enlargement of the gray gray rectangle within the left hand-side diagram. Error bar are presented when available (PM02; 966 mg g^{-1} in THC; 0 % to 3.75 % weight X-100; $R_{S/L}$ = 1:100; t = 40 min; T = 21 °C; $n \geq 1$).

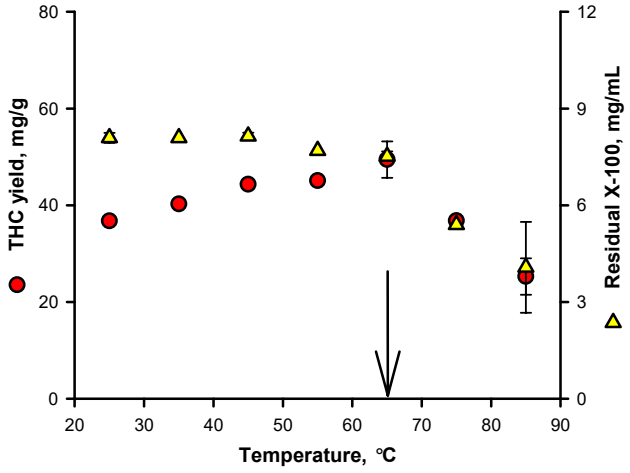

Figure 5.6 Effect of temperature on THC yield and residual surfactant concentration during extraction (PM02; 96 ± 6 mg g^{-1} in THC; 1 % by weight Triton X-100; $R_{S/L}$ = 1:100; t = 40 min; $n \geq 1$). The vertical arrows indicate the cloud point temperature of the pure X100 solution.

to 5.4 mg mL^{-1}, likely lost due to clouding. This result is in agreement with laboratory observations, where we discerned surfactant adhesion onto the cannabis particles at higher temperatures. Cannabis residues extracted below the CPT, easily dispersed upon pouring onto the filter paper. In contrast, those obtained above the cloud point agglomerated and exhibited a paste-like consistency, indicating that the clouded surfactants likely act as binder, coating the cannabis and causing it to flocculate [118]. We believe that the isotropic clouded surfactant phase initially present in the extraction media coalesce onto the cannabis residues, which then act as nucleation sites on which the mesophase accumulates. During filtration, when the cannabis is separated from the extraction, the clouded phase remains adhered to the biomass, thus retaining any extracted cannabinoids within its micelles. The reduction in THC yield above 65 °C can hence be associated to a depletion of the active micelles in solution. Such coalescence likely occurs through non polar interactions between micelles clusters and aliphatic compounds on the cannabis' surface, becoming more pronounced at higher temperatures where the polyoxyethylene heads of surfactants are most hydrophobic.

5.2.5 Effect of post-extraction cooling

Given the reversible nature of the clouded phase, we hypothesized that the surface-aggregated phase could be redissolved into the aqueous bulk by cooling the system below its CPT prior to filtration. We tested this hypothesis by introducing an additional cooling step to the protocol. The cooling was applied to an extraction at 65 °C in a new set of experiments (extraction time was reduced to 30 min). 5 min before the extraction time elapsed, the flask was transferred from the thermostatic bath to an ice bath where the extraction pursued without agitation. Figure 5.7 presents the results as well as those of a benchmark tests conducted without cooling at 65 °C. The two sets of data were obtained in duplicates.

At a concentration of 6.48 ± 0.02 mg mL^{-1}, residual X100 content of the ice bath treated extract was 23 % superior to that in the untreated extract, which contained 5.25 ± 0.06 mg mL^{-1}. Hence, the loss in surfactant was reversed, which confirms that the adhered surfactant is composed of an isotropic clouded phase. Simultaneously, THC yield improved from (13 ± 1) mg g^{-1} to (22.8 ± 0.4) mg g^{-1}. The latter corresponds to a 57 % improvement, which is far superior to the amount of additional surfactant recovered, indicating that, above the CPT, extraction occurs by a mesophase solubilization mechanism. This result comes in agreement with detergency studies on soiled fabrics where oil removal improved in the presence of a mesophase phase [82].

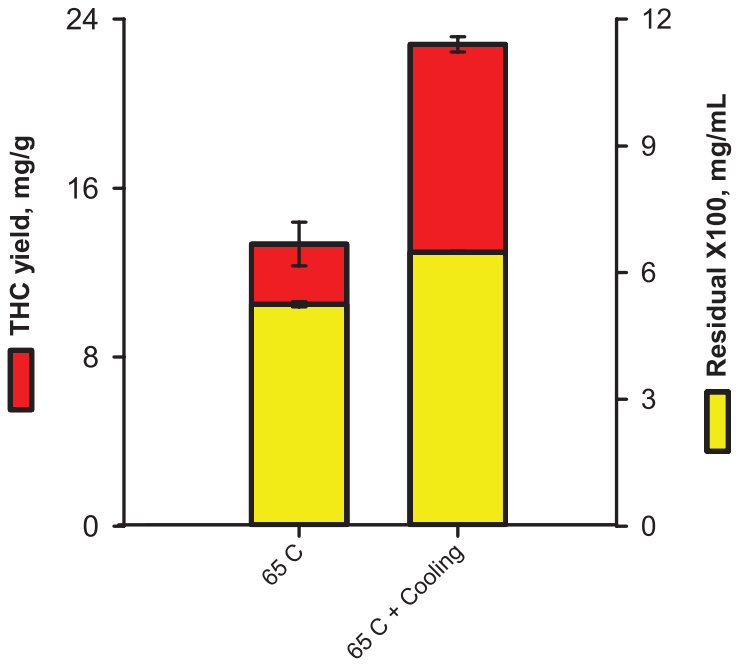

Figure 5.7 Effect of an additional cool-down on THC yield and residual X100 concentration.

5.2.6 Effect of particle Size

Particle size (D_p) was investigated at three levels from 300 µm to 700 µm. Following the surfactant adhesion observed during the temperature experiments, D_p was studied at both the control temperature of 21 °C and at 65 °C in order to identify potential interactions. Figure 5.8a present the THC yields at both temperatures and figure 5.8b shows the residual X100 concentrations.

At both temperatures, smaller particles yielded extracts with improved THC content. The maximum yield, obtained at 300 µm and 65 °C, was $52.5 \pm 0.4\,\mathrm{mg\,g^{-1}}$ and represents approximately a 60 % extraction with respect to PM01. It should be noted that any improvement in yield with particle diameter is likely a result of an increase in the fraction of broken trichomes rather then better diffusivity. The incremental milling procedure we applied, does not significantly alter the size of the glandular trichomes relative to the much larger leaves on which they grow. However, it progressively fractures the glands. During extraction of intracellular metabolites with traditional solvents, the compound of interest is uniformly dispersed in the plant's cells. Reducing the material's diameter then improves the extraction by reducing the diffusion path and enhancing solvent permeation. In the case marijuana, the cannabinoids are concentrated in glands already present at the surface of the leaves. The diameter of these structures ranges from 50 µm to 70 µm, six times smaller then the lowest

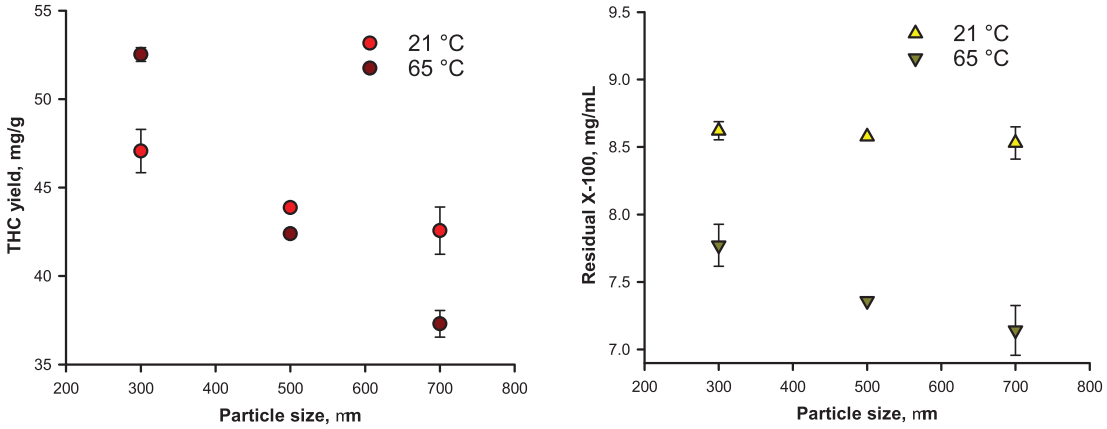

(a) (b)

Figure 5.8 Effect of particle size $D_p = 300\,\mu m$ to $700\,\mu m$ on extraction yield **(a)** and residual surfactant concentration **(b)** at 21 °C and 65 °C (PM01; 1 wt.% X100; $R_{S/L}$ = 1:100; 40 min; $n \geq 1$).

average size of the tested starting material. Hence, extraction yield was expected likely to be independent of particle size, as the trichomes immediately comes in contact with the solvent when submerged.

With respect to residual surfactant content, at 21 °C, it was not affected by D_p and remained constant at $8.6\,mg\,mL^{-1}$ (figure 5.8b). Surprisingly, at 65 °C, as X100 loss was most prominent in the largest particles. An increase from 300 µm to 700 µm correlates with a reduction in C_{X100}^{ext} from $(0.77 \pm 0.02)\,mg\,mL^{-1}$ to $(0.71 \pm 0.02)\,mg\,mL^{-1}$. As a results of the lose in effective micelle phase, SEE at 65 °C yields better then at 21 °C for smaller particles but not for larger ones.

Assuming mesophase accumulation, a plausible explanation to the previous result comes from the fluid dynamics of the various cannabis grains sizes. Figure 5.8b shows the plant matters employed. The cannabis power of 300 µm is granular and spherical in shape, whereas the one of 700 µm is composed of slabs and flakes reminiscent of the leaves prior to milling. We hypothesize that smaller diameters limits accumulation of the clouded phase as the surfactant aggregates are broken off by the liquid stream generated by the stirrer. In contrast, the larger cannabis grain provides areas of low current, which favor growth of the aggregates and prevents them from reintegrating the aqueous bulk, therefore leading to less residual surfactant in the extract.

(a) (b) (c)

Figure 5.9 PM01 cannabis powders employed during particle size experiments. From left to right, the average diameters are 300 µm, 500 µm and 700 µm.

5.2.7 Effect of solid to liquid ratio

Herein, the solid to liquid ratio ($R_{S/L}$) was defined as follows:

$$\text{Solid to liquid ratio} = \text{Mass of cannabis:Mass of surfactant solution} \tag{5.1}$$

To measure the effect of $R_{S/L}$, some modifications were made to our experimental protocol to account for a larger volumes in solvent. The 50 mL extraction vessel was replaced with a 150 mL Erlenmeyer flask. All other parameters were otherwise kept identical to the original protocol presented in chapter 4. Extraction yields are displayed in figure 5.10.

Extraction yield positively correlated with the solid to liquid ratio, increasing from 46.3 ± 0.7 mg g^{-1} to 36.3 ± 0.2 mg g^{-1}. These results are in agreement with mass transfer principles. The additional solvent maintains a concentration gradient between the cannabis and the solution, which leads to higher diffusion rates. Once extraction reaches an equilibrium, a steady state is expected, where increasing the solid to liquid ratio no longer enhances extraction [119]. With respect to the THC yield we obtained, such equilibrium was not observed. Its variation was linear up to an $R_{S/L}$ of 1:370, indicating that SEE efficiency may further improve with more solvent.

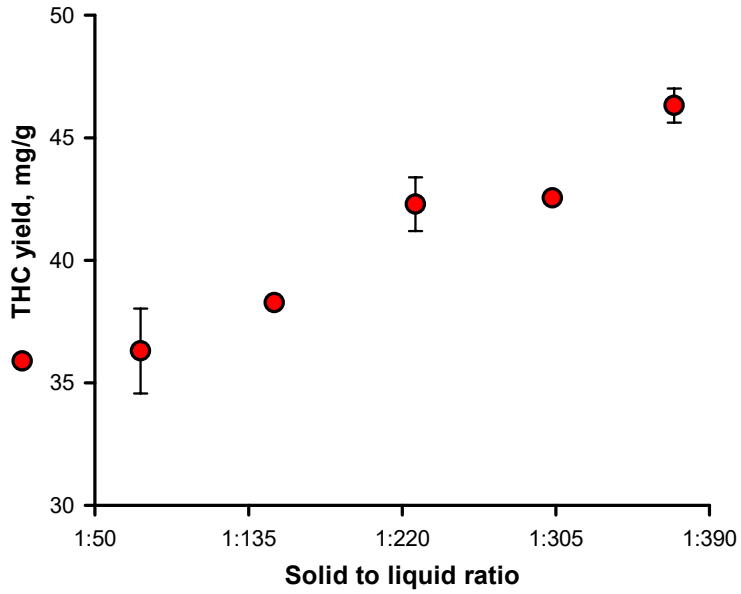

Figure 5.10 Effect of solid to liquid ratio between 1:75 to 1:370 on extraction yield (PM01; 25 °C; 1 wt.% X100; 0 wt.% Na_2SO_4; 40 min; $n \geq 1$).

5.3 Cloud point separation

The previous section provided insight on the behavior of nonionic surfactants and established optimization avenues for the continued development of such SEE process. The ability to concentrate cannabinoids into a small fragment of the raw extract's initial volume is perhaps the most appealing aspect of a surfactant mediated process. This section assesses the efficiency of cloud point separation

A 300 g batch of crude extract was purposely produced for the CPS experiments using cannabis ground from lot PM04. Table 5.3 presents the intial extract's concentration in cannabinoid, X100 and TPC as well as the operating conditions. Sodium sulphate was added to the crude extract until weight fractions ranging from 0 4%. The samples were then submitted to CPS at 95 °C and centrifuged at 2540 x g for 1 min.

5.3.1 Effect of salt on THC and CBD

In the absence of added sodium sulphate, CPS achieved its highest recovery. In fact, nearly all cannabinoids (more then 96 %) were recovered in the coacervate. An appreciable concentration factor was simultaneously achieved: the THC weight fraction in the coacervate

Table 5.3 Composition of the raw extract employed during CPS

	THC	CBD	X100	TPC
Concentration, $\mathrm{mg\,mL^{-1}}$	0.6578 ± 3	0.0995 ± 5	20.74 ± 8	0.31 ± 1

The extract was obtained under the following conditions: cannabis lot PM04 ($87 \pm 4\,\mathrm{mg\,g^{-1}}$ in THC); $R_{S/L}$= 0.01; t = 50 min; T = 63 °C; w_{x100} = 2.25 %. The extraction parameters were modeled after an set of optimization experiments which will be published elsewhere and are not presented in this manuscript. Nonetheless, it is worth mentioning that these conditions achieved the highest yields throughout all of our SEE experiment with a percentage recovery of 80 % with respect to the starting cannabis.

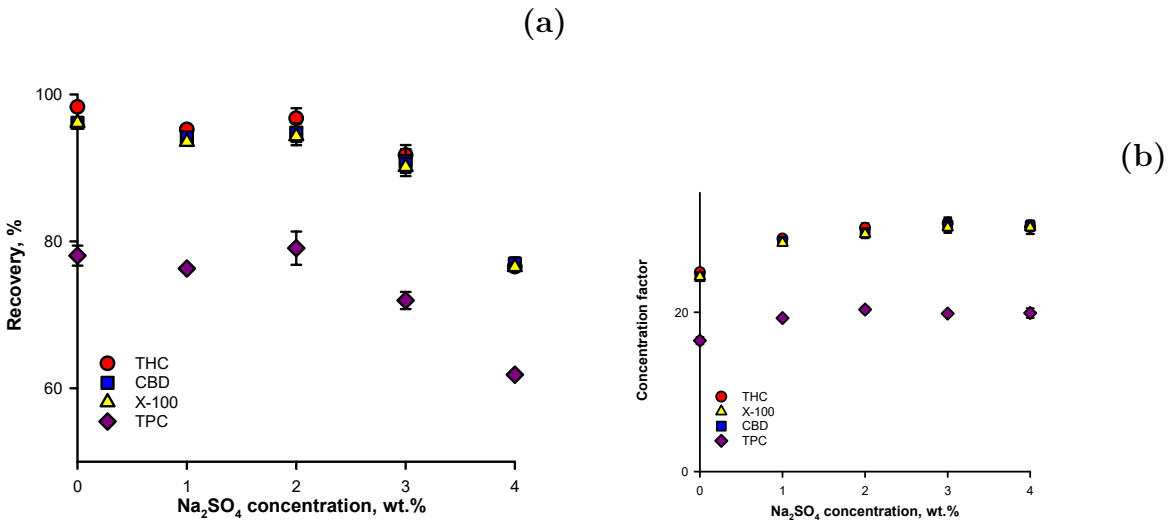

Figure 5.11 Effect of Na_2SO_4 on cloud point separation recovery and concentration factor. **(a)**. With respect to the initial extract, the recovery is the mass percentage of THC, CBD, X100 and TPC transfered to the surfactant-rich phase. **(b)**. The concentration factor is the multiplicative factor relating the weight fractions of each compound in the crude extract to that in the surfactant-rich phase.

was 25 times that of the initial extract. THC and CBD accounted for 1.99 ± 0.05 % and 0.296 ± 0.007 % of the surfactant-rich phase's mass, whereas the mass of X100 was superior by over one order of magnitude at a weight fraction of 61 ± 1 %.

At 2 % (w/w) in $NaCO_4$, the concentration factor of cannabinoids rose to 30. Further increase in salt content did not significantly alter their concentrations. When sodium sulphate was added, we observed two opposing effects on CPS efficiency: Although the surfactant-rich phase was more concentrated, less cannabinoids were recovered.

The increased concentration is explained by a reduction of the water fraction within the coacervate. In section 3.1.4 of the literature review, we detailed the salting-out mechanism

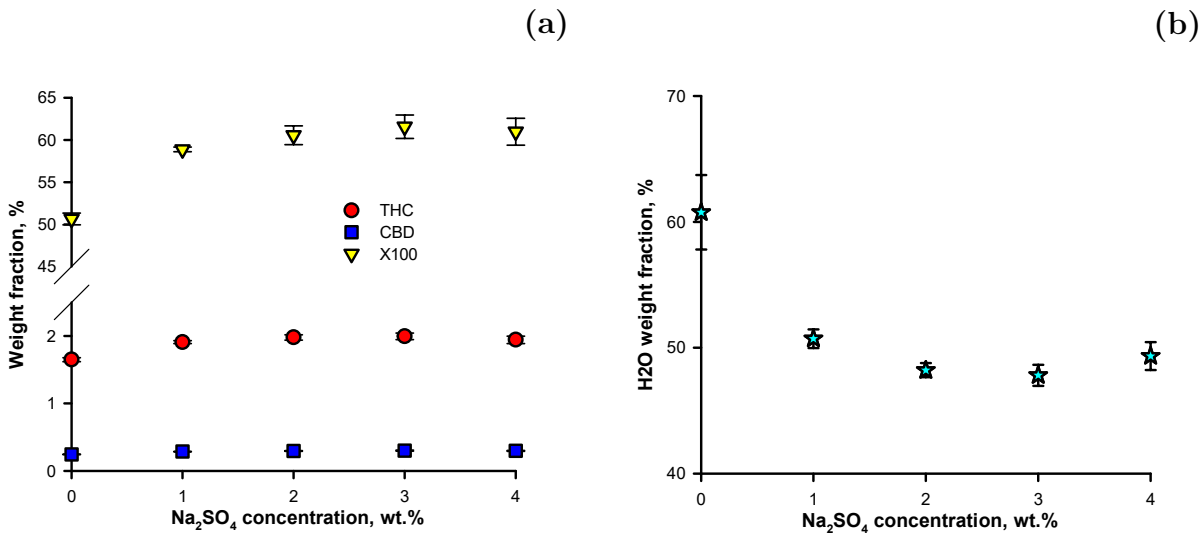

Figure 5.12 Effect of Na_2SO_4 on the surfactant-rich phase's weight fraction in **(a)** THC, CBD and X100 as well as on the weight fraction of **(b)** water.

by which added salt promotes polar binding between water molecules. This reduces the equilibrium water content and, thus, the total mass of surfactant-rich phase. As such, the surfactants and the cannabinoids then occupy a larger fraction of the coacervate. As a matter of fact, Karl-Fisher titration revealed a drop in water weight fraction from $61 \pm 3\,\%$ to $48.1 \pm 0.4\,\%$ from $0\,\%$ to $2\,\%$ in Na_2SO_4.

The reduction in cannabinoid recovery results from a decreasing density difference between aqueous and surfactant phases. At ambient conditions, Triton X-100 and water exhibit comparable density ($1.07\,\mathrm{g\,mL^{-1}}$ and $0.997\,\mathrm{g\,mL^{-1}}$, respectively). The dissolved salt renders the water denser, increasing buoyancy forces which the surfactant phase must overcome to phase out. This effect is highlighted by figure 5.13, which shows post-centrifugation samples obtained during our preliminary tests. In a extract containing $6\,\%$ (w/w) in sodium sulphate, the surfactant-rich phase starts to experiences neutral force balance and does not completely settle after centrifugation. Further increase above $8\,\%$ causes the top and bottom phases to invert positions (figure 5.13b).

Interestingly, for a given ionic strength, the recovery and concentration factor of both cannabinoids were identical to that of X100. Independently of the system's ionic strength, all three compounds partition to the surfactant-rich phase equally. This result indicates that the cannabinoids possess high affinity for the micelle phase and remain contained in the hydrophobic core during clouding and separation.

There are other methods by which electrolyte disturbs surfactant behavior during CPS which may explain some of the data irregularities. For instance, salt species can also alter the volumetric mass of the surfactant phase. First by dehydration, but also by compacting the water inherently bound to surfactant monomers. Studies have shown electrolyte content caused oscillations in the equilibrium density of the clouded phase [120]. In addition, ionic species and temperature both increase aggregation number and influences micelle size [121]. A combination of the above-mentioned behavior affects sedimentation hydrodynamics, leading to non-optimal separation.

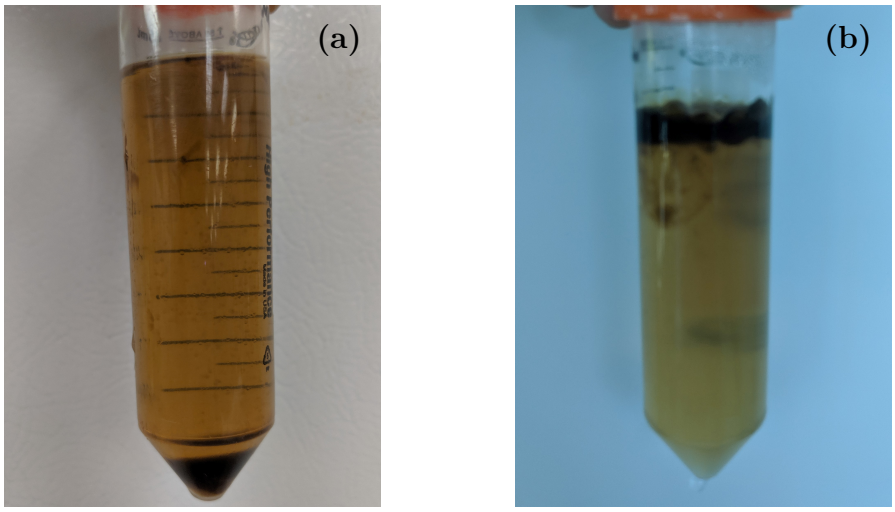

Figure 5.13 Supernatant and coacervate inversion during cloud point separation. A 50 mL sample was clouded for 15 min at 95 °C and centrifuged for 1 min at 3000 x g. **(a)**. Following clouding, the extract with 6 % by weight in Na_2SO_4 contained brown droplets throughout it's length. In addition, a thin layer of surfactant-rich phase could be observed on top of the water phase. **(b)**. Increasing Na_2SO_4 weight fraction to 8 % reversed the relative position of the two phases, with the water-rich phase now at the bottom and the surfactant-rich phase on top.

5.3.2 Effect of salt on total polyphenolic content

Polyphenolics constitute a large class of secondary metabolites produces by plants and accounts for up to 25 % of the mass of dry leaves. Low molecular weight phenolics are particularly susceptible to extraction. Hence, quantification of total polyphenolic content before and after CPS provided an indication of the cannabinoids performance relative to other co-extracted biomolecules.

At best, total polyphenolic content (TPC) achieves a concentration factor of 20.3 ± 0.4 (at

4 % (w/w) in $NaSO_4$). For all salt weight fractions, TPC exhibited proportional, but inferior, concentration factors and recoveries than THC and CBD. As cannabinoids themselves are phenolic, the similarity in data trends is likely explained by the fact that THC and CBD account for a large portion of the TPC response.

Nonetheless, a compelling conclusion can be drawn from the gap in recovery between the TPC and X100. Specifically, we consider the data at 0 % weight fraction in $NaSO_4$ where a nearly complete phase segragation was obtained. Contrarily to the cannabinoids, TPC did not partition equally with the surfactant and was recovered at 78 ± 1 %. The remaining phenolic is accounted for in the water-rich supernatant, which upon analysis contained 22.4 ± 0.8 % of the TPC present in the initial extract. During our screening experiments (section 5.1), we have demonstrated that water, although capable of extracting polyphenolics, does not readily dissolve the cannabinoids. The polyphenolic composition of biomass is inherently heterogeneous with some compounds possessing more hydrophilic attributes, whereas other are more hydrophobic. In the crude extract, this difference in affinity causes them to unevenly partition between the micelles and the aqueous bulk. When CPS is applied, the water soluble molecules remain in the aqueous phase and therefore are not recovered in the coacervate along with the cannabinoids. This is in agreement with the high octanol–water partition coefficients ($K_{ow} > 4.5$) of cannabinoids [122]. A larger K_{ow} indicates a more hydrophobic solute and correlates with a tendency for partitioning towards the micellar phase [123].

Fractioning between hydrophilic and hydrophobic cellular proteins has previously been employed during CPE to concentrate proteins of interest from cell lysates [124]. Such behavior in cannabinoids may be similarly applied to the development of a surfactant assisted process, as a preliminary purification step by removing water-soluble impurities while simultaneously enriching cannabinoid content.

CHAPTER 6 SUPPLEMENTARY RESULTS

6.1 Decarboxylation experiments

Decarboxylation converts the naturally synthesized acidic cannabinoids to their biologically active neutral moieties. During kinetic experiments of methanolic samples of CBDA, [7] observed an 8 % increase in CBD concentration in experiments at 80 °C after 60 min. These experiments closely resemble our SEE and CPS conditions. As our HPLC-UV method was unable to quantify acidic cannabinoids, achieving full decarboxylating in the starting material ensured its compatibility with the analysis. This avoids potential overestimation of the calculated yield due to conversion of the carboxylic acids during high temperature SEE and CPS. We therefore devised a preliminary test to determine optimum decarboxylation time and temperature.

Based on our literature survey, at 100 °C, the reaction requires in excess of 2 h to achieve complete conversion, whereas, at 150 °C and above, cannabinoids are prone to degradative and evaporative losses [125, 52]. Hence, temperature was set at 120 °C. Milled cannabis samples of 100 µg were measured in sealed 20 mL vials and placed in a temperature equilibrated furnace for 0 min to 105 min. After the thermal processing, we extracted the the resulting material in 15 mL of methanol. The step was repeated once and the yield from both extracts were combined to quantify the neutral cannabinoids content (table F.1). Each data point was performed in triplicate.

The untreated material contained $5 \pm 1\,\mathrm{mg\,g^{-1}}$, $3.8 \pm 0.7\,\mathrm{mg\,g^{-1}}$ and $0.3 \pm 0.1\,\mathrm{mg\,g^{-1}}$ for THC, CBD and CBN, respectively. Concentration of THC increased sharply within the first 60 min before plateauing at a concentration of approximately $90\,\mathrm{mg\,g^{-1}}$ (figure 6.1). The maximum THC concentration of $100 \pm 20\,\mathrm{mg\,g^{-1}}$ was obtained after 105 min. CBD exhibited an identical trend with a maximum concentration of $70 \pm 10\,\mathrm{mg\,g^{-1}}$ after an equal period of time. A negligible increase in concentration of CBN was observed up to 105 min.

$$r_{CB} = \frac{\text{weight fraction THC}}{\text{weight fraction THC}} \tag{6.1}$$

Although the THCA and CBDA could not be quantified, the relative reaction rates can be inferred by considering time variation in THC to CBD ratio (r_{CB}), defined in equation (6.1). This ratio increased from an initial value of 1.32 to 2.94 during the first 30 min, indicating that conversion of THCA occurs more rapidly than CBDA. The faster kinetic of THCA is

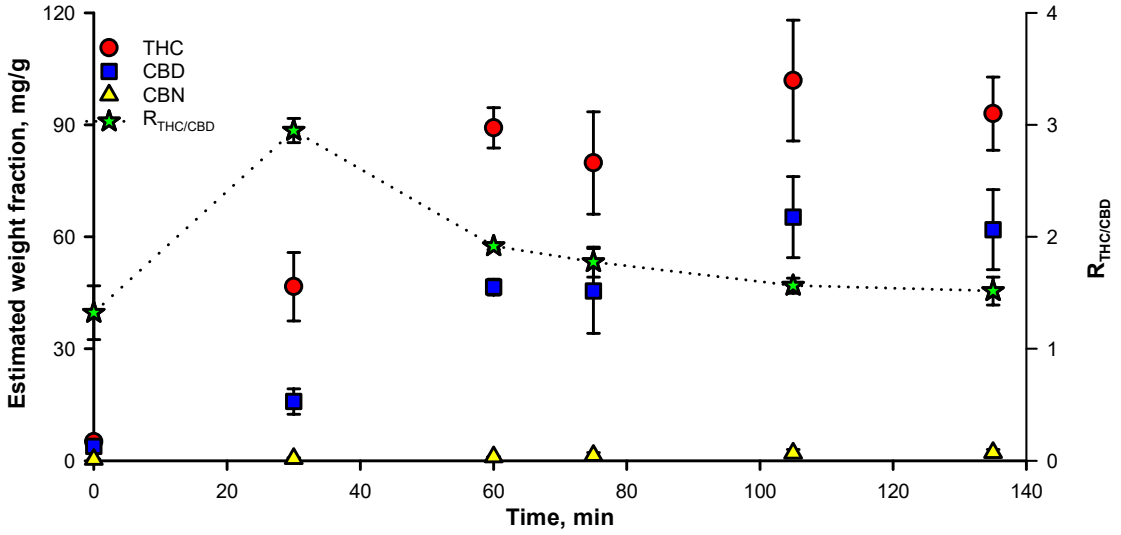

Figure 6.1 Effect of decarboxylation time on neutral cannabinoid content of cannabis powder and THC/CBD ratio (PM03; T = 120 °C; t = 0 min to 135 min, $n = 3$).

consistent with our literature review in section 2.5. Following its peak, r_{CB} then decreased to of 1.48 at 105 min, approaching its initial value. Base on these results, a 105 min decarboxylation at either 120 °C or 140 °C were employed for our starting material.

6.2 Effect of ionorganic salts on the cloud point temperature

Data on the cloud point temperature (CPT) ternary water-surfactant-salt systems were not widely available in the literature. We investigated the dependence of CPT on the solution's concentration in surfactants (1 % and 4 % weight X-100) and inorganic salts (0 % to 8 % by weight in Na_2SO_4 and NaCl).

We visually determined cloud point temperatures of our surfactant following standardized method ASTM D2024 [110]. Briefly, test tubes containing 15 g of aqueous surfactant solutions were submerged and heated in a thermostatic water bath until sustained formation of a turbid second phase indicated attainment of the CPT. A thermocouple recorded the corresponding temperature. The tube was then allowed to cool at room temperature. The temperature was recorded a second time upon it dropping below the CPT characterized by the remixing of the two phases into a single translucent fluid. Tests were performed in duplicate, with a maximum relative standard deviation of 1.4 %.

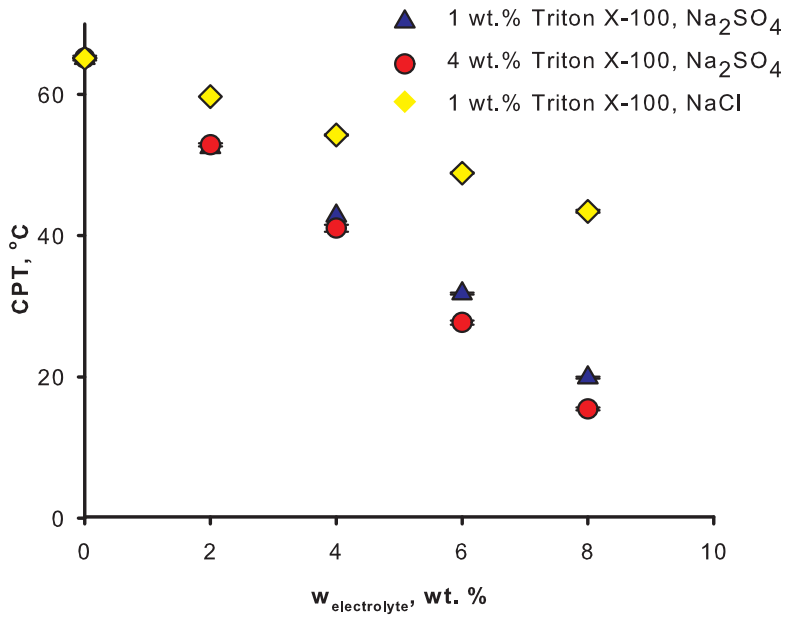

Figure 6.2 Effect of X100 and electrolyte (Na_2SO_4 and NaCl) weight fraction on cloud point temperature (n=4).

The results, presented in figure 6.2, were linearly regressed to obtained a direct correlation between the CPT and the salt weight fraction. The regression equation is:

$$CPT(w^0_{salt}) = k_{cpt} * w^0_{salt} + 65 \tag{6.2}$$

CPT of both 1 % and 4 % solutions occurred 65 °C, in accordance with the range of 63 °C to 69 °C reported by the supplier (Sigma Aldrich, United States). It exhibited a strong negative linear dependence on salt ions weight fraction ($R^2 \geq 0.998$). Na_2SO_4 was twice as efficient in reducing the CPT as NaCl with α of 2.7 °C and 5.6 °C, respectively (table 6.1). This effect reflects the greater anionic charge of SO_4^{2-} over Cl^-, resulting in increased disruption and dehydration of EO-water interactions [126].

Table 6.1 CPT regression coefficient

Salt type	w^0_{X100}, wt.%	α	R^2
NaCl	1	-2.69	0.999
Na2SO4	1	-5.56	0.998
Na2SO4	4	-6.17	1.000

6.3 Supplementary extraction results: effect of electrolyte content

Cloud point extraction employs inorganic salts to reduces the CPT and the surfactant-rich phase's water content. With the prospect of simplifying an integrated SEE-CPS process, we experimented by adding sodium sulfate to the SEE solvent. The presence of electrolytes in the SEE solvent streamlines the process, removing the necessity of an additional mixing step prior to CPS. Two different types of experiments were performed according to our standard protocol to evaluate (1) the effect of salt concentration and (2) interactions between salt and temperature.

6.3.1 Effect of salt content

In a first test, we altered the ionic strenght of the SEE solvent while maintain operative temperature at 21 °C. X100 and Na_2SO_4 were incorporated in water to obtain respective weight fractions of 1 % and 0 % to 2.5 %. Due to the limited amount of cannabis, three separate sets of experiments were performed without duplicates (figure 6.3).

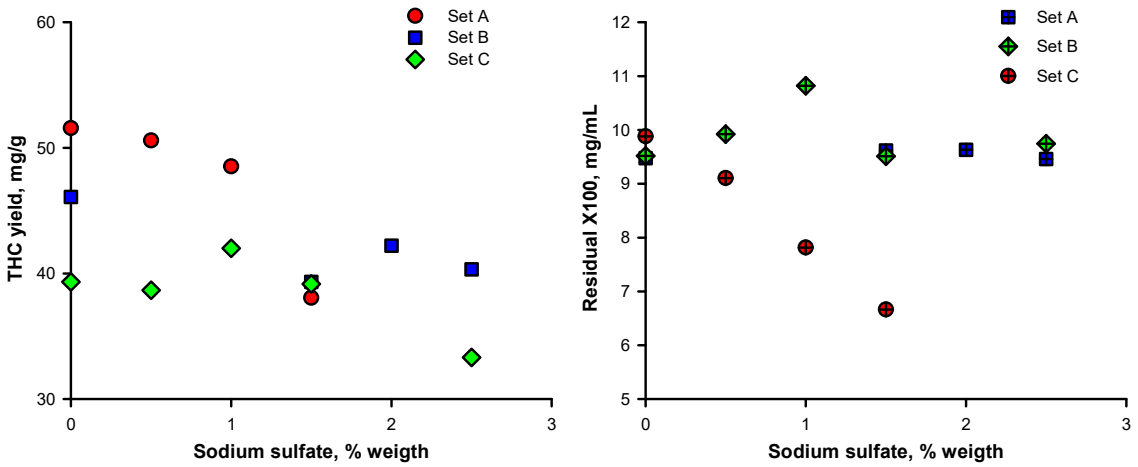

(a) THC extraction yield

(b) Residual X100 concentration

Figure 6.3 Effect of 0 % to 2.5 % weight Na_2SO_4 on **(a)** extraction yield and **(b)** residual X100 with PM03 (set A), PM01 (set B), and PM04 (set C) (1 % Triton X-100; $R_{S/L}$ = 1:100; t = 40 min; T=21 °C; $n = 1$).

We were unable to discern any conclusive trends when the ionic strength of the solvent was altered. In the first set of experiments (set A), THC yield decreased by 25 % between 0 % and

1.5 % in sodium sulphate and was accompanied by a loss in X100. Nonetheless, this effect was not replicated in the subsequent sets of extractions, where both compounds followed non specific trends.

Based on the regression of section 6.2, the CPT of an X100 solution containing 2.5 % (w/w) in Na_2SO_4 is expected at 51 °C, whereas the results of set A were obtained at room temperatures. In contrast to the surfactant loss observed in a clouded SEE system (section 5.2.3), the decrease in residual X100 could not be attributed to clouding. Hence, we initially attributed this result to a salting out effect. As X100 is nonionic, it does not directly interact with the dissolved salt ions. Instead, the salt increases cohesive polar forces within water [127], which may have caused an increase in surfactant adsorption at the cannabis-water interface. Adsorption of nonionic surfactants on both hydrophilic and hydrophobic surfaces is well documented within the literature and has been demonstrated to increase with electrolyte concentration [128]. Zhao's team previously studied the adsorption isotherms of X100 on hydrophobic polystyrene latex particles and observed a 50 % increase in surface saturation when sodium bromide concentration was raised from 0 mM to 1 mM [129].

Experiment sets B and C appeared unaffected by the ionic strength of the solvent. Specifically, the residual X100 did not display significant difference between each salt concentration. Other factors may have favored their presence in the aqueous bulk. This could be caused by some inconsistencies in the cannabis preparation procedure (e.i. milling and decarboxylation) which can affect the surface properties the cannabis powder. Additionally, pH of the surfactant solution may also be at play. These factors are discussed in greater detail in the general discussion chapter 7.

6.3.2 Effect of temperature in a surfactant solvent containing 1 percent in Na_2SO_4 by weight

In a the second test, the sodium sulphate content was set to 1 % (w/w), while SEE temperature was increased from 25 °C to 85 °C. For each temperature, the extraction was duplicated using cannabis lot PM01. The results are presented along with data obtained without sodium sulphate (reprinted from section 5.2.3 for reference).

Compared to a solvent without Na_2SO_4, increase in temperature was unfavorable to extraction when salt was added. Whereas the CPT of the pure X100-water solution is 65 °C, that of a mixture containing 1 % (w/w) in sodium sulphate shifts from 59°C (as determined in section 6.2). As such, a decrease in residual surfactant was expected at this temperature due to the aggregation of the clouded phase. However, loss in X100 occurred before the cloud point and appeared to be two-stepped. Below the CPT and between 25 °C and 55 °C,

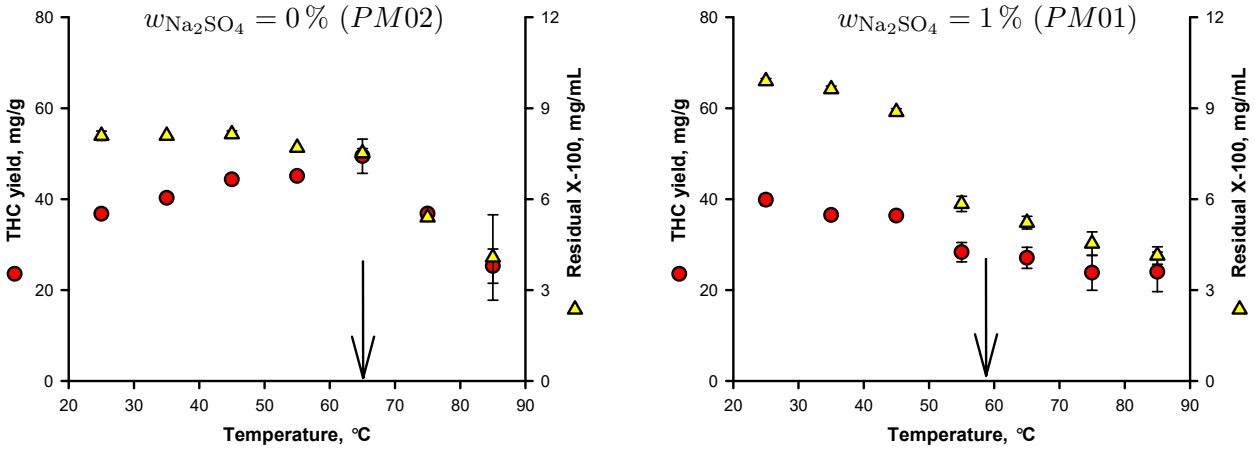

Figure 6.4 Effect of SEE temperature on THC yield and residual surfactant concentration in a surfactant solvent containing 0 % (left) and 1 % (right) in Na_2SO_4. The vertical arrows indicate the cloud point temperature of the pure X100 solution.

the concentration of X100 falls exponentially from $10.2 \pm 0.1\,\mathrm{mg\,mL^{-1}}$ to $6.1 \pm 0.5\,\mathrm{mg\,mL^{-1}}$. As a result of the lowered micelle concentration, THC yield varies from $40 \pm 1\,\mathrm{mg\,mL^{-1}}$ to $28 \pm 5\,\mathrm{mg\,mL^{-1}}$ over this temperature range. Above the CPT and up to 85 °C, X100 further reduces down to $4.5 \pm 0.3\,\mathrm{mg\,mL^{-1}}$.

We hypothesis that adsorption could again be involved, as it also increases with temperature. In particular instances, when the surface's properties and the surfactant's structure are suitable, adsorption occurs not as a monolayer but as two-dimensional hemispheres or multilayered lamella [128, 130]. The combined effect of temperature and salt may have resulted in such structures, which could explain why X100 is lost prior to the cloud point.

CHAPTER 7 GENERAL DISCUSSION

In this thesis, we identified several phenomenon unique to the surfactant assisted extraction of cannabis namely, the selective extraction of cannabinoids over surface lipids and the coalescence and subsequent surface adhesion of a micellar mesophase on cannabis particles above the cloud point temperature. These phenomenon limit the extraction rate during surfactant enhanced extraction. In this section, we discussing with some details there implications for developments of cannabis SEE-CPS.

Surfactant

Triton X-100 was selected for its low cloud point temperature and superior performance in our screening tests. The low CPT allowed for precise separation during in-lab CPS manipulations. It should be noted that this surfactant is of low biocompatibility and potentially harmful for the environment [131]. It is suggested that a consumable and less nontoxic surfactant be chosen before for further process development, while considering the end use of the concentrate. For instance, polysorbate-type surfactants, such as Tween 20, may be considered. These surfactants are currently incorporated in products such as topical cremes and cough syrups.

Trichomes

With respect to the trichomes, release of additional cannabinoids may be increased by combining SEE with mechanical intensification procedures. For instance, several publications have reported the ability of ultrasound assisted extractions (UAE) to substantially enhance extraction of cannabis in conventional solvents such as ethanol [132, 133, 134]. During UAE, propagation of cavitational micro-jets breakdown the plant's cellular matrix. and help in achieving better solvent efficiency and reduced equilibrium time. The effect of these micro-jets on glandular trichomes of rosemary leaves have been analyzed by Khadhraoui et al.[135] during UAE in water at 25 °C and ultrasonic intensity of 41 $\mathrm{W\,cm^{-2}}$. In microscope images the leaves' surface, disruption of the the trichomial structures were important, whereas the leaves' epidermis integrity remained relatively unaffected.

Additionally, the selective extraction of cannabinoids over $C_{32}{}^{+}$ waxes contained in the trichome was inferred from the SEM analysis of extracted residues. These residues were observed for SEE samples obtained at up to 40 °C and 2.6 % (w/w) in X100. It is unknown if intensified conditions (i.e. 85 °C) lead to a substantial co-extraction of the epidermal lipids. Their disintegration may explain the higher yields obtained. Regardless, chemical quantifi-

cation of these compounds is a more rigorous approach and should be implemented in future experiments.

Phase behavior

During SEE-CPS, cannabinoids are distributed between two phases: micelles and water. Ternary phase diagram are useful in predicting equilibrium condition of such systems and to inform the choices in operating conditions. Similarly to that of conventional liquid-liquid extraction, the equilibrium partition coefficients in a binary surfactant-water systems remains constant independently of the concentration of each phase [123]. As such, the respective solubility of THC and CBD may be obtained for various concentrations and temperatures and correlated to the extraction extent. Ternary phase diagrams are not readily available for a large number of cannabinoids and surfactant combinations. For future experiments, it is recommended that they be produced for the chosen SEE-CPS surfactant prior to extraction experiments.

The importance of phase behavior is also highlighted by our CPS results in section 5.2.5, where we observed equal phase partitioning between cannabinoids and surfactants. This result implies that all three compounds maintain the same relative ratio as in the extract:

$$\frac{\text{mass of THC}}{\text{mass of X100}} \text{ of the raw extract } = \frac{\text{mass of THC}}{\text{mass of X100}} \text{ of the surfactant phase} \tag{7.1}$$

An extract containing high fractions of surfactant yields a coacervate with equally high amount of surfactant and a lower concentration factor. In our CPS tests, a coacervate containing $1.99 \pm 0.05\,\mathrm{g\,g^{-1}}$ in THC had a mass in X100 that was 30 times superior ($61 \pm 1\,\mathrm{g\,g^{-1}}$). Rivera et al. [123] studied the effect of surfactant concentration on the CPE polyaromatic hydrocarbons (PAH). They observed an inverse proportionality between surfactant concentration and the concentration factor. When PAH concentration was maintained constant, an increase in Triton X-405 from 1 % to 3 % was correlated with a reduction in concentration factor from 30 to 10.

Clouded mesophase adhesion

With respect to the loss in surfactant during high temperature SEE, we have demonstrated that cooling the extraction vessel or employing smaller particles are efficient recuperating a portion of the micelles. Monomer adsorption innately occurs at the solvent-biomass interface. As such, for all temperature, a reduction in active surfactant concentration relative to the pure water-surfactant solvent is expected. Nonetheless, this phenomenon has not been previously reported in the literature and may be a results of the low amount of surfactant (1 % by weight) of our control conditions. Loss in micelle is most impactful at lower concentrations, where

a smaller mass of adhere surfactant corresponds to a higher fraction of all initial surfactant phase. Comparable SEE-CPS publication extracted with solutions containing upwards of 10 % (w/w) in surfactant [92, 136, 94]. Under these conditions, any adhesion or adsorption becomes negligible relative to the remaining amount of micellar phase.

pH of the aqueous surfactant solvent

The acidity of the extraction media was not studied in this research. pH is known to cause significant changes in the partitions coefficient of organic solutes during CPE as a large quantity of these compounds are ionizable. For examples, during the extraction of polyphenolics compounds from fruits extracts, Hosseinzadeh et al.[137] observed a 40 % increase in concentration, when the pH was reduced from 6 to 2.5. They concluded that the lower pH conditions favored the formation of neutral neutral phenolics which, unlike their ionized form, are extracted in the micellar phase.

The effect of pH may also explained some of the inconsistencies in our data, specifically the results of the salt concentrations experiments section 6.3. For instance, atmospheric CO_2 is known to spontaneously solubilize in aqueous solutions. Depending on the storage time and conditions, this may affect the solvent's pH and therefore the partition coefficients during extraction. The additional electrolytes may also increase the ionic strength, causing an increase in salting-out of the surfactants micelles [64, 138].

Laboratory procedures

We would like to further emit the following recommendations regarding the SEE-CPS laboratory material and procedures.

At the time of our experiments, standardized methods for cannabis characterization were not readily available. In future works, particular emphasis should be placed on the starting material by using a single lot of cannabis and by standardizing their preparation and characterization methods. The design and scale-up of biomass extraction processes greatly benefit from a defined raw material and consistent pretreatment procedures. Modeling is otherwise impossible due to the natural variances which occurs during cultivation and harvest [139]. This holds particularly true for cannabis, unlike other plant matrices such as leaves or seeds, cannabis inflorescence are highly heterogeneous. Along with the trichomes and the flowers leaves themselves, cannabis purchased from dispensaries contain a fraction in branches and in reduced leaves which are not readily separated. These organs differ in shape, size, rigidity and chemical composition and, as such, are not equally affected when preprocessed for extraction.

In fact, for our experiments, the material's heterogeneity had particular implication for par-

ticle size measurements. Milling was the only procedure applied for particle size reduction. For plant matter, studies on particles size generally employ a combination of milling and sieving to obtain the desired particle sizes. The plant is first milled and sifted through various mesh sizes. However, for cannabis, this procedure splits the cannabinoids towards the smaller particles as the smaller and denser trichomes rapidly sinks through the sieves. As a matter of fact, we have demonstrated this effect in appendix E, where THC content of sieved cannabinoids where analyzed.

The method we employed for particle size analysis may also lack reliability. We assessed size distribution by laser diffraction through the Mie theory. The latter requires the refractive index (RI), which is given by chemical composition of the measured compound. A single RI is impractical to define in mixed cannabis ground, as chemical composition vary between leaves, trichomes and stalks. We employed a RI of 1.4, corresponding to that of cellulose. Although cellulose is present in leaves at a average weight fractions between, they are not present in trichomes 10 % to 12 % [140]. Hence, the contribution of these glands to the mean sample diameter may have been underestimated.

With respect to CPS, we observed inconsistencies in the protocol employed by various publications to initiate the two phases-aqueous separation of the extracts. Some performed clouding through decantation in a heated oven [76] while other heavily employed inorganic salt in order to achieve phase separation at room temperature [95]. A majority of papers favored first heating the solution followed by centrifugation [92, 94] with a procedure similar to the one employed in section 4.4.2. During transport and spinning cycles, extracts are subject to temperature fluctuations, namely through convective cooling of the centrifugal tubes. These transient conditions alter the flow properties of the aggregates and are likely not reproducible at scale. For future experiments, studies of separation parameters ideally occur under adiabatic conditions in a heated centrifuge. Nonetheless, obtaining representative data may prove challenging as most bench-top centrifuges operates at a maximum of 40 °C due to mechanical constraints.

CHAPTER 8 CONCLUSION

This project attempted to determine the fundamental parameters for the development of a sequential surfactant enhanced extraction (SEE) and cloud point separation (CPS) process. For the first time, amphoteric aqueous solutions successively recovered and concentrated Δ^9-tetrahydrocannabinol (THC) and cannabidiol (CBD) from the aerial flower buds of *Cannabis L. Sativa*. We adapted two analytical methods to the characterization of emulsified cannabis extracts, which which were then employed to optimize extraction and separation.

High performance liquid chromatography method (appendix B) simultaneously quantified concentrations of THC, CBD and Triton X-100 in a single elution through a C18 column at a detection wavelength of 235 µm. It employed a solvent composed of methanol:water:acetic acid in volume ratio of 85:14.2:0.8, eluted at $0.8\,\mathrm{mL\,min^{-1}}$ and 28 °C. The Folin-Ciocalteu assay (appendix C) was adapted to polyphenolic quantification . The addition of sodium dodecyl sulphate (5000 ppm) was effective to counter precipitation and did not affect reliability of the measurements.

We compared the THC extraction efficiency of water, ethanol and Triton X-100 on cannabis inflorescence. At 21 °C, THC does not extract in water. Their solubilization requires the the presence of micelles aggregates, as with 1 % (w/w) in X100, THC concentration increased to $0.3922 \pm 0.0004\,\mathrm{mg\,mL^{-1}}$. Nonetheless, ethanol was found to extract twice that amount and at four times the rate.

In addition, Triton X-100 extracted the cannabis ground in single-variable experiments to assess the effects of time (t = 0 to 105 min), surfactant concentration (w_{x100} = 0 to 3.75 % (w/w)), temperature (T = 25 to 85 °C), particle size (D_p = 300 to 700 µm) and solid to liquid ratio ($R_{S/L}$ = 1:75 to 1:370). Extraction was found to be limited to superficial THC, as the solvent was unable to access cannabinoids fractions contained in intact secretory glands. As a results, extraction at room temperature did not surpass 50 % after 105 min. Nonetheless, surfactant weight fractions as low as 0.3 % (w/w) were efficient capturing the superficial THC fraction, above 1.5 % (w/w) yields plateaued. When extraction occurred above X100's cloud point temperature of 65 °C, the surfactant precipitated on to the plant particles and entrained with it a portion of the cannabinoids, thus reducing extraction yield. This effect has not been previously been reported for SEE of plant matter and is believe to be caused by hydrophilic interactions between the surfactant and lipidic cuticular waxes on the plant's surface. This adhesion effect was demonstrated to be reversible as the clouded surfactant was resolubilized by reducing the system's temperature to 5 °C. Nonetheless, we were able to

acheive an extraction recovery of 80 % under the following SEE conditions: $D_p = 300$ to 700; $R_{S/L}$= 1:100; t = 50 min; T = 63 °C; $w_{x100} = 2.25$ %. This extract was then used to evaluate the effects of inorganic salt (Na_2SO_4) between weight fraction of 0 % to 4 %) on CPS. At high ionic concentrations, the enhanced concentration factor is offset by poor hydrodynamics which leads to diminished recovery. Even so, CPS successfully recovers from the crude extract 98.3 ± 0.3 %, 96.2 ± 0.6 % and 96.2 ± 0.1 % of THC, CBD and X100, respectively. In additional, the cannabinoids favorably partitioned in the surfactant-rich phase in equal ratio to the surfactants. Simultaneously, it was observed that a portion (approximately 20 %) of hydrophobic polyphenolic compounds were removed in the water-rich phase.

Our results demonstrate an environmentally benign and energy efficient method for the concurrent extraction-purification of phytocannabinoids. In addition to the content of the present document, a report of invention titled *"Surfactant enhanced extraction of tetrahydrocannabinol and cannabidiol and subsequent purification by cloud point separation"* was submitted to Univalor with the intent of patenting the SEE-CPS process detailed herein. Another part of this project includes a currently unpublished review article covering the literature and patents on cannabis processing and extraction (approximately 30 pages at the time of submitting).

The proposed process remains limited by SEE performance. Several recommendations have been made in that regards in our discussion of chapter 7. Some of those recommendations are reiterated below, along with more general suggestions for future work:

1. Replace the nonionic surfactant used herein (Triton X-100) with one that is suitable for direct formulations into consumer products.

2. Perform economic assessment of SEE-CPS to compare its performance to traditional organic solvent such as ethanolic maceration of cannabis

3. Develop new purification methods for the surfactant-rich concentrate obtained following CPS.

4. Complete characterization of nonionic surfactant-water-cannabinoids systems to obtain phase densities and phase compositions at various temperatures. Composition measurement will allow the determination of equilibrium partition coefficients of THC and CBD and the modeling of the SEE kinetics. Whereas, the density of the water and surfactant-rich phases are required in the design of a CPS separation apparatus (i.e. centrifuges).

5. Study the effect of pH and ionic strength on cannabinoid yields and recovery during SEE and CPS, respectively.

REFERENCES

[1] J. M. Chatkin, L. Zani-Silva, I. Ferreira, and N. Zamel, "Cannabis-Associated Asthma and Allergies," *Clinical Reviews in Allergy & Immunology*, vol. 56, no. 2, pp. 196–206, Apr. 2019.

[2] J. L. Bottorff, L. J. Bissell, L. G. Balneaves, J. L. Oliffe, N. R. Capler, and J. Buxton, "Perceptions of cannabis as a stigmatized medicine: A qualitative descriptive study," *Harm Reduction Journal*, vol. 10, no. 1, p. 2, Feb. 2013.

[3] R. D. Richins, L. Rodriguez-Uribe, K. Lowe, R. Ferral, and M. A. O'Connell, "Accumulation of bioactive metabolites in cultivated medical Cannabis," *PLOS ONE*, vol. 13, no. 7, p. e0201119, 2018.

[4] S. Elzinga, O. Ortiz, and J. Raber, "The Conversion and Transfer of Cannabinoids from Cannabis to Smoke Stream in Cigarettes," *Natural Products Chemistry & Research*, vol. 3, p. 163, Dec. 2014.

[5] A. L. Stinchcomb, S. Valiveti, D. C. Hammell, and D. R. Ramsey, "Human skin permeation of Δ8-tetrahydrocannabinol, cannabidiol and cannabinol," *Journal of Pharmacy and Pharmacology*, vol. 56, no. 3, pp. 291–297, Mar. 2004.

[6] M. Wang, Y.-H. Wang, B. Avula, M. M. Radwan, A. S. Wanas, J. van Antwerp, J. F. Parcher, M. A. ElSohly, and I. A. Khan, "Decarboxylation Study of Acidic Cannabinoids: A Novel Approach Using Ultra-High-Performance Supercritical Fluid Chromatography/Photodiode Array-Mass Spectrometry," *Cannabis and Cannabinoid Research*, vol. 1, no. 1, pp. 262–271, Dec. 2016.

[7] C. Citti, B. Pacchetti, M. A. Vandelli, F. Forni, and G. Cannazza, "Analysis of cannabinoids in commercial hemp seed oil and decarboxylation kinetics studies of cannabidiolic acid (CBDA)," *Journal of Pharmaceutical and Biomedical Analysis*, vol. 149, pp. 532–540, Feb. 2018.

[8] L. Romano and A. Hazekamp, "Cannabis oil: Chemical evaluation of an upcoming cannabis- based medicine," *Cannabinoids*, vol. 1, pp. 1–11, Jan. 2013.

[9] K. S. Romanowski, A. Barsun, P. Kwan, E. H. Teo, T. L. Palmieri, S. Sen, P. Maguina, and D. G. Greenhalgh, "Butane Hash Oil Burns: A 7-Year Perspective on a Growing Problem," *Journal of Burn Care & Research*, vol. 38, no. 1, pp. E165–E171, Jan. 2017.

[10] M. Szalata and K. Wielgus, "Extraction of CBD and Δ9-THC from three varieties of fibre hemp by different concentrations of ethanol," *New Biotechnology*, vol. 33, p. S162, Jul. 2016.

[11] C. Da Porto, D. Voinovich, D. Decorti, and A. Natolino, "Response surface optimization of hemp seed (Cannabis sativa L.) oil yield and oxidation stability by supercritical carbon dioxide extraction," *The Journal of Supercritical Fluids*, vol. 68, pp. 45–51, Aug. 2012.

[12] D. R. Grijo, I. A. Vieitez Osorio, and L. Cardozo-Filho, "Supercritical extraction strategies using CO2 and ethanol to obtain cannabinoid compounds from Cannabis hybrid flowers," *Journal of CO2 Utilization*, vol. 28, pp. 174–180, 2018.

[13] Witkamp, G.J., Verpoorte, R., Kroon, M.C., and Perrotin-Brunel, H., "Sustainable Production of Cannabinoids with Supercritical Carbon Dioxide Technologies," Ph.D. dissertation, Apr. 2011.

[14] A. Leghissa, Z. L. Hildenbrand, and K. A. Schug, "A review of methods for the chemical characterization of cannabis natural products," *Journal of Separation Science*, vol. 41, no. 1, pp. 398–415, Jan. 2018.

[15] D. o. J. Government of Canada, "Cannabis Legalization and Regulation," Jun. 2018.

[16] A. K. Ressmann, P. Gaertner, and K. Bica, "From plant to drug: Ionic liquids for the reactive dissolution of biomass," *Green Chemistry*, vol. 13, no. 6, pp. 1442–1447, Jun. 2011.

[17] L. Romano and A. Hazekamp, "Cannabis oil: Chemical evaluation of an upcoming cannabis- based medicine," *Cannabinoids*, vol. 1, pp. 1–11, Jan. 2013.

[18] M. Ellis, "Apparatus for extracting oil from oil-bearing plants," US Patent US20 160 303 490A1, Oct., 2016.

[19] Z. Mehmedic, S. Chandra, D. Slade, H. Denham, S. Foster, A. S. Patel, S. A. Ross, I. A. Khan, and M. A. ElSohly, "Potency Trends of Δ9-THC and Other Cannabinoids in Confiscated Cannabis Preparations from 1993 to 2008," *Journal of Forensic Sciences*, vol. 55, no. 5, pp. 1209–1217, Sep. 2010.

[20] M. Taschwer and M. G. Schmid, "Determination of the relative percentage distribution of THCA and Δ9-THC in herbal cannabis seized in Austria – Impact of different storage

temperatures on stability," *Forensic Science International*, vol. 254, pp. 167–171, Sep. 2015.

[21] M. Iqbal, Y. Tao, S. Xie, Y. Zhu, D. Chen, X. Wang, L. Huang, D. Peng, A. Sattar, M. A. B. Shabbir, H. I. Hussain, S. Ahmed, and Z. Yuan, "Aqueous two-phase system (ATPS): An overview and advances in its applications," *Biological Procedures Online*, vol. 18, Oct. 2016.

[22] S. Ameur, B. Haddou, Z. Derriche, J. P. Canselier, and C. Gourdon, "Cloud point extraction of Δ9-tetrahydrocannabinol from cannabis resin," *Analytical and Bioanalytical Chemistry*, vol. 405, no. 10, pp. 3117–3123, Apr. 2013.

[23] P. Morales and P. H. Reggio, "CBD: A New Hope?" *ACS Medicinal Chemistry Letters*, vol. 10, no. 5, pp. 694–695, May 2019.

[24] S. Pisanti and M. Bifulco, "Medical Cannabis: A plurimillennial history of an evergreen," *Journal of Cellular Physiology*, vol. 234, no. 6, pp. 8342–8351, 2019.

[25] W. B. O'Shaughnessy, "On the Preparations of the Indian Hemp, or Gunjah," *Provincial Medical Journal and Retrospect of the Medical Sciences*, vol. 5, no. 123, pp. 363–369, Feb. 1843.

[26] M. Broughton, "The Prohibition of Marijuana," *Manitoba Policy Perspectives Journal*, vol. 1, no. 1, p. 14, 2014.

[27] S. C. o. C. , "R. v. Clay," Dec. 2003.

[28] C. Leos-Toro, L. Reid, Ulaina, M. SR, V. Rynard, and O. Douglas, "Tobacco Use in Canada: Patterns and Trends - Special Supplement: Cannabis in Canada," Propel Centre for Population Health Impact. University of Waterloo., Waterloo, ON, Special Supplement 2017 Edition, 2017.

[29] Ministère de la Justice, "Access to Cannabis for Medical Purposes Regulations," Oct. 2018.

[30] B. Spitzer-Rimon, S. Duchin, N. Bernstein, and R. Kamenetsky, "Architecture and Florogenesis in Female Cannabis sativa Plants," *Frontiers in Plant Science*, vol. 10, 2019.

[31] B. Shamblen, "Cannabis Flower," Sep. 2018.

[32] C. T. Hammond and P. G. Mahlberg, "Morphogenesis of Capitate Glandular Hairs of Cannabis sativa (Cannabaceae)," *American Journal of Botany*, vol. 64, no. 8, pp. 1023–1031, 1977.

[33] ——, "Morphology of Glandular Hairs of Cannabis Sativa from Scanning Electron Microscopy," *American Journal of Botany*, vol. 60, no. 6, pp. 524–528, 1973.

[34] D. Hegebarth, C. Buschhaus, M. Wu, D. Bird, and R. Jetter, "The composition of surface wax on trichomes of *Arabidopsis thaliana* differs from wax on other epidermal cells," *The Plant Journal*, vol. 88, no. 5, pp. 762–774, Dec. 2016.

[35] V. Brighenti, F. Pellati, M. Steinbach, D. Maran, and S. Benvenuti, "Development of a new extraction technique and HPLC method for the analysis of non-psychoactive cannabinoids in fibre-type Cannabis sativa L. (hemp)," *Journal of Pharmaceutical and Biomedical Analysis*, vol. 143, pp. 228–236, Sep. 2017.

[36] V. Raman, H. Lata, S. Chandra, I. A. Khan, and M. A. ElSohly, "Morpho-Anatomy of Marijuana (Cannabis sativa L.)," in *Cannabis Sativa L. - Botany and Biotechnology*, S. Chandra, H. Lata, and M. A. ElSohly, Eds. Cham: Springer International Publishing, 2017, pp. 123–136.

[37] N. Happyana, S. Agnolet, R. Muntendam, A. Van Dam, B. Schneider, and O. Kayser, "Analysis of cannabinoids in laser-microdissected trichomes of medicinal Cannabis sativa using LCMS and cryogenic NMR," *Phytochemistry*, vol. 87, pp. 51–59, Mar. 2013.

[38] C. M. Andre, J.-F. Hausman, and G. Guerriero, "Cannabis sativa: The Plant of the Thousand and One Molecules," *Frontiers in Plant Science*, vol. 7, Feb. 2016.

[39] M. A. ElSohly and D. Slade, "Chemical constituents of marijuana: The complex mixture of natural cannabinoids," *Life Sciences*, vol. 78, no. 5, pp. 539–548, Dec. 2005.

[40] O. Aizpurua-Olaizola, U. Soydaner, E. Öztürk, D. Schibano, Y. Simsir, P. Navarro, N. Etxebarria, and A. Usobiaga, "Evolution of the Cannabinoid and Terpene Content during the Growth of Cannabis sativa Plants from Different Chemotypes," *Journal of Natural Products*, vol. 79, no. 2, pp. 324–331, Feb. 2016.

[41] E. B. Russo, "Current Therapeutic Cannabis Controversies and Clinical Trial Design Issues," *Frontiers in Pharmacology*, vol. 7, no. 309, Sep. 2016.

[42] R. D. Richins, L. Rodriguez-Uribe, K. Lowe, R. Ferral, and M. A. O'Connell, "Accumulation of bioactive metabolites in cultivated medical Cannabis," *PLOS ONE*, vol. 13, no. 7, p. e0201119, 2018.

[43] "UNODC - Bulletin on Narcotics - 1972 Issue 4 - 004," //www.unodc.org/unodc/en/data-and-analysis/bulletin/bulletin_1972-01-01_4_page005.html.

[44] P. Lazzari, P. Fadda, G. Marchese, G. L. Casu, and L. Pani, "Antinociceptive activity of Δ9-tetrahydrocannabinol non-ionic microemulsions," *International Journal of Pharmaceutics*, vol. 393, no. 1, pp. 239–244, Jun. 2010.

[45] "Yaws' Handbook of Properties for Aqueous Systems - Knovel," https://app.knovel.com/web/toc.v/cid:kpYHPAS006/viewerType:toc//root_slug:yaws-handbook-properties/url_slug:yaws-handbook-properties?b-q=Yaws%26%2339%3B%20Handbook%20of%20Properties%20for%2 0Aqueous%20Systems&sort_on= default&b-group-by=true&b-sort-on=defaul t&b-content-type=all_references.

[46] H. Perrotin-Brunel, M. C. Kroon, M. J. van Roosmalen, J. van Spronsen, C. J. Peters, and G.-J. Witkamp, "Solubility of non-psychoactive cannabinoids in supercritical carbon dioxide and comparison with psychoactive cannabinoids," *The Journal of Supercritical Fluids*, vol. 55, no. 2, pp. 603–608, Dec. 2010.

[47] P. Bhatarah, D. Mchattie, and A. K. Greenwood, "Production of delta 9 tetrahydrocannabinol," WO Patent WO2 009 133 376A1, Nov., 2009.

[48] J. M. McPartland, C. MacDonald, M. Young, P. S. Grant, D. P. Furkert, and M. Glass, "Affinity and Efficacy Studies of Tetrahydrocannabinolic Acid A at Cannabinoid Receptor Types One and Two," *Cannabis and Cannabinoid Research*, vol. 2, no. 1, pp. 87–95, Jan. 2017.

[49] H. Perrotin-Brunel, W. Buijs, J. van Spronsen, M. J. E. van Roosmalen, C. Peters, R. Verpoorte, and G.-J. Witkamp, "Decarboxylation of Δ 9-tetrahydrocannabinol: Kinetics and molecular modeling," *Journal of Molecular Structure - J MOL STRUCT*, vol. 987, pp. 67–73, Feb. 2011.

[50] T. Veress, J. Szanto, and L. Leisztner, "Determination of cannabinoid acids by high-performance liquid chromatography of their neutral derivatives formed by thermal decarboxylation," *Journal of Chromatography A*, vol. 520, pp. 339–347, Nov. 1990.

[51] C. Citti, B. Pacchetti, M. A. Vandelli, F. Forni, and G. Cannazza, "Analysis of cannabinoids in commercial hemp seed oil and decarboxylation kinetics studies of cannabidiolic acid (CBDA)," *Journal of Pharmaceutical and Biomedical Analysis*, vol. 149, pp. 532–540, Feb. 2018.

[52] M. Wang, Y.-H. Wang, B. Avula, M. M. Radwan, A. S. Wanas, J. van Antwerp, J. F. Parcher, M. A. ElSohly, and I. A. Khan, "Decarboxylation Study of Acidic Cannabinoids: A Novel Approach Using Ultra-High-Performance Supercritical Fluid Chromatography/Photodiode Array-Mass Spectrometry," *Cannabis and Cannabinoid Research*, vol. 1, no. 1, pp. 262–271, Dec. 2016.

[53] "Decarboxylation of Δ9-tetrahydrocannabinol: Kinetics and molecular modeling - ScienceDirect," https://www.sciencedirect.com/science/article/pii/S0022286010009270.

[54] *The HLB System: A Time-Saving Guide to Emulsifier Selection.*

[55] D. Rubingh, *Cationic Surfactants: Physical Chemistry.* CRC Press, Oct. 1990.

[56] J. Falbe, Ed., *Surfactants in Consumer Products: Theory, Technology and Application.* Berlin Heidelberg: Springer-Verlag, 1987.

[57] "Surfactant Self-Assembly," in *Surface Chemistry of Surfactants and Polymers.* John Wiley & Sons, Ltd, 2014, pp. 75–94.

[58] S. D. Christian and J. F. Scamehorn, *Solubilization in Surfactant Aggregates.* CRC Press, Apr. 1995.

[59] I. Kralova and J. Sjöblom, "Surfactants Used in Food Industry: A Review," *Journal of Dispersion Science and Technology*, vol. 30, no. 9, pp. 1363–1383, Sep. 2009.

[60] "Interfacial Energetics," in *Emulsions, Foams, and Suspensions.* John Wiley & Sons, Ltd, 2006, pp. 53–100.

[61] P. G. Nilsson, H. Wennerstroem, and B. Lindman, "Structure of micellar solutions of nonionic surfactants. Nuclear magnetic resonance self-diffusion and proton relaxation studies of poly(ethylene oxide) alkyl ethers," *The Journal of Physical Chemistry*, vol. 87, no. 8, pp. 1377–1385, Apr. 1983.

[62] "Higher-Level Surfactant Aggregate Structures: Liquid Crystals, Continuous Biphases, and Microemulsions," in *Surfactant Science and Technology.* John Wiley & Sons, Ltd, 2005, pp. 160–190.

[63] A. A. Ribeiro and E. A. Dennis, "Structure and Dynamics by NMR and Other Methods," in *Nonionic Surfactants: Physical Chemistry*, ser. Surfactant Science Series, M. J. SCHICK, Ed. Marcel DEKKER Inc., Mar. 1987, vol. 23, pp. 971–1009.

[64] E. K. Paleologos, D. L. Giokas, and M. I. Karayannis, "Micelle-mediated separation and cloud-point extraction," *TrAC Trends in Analytical Chemistry*, vol. 24, no. 5, pp. 426–436, May 2005.

[65] W. L. Hinze and E. Pramauro, "A Critical Review of Surfactant-Mediated Phase Separations (Cloud-Point Extractions): Theory and Applications," *Critical Reviews in Analytical Chemistry*, vol. 24, no. 2, pp. 133–177, Jan. 1993.

[66] A. M. Hyde, S. L. Zultanski, J. H. Waldman, Y.-L. Zhong, M. Shevlin, and F. Peng, "General Principles and Strategies for Salting-Out Informed by the Hofmeister Series," *Organic Process Research & Development*, vol. 21, no. 9, pp. 1355–1370, Sep. 2017.

[67] A. Appusamy, K. Ponnusamy, S. Cherukuri, and A. Vijayan, "Studies on removal of Reactive Blue dye using cloud point extraction," *Int. J. Chem. Environ. Eng.*, vol. 3, pp. 16–23, Jan. 2012.

[68] R. P. Frankewich and W. L. Hinze, "Evaluation and Optimization of the Factors Affecting Nonionic Surfactant-Mediated Phase Separations," *Analytical Chemistry*, vol. 66, no. 7, pp. 944–954, Apr. 1994.

[69] V. Jordan and U. Müller, "Alternative Solvents in Plant Extraction," in *Industrial Scale Natural Products Extraction*. John Wiley & Sons, Ltd, 2011, pp. 55–86.

[70] H. Tani, T. Kamidate, and H. Watanabe, "Aqueous Micellar Two-Phase Systems for Protein Separation." *Analytical Sciences*, vol. 14, no. 5, pp. 875–888, 1998.

[71] "Emulsions," in *Surfactant Science and Technology*. John Wiley & Sons, Ltd, 2005, pp. 280–322.

[72] T. F. Tadros, "Emulsion Formation, Stability, and Rheology," in *Emulsion Formation and Stability*. John Wiley & Sons, Ltd, 2013, pp. 1–75.

[73] Y. Maphosa and V. A. Jideani, "Factors Affecting the Stability of Emulsions Stabilised by Biopolymers," *Science and Technology Behind Nanoemulsions*, Aug. 2018.

[74] "Phase Behavior of Surface-Active Solutes," https://lubrizolcdmo.com/technical-briefs/phase-behavior-of-surface-active-solutes/, Oct. 2019.

[75] MKD, "English: HLB scale showing classification of surfactant function." Aug. 2014.

[76] A. C. Leite, A. M. Ferreira, E. S. Morais, I. Khan, M. G. Freire, and J. A. P. Coutinho, "Cloud Point Extraction of Chlorophylls from Spinach Leaves Using Aqueous Solutions of Nonionic Surfactants," *ACS Sustainable Chemistry & Engineering*, vol. 6, no. 1, pp. 590–599, Jan. 2018.

[77] R. C. Pasquali, N. Sacco, and C. Bregni, "The studies on hydrophilic-lipophilic balance (HLB): Sixty years after William C. Griffin's pioneer work (1949-2009)," *Latin American Journal of Pharmacy*, vol. vol. 28, no. 2, 2009.

[78] J. A. Poce-Fatou, "A Superficial Overview of Detergency," *Journal of Chemical Education*, vol. 83, no. 8, p. 1147, Aug. 2006.

[79] K. H. Raney, W. J. Benton, and C. A. Miller, "Optimum detergency conditions with nonionic surfactants: I. Ternary water-surfactant-hydrocarbon systems," *Journal of Colloid and Interface Science*, vol. 117, no. 1, pp. 282–290, May 1987.

[80] S. K. Goel, "Measuring detergency of oily soils in the vicinity of phase inversion temperatures of commercial nonionic surfactants using an oil-soluble dye," *Journal of Surfactants and Detergents*, vol. 1, no. 2, pp. 221–226, Apr. 1998.

[81] A. A. Peña and C. A. Miller, "Solubilization rates of oils in surfactant solutions and their relationship to mass transport in emulsions," *Advances in Colloid and Interface Science*, vol. 123-126, pp. 241–257, Nov. 2006.

[82] C. A. Miller and K. H. Raney, "Solubilization—emulsification mechanisms of detergency," *Colloids and Surfaces A: Physicochemical and Engineering Aspects*, vol. 74, no. 2-3, pp. 169–215, Jul. 1993.

[83] A. Hutin, "Application Notes -Theory: 3. Detergency," Feb. 2019.

[84] A. B. Tabrizi, "Development of a cloud point extraction-spectrofluorimetric method for trace copper(II) determination in water samples and parenteral solutions," *Journal of Hazardous Materials*, vol. 139, no. 2, pp. 260–264, Jan. 2007.

[85] M. Buggert, L. Mokrushina, I. Smirnova, R. Schomäcker, and W. Arlt, "Prediction of Equilibrium Partitioning of Nonpolar Organic Solutes in Water- Surfactant Systems by UNIFAC and COSMO-RS Models," *Chemical Engineering & Technology*, vol. 29, no. 5, pp. 567–573, 2006.

[86] H. Watanabe and H. Tanaka, "A non-ionic surfactant as a new solvent for liquid—liquid extraction of zinc(II) with 1-(2-pyridylazo)-2-naphthol," *Talanta*, vol. 25, no. 10, pp. 585–589, Oct. 1978.

[87] S. S. Arya, A. M. Kaimal, M. Chib, S. K. Sonawane, and P. L. Show, "Novel, energy efficient and green cloud point extraction: Technology and applications in food processing," *Journal of Food Science and Technology*, vol. 56, no. 2, pp. 524–534, Feb. 2019.

[88] A. S. Yazdi, "Surfactant-based extraction methods," *TrAC Trends in Analytical Chemistry*, vol. 30, no. 6, pp. 918–929, Jun. 2011.

[89] B. Lindman, B. Medronho, and G. Karlström, "Clouding of nonionic surfactants," *Current Opinion in Colloid & Interface Science*, vol. 22, pp. 23–29, Apr. 2016.

[90] Q. Fang, H. W. Yeung, H. W. Leung, and C. W. Huie, "Micelle-mediated extraction and preconcentration of ginsenosides from Chinese herbal medicine," *Journal of Chromatography A*, vol. 904, no. 1, pp. 47–55, Dec. 2000.

[91] P. Trivedi, R. Singh, and K. Shanker, "Micellar Extraction and Cloud-Point Preconcentration of Labdane Diterpenoids from Andrographis Paniculata," *Journal of Liquid Chromatography & Related Technologies*, vol. 34, no. 18, pp. 2085–2102, Nov. 2011.

[92] X. Tang, D. Zhu, W. Huai, W. Zhang, C. Fu, X. Xie, S. Quan, and H. Fan, "Simultaneous extraction and separation of flavonoids and alkaloids from Crotalaria sessiliflora L. by microwave-assisted cloud-point extraction," *Separation and Purification Technology*, vol. 175, pp. 266–273, Mar. 2017.

[93] W. Xing and L. Chen, "Micelle-mediated extraction and cloud point preconcentration of bergenin from Ardisia japonica," *Separation and Purification Technology*, vol. 110, pp. 57–62, Jun. 2013.

[94] W. Liu, W.-j. Zhao, J.-b. Chen, and M.-m. Yang, "A cloud point extraction approach using Triton X-100 for the separation and preconcentration of Sudan dyes in chilli powder," *Analytica Chimica Acta*, vol. 605, no. 1, pp. 41–45, Dec. 2007.

[95] K. Stamatopoulos, E. Katsoyannos, and A. Chatzilazarou, "Antioxidant Activity and Thermal Stability of Oleuropein and Related Phenolic Compounds of Olive Leaf Extract after Separation and Concentration by Salting-Out-Assisted Cloud Point Extraction," *Antioxidants*, vol. 3, no. 2, pp. 229–244, Apr. 2014.

[96] K. Śliwa, E. Sikora, J. Ogonowski, J. Oszmiański, and J. Kolniak-Ostek, "A micelle mediated extraction as a new method of obtaining the infusion of Bidens tripartita." *Acta biochimica Polonica*, vol. 63, no. 3, pp. 543–548, 2016.

[97] C. Sun, Y. Xie, Q. Tian, and H. Liu, "Cloud Point Extraction of Glycyrrhizic Acid from Licorice Root," *Separation Science and Technology*, vol. 42, no. 14, pp. 3259–3270, Oct. 2007.

[98] Z. Shi, X. Zhu, and H. Zhang, "Micelle-mediated extraction and cloud point preconcentration for the analysis of aesculin and aesculetin in Cortex fraxini by HPLC," *Journal of Pharmaceutical and Biomedical Analysis*, vol. 44, no. 4, pp. 867–873, Aug. 2007.

[99] *HPLC Detection: Newer Methods | Wiley*, 1st ed. John Wiley & Sons, Inc., 1993.

[100] "Chromatographic Analysis of Pharmaceuticals," *Journal of Liquid Chromatography & Related Technologies*, vol. 20, no. 11, pp. 1810–1811, Jun. 1997.

[101] G. Wypych, "1 - PHOTOPHYSICS," in *Handbook of Material Weathering (Sixth Edition)*, G. Wypych, Ed. ChemTec Publishing, Jan. 2018, pp. 1–26.

[102] J. C. Sánchez-Rangel, J. Benavides, J. B. Heredia, L. Cisneros-Zevallos, and D. A. Jacobo-Velázquez, "The Folin–Ciocalteu assay revisited: Improvement of its specificity for total phenolic content determination," *Analytical Methods*, vol. 5, no. 21, pp. 5990–5999, Oct. 2013.

[103] R. M. Lamuela-Raventós, "Folin-Ciocalteu method for the measurement of total phenolic content and antioxidant capacity," in *Measurement of Antioxidant Activity & Capacity*, R. Apak, E. Capanoglu, and F. Shahidi, Eds. Chichester, UK: John Wiley & Sons, Ltd, Dec. 2017, pp. 107–115.

[104] M. Menezes Maciel Bindes, V. Luiz Cardoso, M. Reis, and D. Camilla Boffito, "Maximization of the polyphenols extraction yield from green tea leaves and sequential clarification," *Journal of Food Engineering*, vol. 241, Aug. 2018.

[105] E. A. Ainsworth and K. M. Gillespie, "Estimation of total phenolic content and other oxidation substrates in plant tissues using Folin–Ciocalteu reagent," *Nature Protocols*, vol. 2, no. 4, pp. 875–877, Apr. 2007.

[106] J. C. Sánchez-Rangel, J. Benavides, J. B. Heredia, L. Cisneros-Zevallos, and D. A. Jacobo-Velázquez, "The Folin–Ciocalteu assay revisited: Improvement of its specificity

for total phenolic content determination," *Analytical Methods*, vol. 5, no. 21, pp. 5990–5999, Oct. 2013.

[107] M. A. Makhlouf, Abdel Salam Hamdy, "XRF spectroscopy," p. 304, 2016.

[108] R. A. F. Gordon, Arnold J., "Karl fischer titration and water analysis," p. 448, 1972.

[109] S. Grünke, "Main and side reactions in the Karl Fischer solution," *Food Control*, vol. 12, no. 7, pp. 419–426, Oct. 2001.

[110] ASTM International, "ASTM D2024, Test Method for Cloud Point of Nonionic Surfactants," *West Conshohocken, PA*, 2017.

[111] V. Camel, "Recent extraction techniques for solid matrices—supercritical fluid extraction, pressurized fluid extraction and microwave-assisted extraction: Their potential and pitfalls," *The Analyst*, vol. 126, no. 7, pp. 1182–1193, 2001.

[112] World Health Organization, "Internation program on chemical safety - Sodium sulfate - WHO Food Additives Series No. 44," http://www.inchem.org/documents/jecfa/jecmono/v44jec07.htm.

[113] C. Kaur and H. C. Kapoor, "Anti-oxidant activity and total phenolic content of some Asian vegetables," *International Journal of Food Science & Technology*, vol. 37, no. 2, pp. 153–161, 2002.

[114] Z. Drinic, J. Vladic, A. Koren, T. Zeremski, N. Stojanov, B. Kiprovski, and S. Vidovic, "Microwave-assisted extraction of cannabinoids and antioxidants from Cannabis sativa aerial parts and process modeling," *Journal of Chemical Technology and Biotechnology*.

[115] N. Garti, L. S. GARTI, and R. EDRI, "Method for selective extraction of cannabinoids from a plant source," WO Patent WO2 018 061 009A1, Apr., 2018.

[116] Jorge Cervantes, "Chapter 15: Hash and Oil Making," in *Marijuana Horticulture: The Indoor/Outdoor Medical Grower's Bible*. Van Patten Publishing, 2006, pp. 381–412.

[117] T. M. Attard, C. Bainier, M. Reinaud, A. Lanot, S. J. McQueen-Mason, and A. J. Hunt, "Utilisation of supercritical fluids for the effective extraction of waxes and Cannabidiol (CBD) from hemp wastes," *Industrial Crops and Products*, vol. 112, pp. 38–46, Feb. 2018.

[118] Y. Sun, H. Zheng, J. Zhai, H. Teng, C. Zhao, C. Zhao, and Y. Liao, "Effects of Surfactants on the Improvement of Sludge Dewaterability Using Cationic Flocculants," *PLOS ONE*, vol. 9, no. 10, p. e111036, Oct. 2014.

[119] C. Papuc, V. Nicorescu, I. Gâjâilă, G. V. Goran, C. D. Petcu, and G. Stefan, "The Influence of Solid-to-Solvent Ratio and Extraction Method on Total Phenolic Content , Flavonoid Content and Antioxidant Properties of Some Ethanolic Plant Extracts," 2016.

[120] W. Rao, Y. Wang, J. Han, L. Wang, T. Chen, Y. Liu, and L. Ni, "Cloud Point and Liquid–Liquid Equilibrium Behavior of Thermosensitive Polymer L61 and Salt Aqueous Two-Phase System," *The Journal of Physical Chemistry B*, vol. 119, no. 25, pp. 8201–8208, Jun. 2015.

[121] P. Mukherjee, S. K. Padhan, S. Dash, S. Patel, and B. K. Mishra, "Clouding behaviour in surfactant systems," *Advances in Colloid and Interface Science*, vol. 162, no. 1, pp. 59–79, Feb. 2011.

[122] B. F. Thomas, D. R. Compton, and B. R. Martin, "Characterization of the lipophilicity of natural and synthetic analogs of delta 9-tetrahydrocannabinol and its relationship to pharmacological potency," *The Journal of Pharmacology and Experimental Therapeutics*, vol. 255, no. 2, pp. 624–630, Nov. 1990.

[123] F. Ravera, M. Ferrari, L. Liggieri, R. Miller, and A. Passerone, "Measurement of the Partition Coefficient of Surfactants in Water/Oil Systems," *Langmuir*, vol. 13, no. 18, pp. 4817–4820, Sep. 1997.

[124] C. R. Parish, B. J. Classon, J. Tsagaratos, I. D. Walker, L. Kirszbaum, and I. F. C. McKenzie, "Fractionation of detergent lysates of cells by ammonium sulphate-induced phase separation," *Analytical Biochemistry*, vol. 156, no. 2, pp. 495–502, Aug. 1986.

[125] K. Iffland, M. Carus, and F. Grotenhermen, "Decarboxylation of Tetrahydrocannabinolic acid (THCA) to active THC," *European Industrial Hemp Association*, pp. 1–3, Oct. 2016.

[126] Y. Zhang and P. S. Cremer, "Interactions between macromolecules and ions: The Hofmeister series," *Current Opinion in Chemical Biology*, vol. 10, no. 6, pp. 658–663, Dec. 2006.

[127] P. Palladino and R. Ragone, "Ionic Strength Effects on the Critical Micellar Concentration of Ionic and Nonionic Surfactants: The Binding Model," *Langmuir*, vol. 27, no. 23, pp. 14 065–14 070, Dec. 2011.

[128] S. Paria and K. C. Khilar, "A review on experimental studies of surfactant adsorption at the hydrophilic solid–water interface," *Advances in Colloid and Interface Science*, vol. 110, no. 3, pp. 75–95, Aug. 2004.

[129] J. Zhao and W. Brown, "Comparative Study of the Adsorption of Nonionic Surfactants: Triton X-100 and C $_{12}$ E $_{7}$ on Polystyrene Latex Particles Using Dynamic Light Scattering and Adsorption Isotherm Measurements," *The Journal of Physical Chemistry*, vol. 100, no. 9, pp. 3775–3782, Jan. 1996.

[130] P. Somusundurun and L. Huung, "Thermodynamics of adsorption of surfactants a t solid-I iquid interface," *Pure & Appl. Chem.*, vol. 70, no. 3, pp. 621–626, 1998.

[131] Sigma-Aldrich, Inc., "Triton X-100 Data Sheet," https://www.sigmaaldrich.com/content/dam/sigma-aldrich/docs / Sigma/Product_Information_Sheet/1/t8532pis.pdf.

[132] C. Agarwal, K. Máthé, T. Hofmann, and L. Csóka, "Ultrasound-Assisted Extraction of Cannabinoids from *Cannabis Sativa* L. Optimized by Response Surface Methodology: Extraction of cannabinoids. . . ," *Journal of Food Science*, vol. 83, no. 3, pp. 700–710, Mar. 2018.

[133] C.-W. Chang, C.-C. Yen, M.-T. Wu, M.-C. Hsu, and Y.-T. Wu, "Microwave-Assisted Extraction of Cannabinoids in Hemp Nut Using Response Surface Methodology: Optimization and Comparative Study," *Molecules*, vol. 22, no. 11, p. 1894, Nov. 2017.

[134] V. Brighenti, F. Pellati, M. Steinbach, D. Maran, and S. Benvenuti, "Development of a new extraction technique and HPLC method for the analysis of non-psychoactive cannabinoids in fibre-type Cannabis sativa L. (hemp)," *Journal of Pharmaceutical and Biomedical Analysis*, vol. 143, pp. 228–236, Sep. 2017.

[135] B. Khadhraoui, M. Turk, A. Fabiano-Tixier, E. Petitcolas, P. Robinet, R. Imbert, M. El Maâtaoui, and F. Chemat, "Histo-cytochemistry and scanning electron microscopy for 3 studying spatial and temporal extraction of metabolites induced by ultrasound. Towards chain detexturation mechanism." *Ultrasonics Sonochemistry*, vol. 42, Nov. 2017.

[136] E. H. Papaioannou and A. J. Karabelas, "Lycopene recovery from tomato peel under mild conditions assisted by enzymatic pre-treatment and non-ionic surfactants," *Acta Biochimica Polonica*, vol. 59, no. 1, pp. 71–74, 2012.

[137] R. Hosseinzadeh, K. Khorsandi, and S. Hemmaty, "Study of the Effect of Surfactants on Extraction and Determination of Polyphenolic Compounds and Antioxidant Capacity of Fruits Extracts," *PLOS ONE*, vol. 8, no. 3, p. e57353, Mar. 2013.

[138] J. Li and H. Tang, "A theoretical calculation model for the acidification capacity of natural waters," *Science of The Total Environment*, vol. 212, no. 2, pp. 163–172, Apr. 1998.

[139] M. Kassing, U. Jenelten, J. Schenk, and J. Strube, "A New Approach for Process Development of Plant-Based Extraction Processes," *Chemical Engineering & Technology*, vol. 33, no. 3, pp. 377–387, 2010.

[140] R. Sharma, "Surfactants: Basics and Versatility in Food Industries," vol. 2, pp. 17–29, Oct. 2018.

[141] S. Zivovinovic, R. Alder, M. D. Allenspach, and C. Steuer, "Determination of cannabinoids in Cannabis sativa L. samples for recreational, medical, and forensic purposes by reversed-phase liquid chromatography-ultraviolet detection," *Journal of Analytical Science and Technology*, vol. 9, no. 1, p. 27, Nov. 2018.

[142] J. R. Dulley and P. A. Grieve, "A simple technique for eliminating interference by detergents in the Lowry method of protein determination," *Analytical Biochemistry*, vol. 64, no. 1, pp. 136–141, Mar. 1975.

APPENDIX A STABILITY TEST

Our laboratory setup could not be adapted for sterile experiments and samples were subject to microbiological contamination. Assessing the stability allowed us to store our samples in case of fail or delayed analysis.

A 2 mL extract sample was stored at 4 °C for two weeks. We punctually performed FC (figure A.1a) and HPLC-UV (figure A.1b) analysis to assess TPC, THC and CBD content.

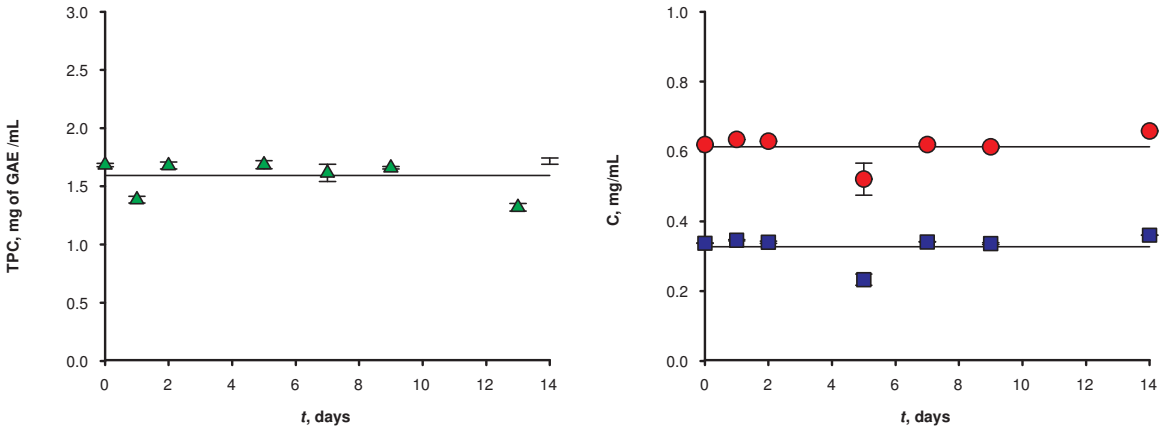

(a) (b)

Figure A.1 14 days stability test. **(a)** Total phenolic concentration ($n = 3$). **(b)** THC and CBD concentration ($n = 2$).

Initial TPC, THC and CBD content were respectively of $1.68 \pm 0.01\,\mathrm{mg_{GAE}\,mL^{-1}}$, $0.619 \pm 0.001\,\mathrm{mg\,mL^{-1}}$ and $0.3371 \pm 0.0006\,\mathrm{mg\,mL^{-1}}$. These concentrations did not deviate over the test period proving that the raw extract was suitable for long-term storage.

APPENDIX B HPLC-UV

Method development

The suitable wavelength for detection was determined using UV/Vis spectrophotometry. The absorbance spectra of standard solutions of THC, CBD and X-100 between wavelengths of 200 nm to 900 nm were quantified using Evolution 220 UV/Vis spectrophotometer (Thermo Scientific, MA, US) and expressed as a percentage of the maximum absorbance (appendix B). Base on the spectrograms, a detection wavelength was set at 235 nm. Although at lower

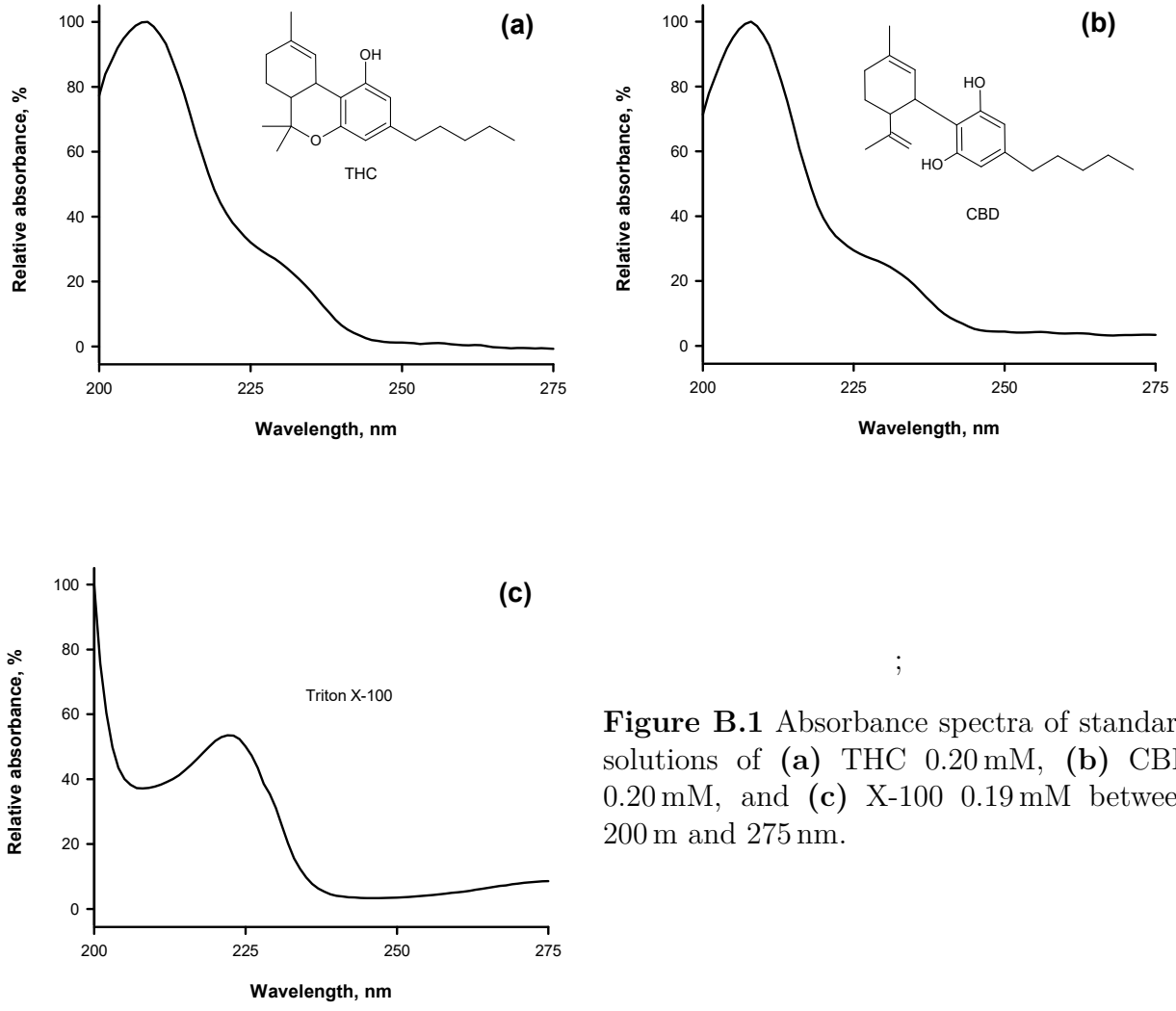

;

Figure B.1 Absorbance spectra of standard solutions of **(a)** THC 0.20 mM, **(b)** CBD 0.20 mM, and **(c)** X-100 0.19 mM between 200 m and 275 nm.

wavelength, absorbance continues to improves for all three compounds, interference with the

eluant (high in methanol) saturated the UV detector of our Prostar HPLC system.

?? presents the chromatograms obtained for cannabinoid (THC, CBD and CBN) and X100 standard solutions. We experimented with multiple eluant compositions, elution flow rates and temperatures to obtain the suitable separation between each peaks. Finally, we confirmed th peak elution time by spiking the extracted solutions with small volumes of standards containing each individual cannabinoids [141].

HPLC-UV method

HPLC calibration lines were traced for THC, CBD, CBN and Triton X-100. THC, CBD, CBN mixture calibration standard were obtained from Sigma-Aldrich in 1 mL aliquots of $1.000\,\mathrm{mg\,mL^{-1}}$ in methanol. The standards were dissolved in appropriate amounts of methanol to yield concentrations of $0.01\,\mathrm{mg\,mL^{-1}}$ to $0.10\,\mathrm{mg\,mL^{-1}}$. Triton X-100 calibration standards were prepared in house by dissolving the reagent until concentrations of $0.333\,\mathrm{mg\,mL^{-1}}$ to $1.70\,\mathrm{mg\,mL^{-1}}$. The standards were injected in the HPLC and the resulting chromatogram were integrated in Varian ProStar 6.41 Software and use to trace calibration lines (figures B.2 and B.3). Abscissa of the calibration graphs corresponds to the total area under the peak corresponding to each compound while the Y axis correspond to the volumetric concentration.

Sample calculation

Mass concentration of extract samples were determined by interpolating integration area of peaks with calibration curves. One of the replicate at 25 °C, shown in our temperature tests (figure 5.6), is used for this example. The density of the extract was assumed equal to that of water at room temperature ($\rho_{ext}^{21\,^{\circ}\mathrm{C}} = 0.998\mathrm{g\,mL^{-1}}$).

Table B.1 Calibration constants and raw data

Sample Raw Data		
A	20833430	AU
m_{pm}	0.3005	g
m^{ext}	28.4700	g
DF	10	

Calibration Constants		
α_{THC}	558770934	$\mathrm{mL\,AU^{-1}\,mg^{-1}}$
β_{THC}	-549944	AU

From equation (4.7), THC concentration in the diluted sample is obtained as follows:

$$\gamma_{THC}^{dil} = \frac{A - \beta_{THC}}{\alpha_{THC}} = \frac{20\,833\,430\,\mathrm{AU} - (-549\,944\,\mathrm{AU})}{558\,770\,934\,\mathrm{mL\,AU^{-1}\,mg^{-1}}} = 0.0383\,\mathrm{mg\,mL^{-1}} \tag{B.1}$$

The concentration of the extract is then:

$$\gamma_{THC}^{ext} = \gamma_{THC}^{dil} \times DF = 0.0383\,\mathrm{mg\,mL^{-1}} \times 10 = 0.383\,\mathrm{mg\,mL^{-1}} \tag{B.2}$$

Finally, THC yield is calculated as follows, according to:

$$Y_{THC} = \frac{\gamma_{THC}^{ext}\, m^{ext}}{m^{pm}\, \rho_{ext}^{21\,^{\circ}\mathrm{C}}} = \frac{0.382\,\mathrm{mg\,mL^{-1}} 28.4700\,\mathrm{g}}{0.3005\,\mathrm{g} 0.998\,\mathrm{g\,mL^{-1}}} = 36.3\,\mathrm{mg\,g^{-1}} \tag{B.3}$$

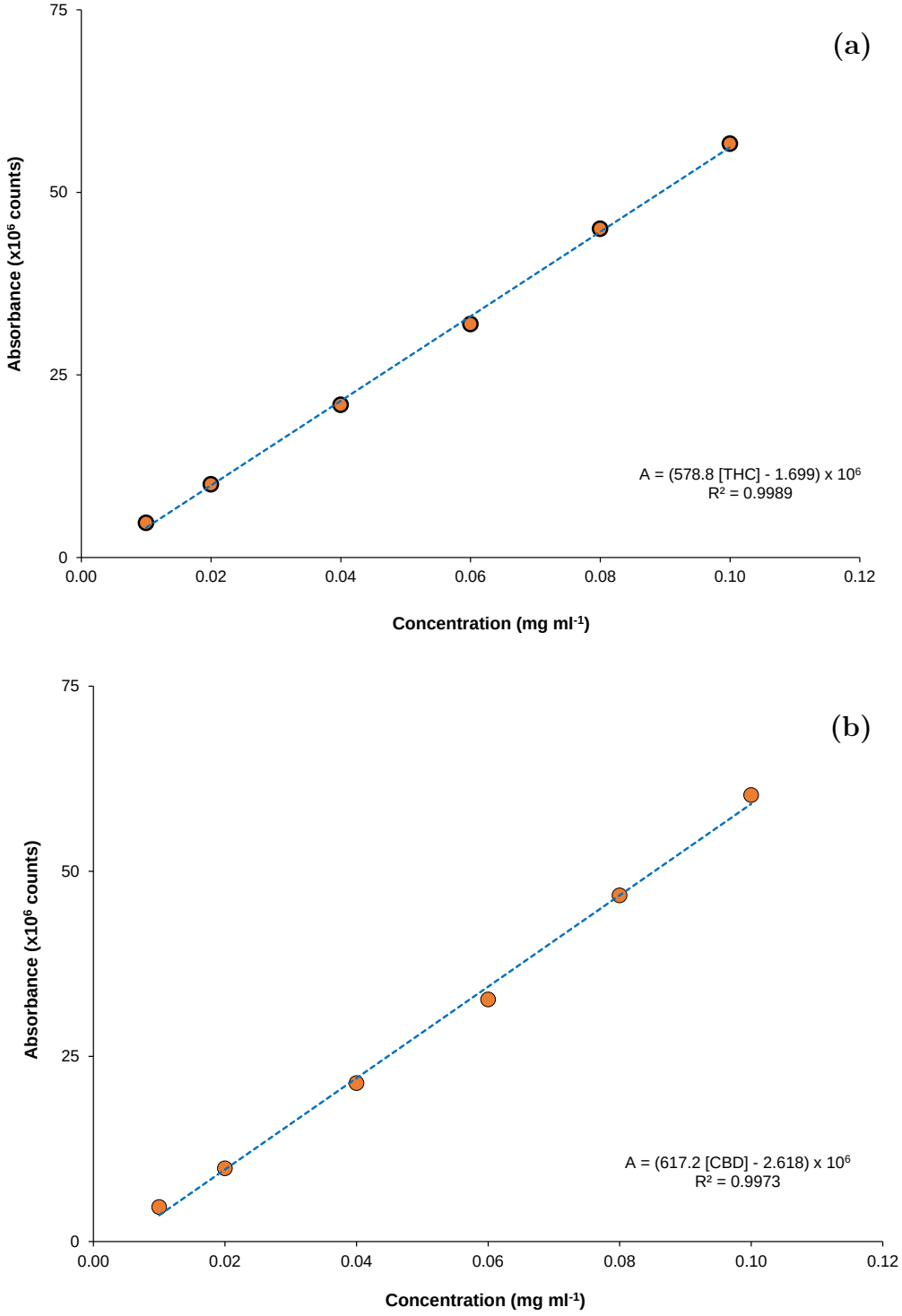

Figure B.2 Sample calibration lines for **(a)** THC and **(b)** CBD

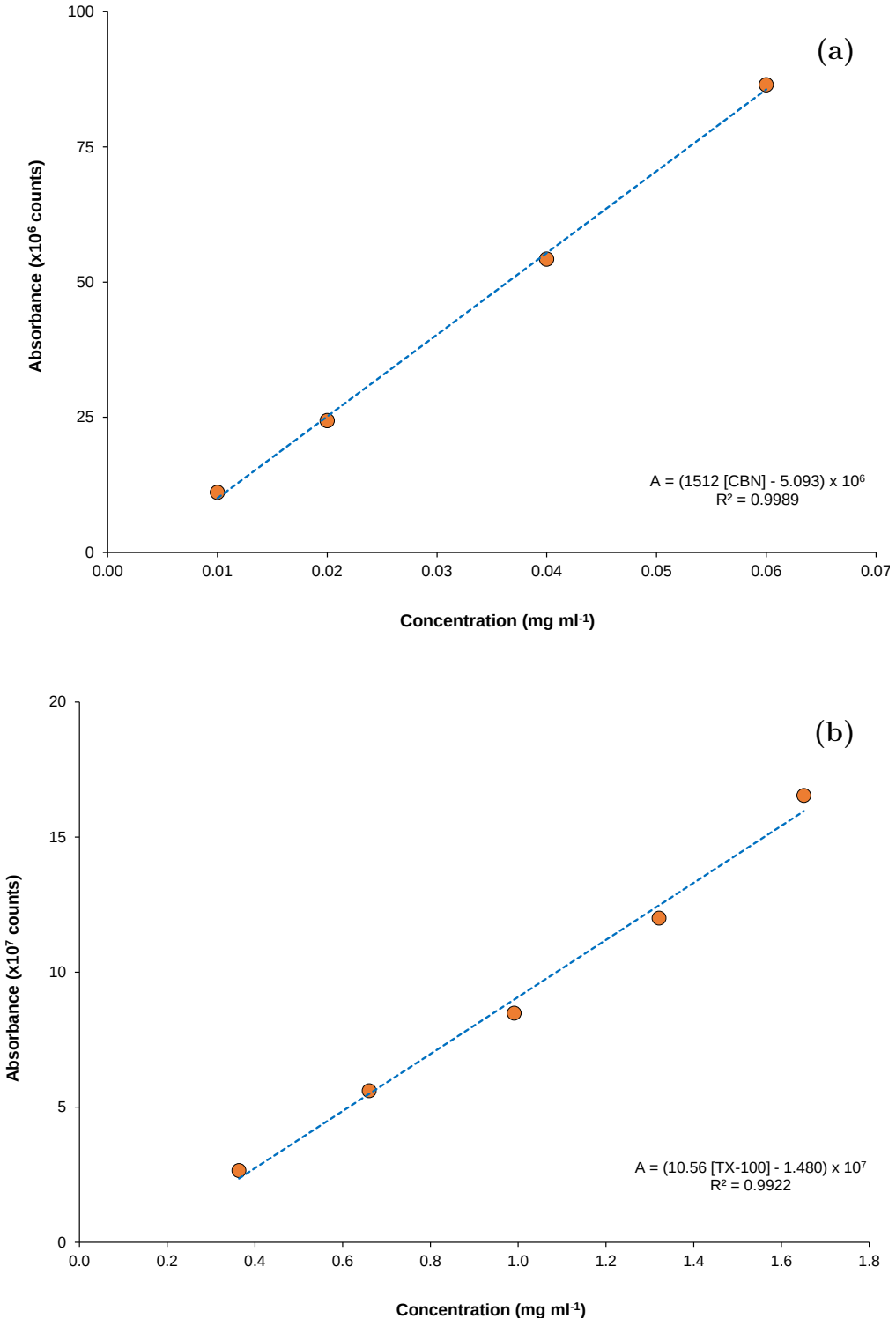

Figure B.3 Sample calibration lines for **(a)** CBN and **(b)** X100.

Sample chromatograph

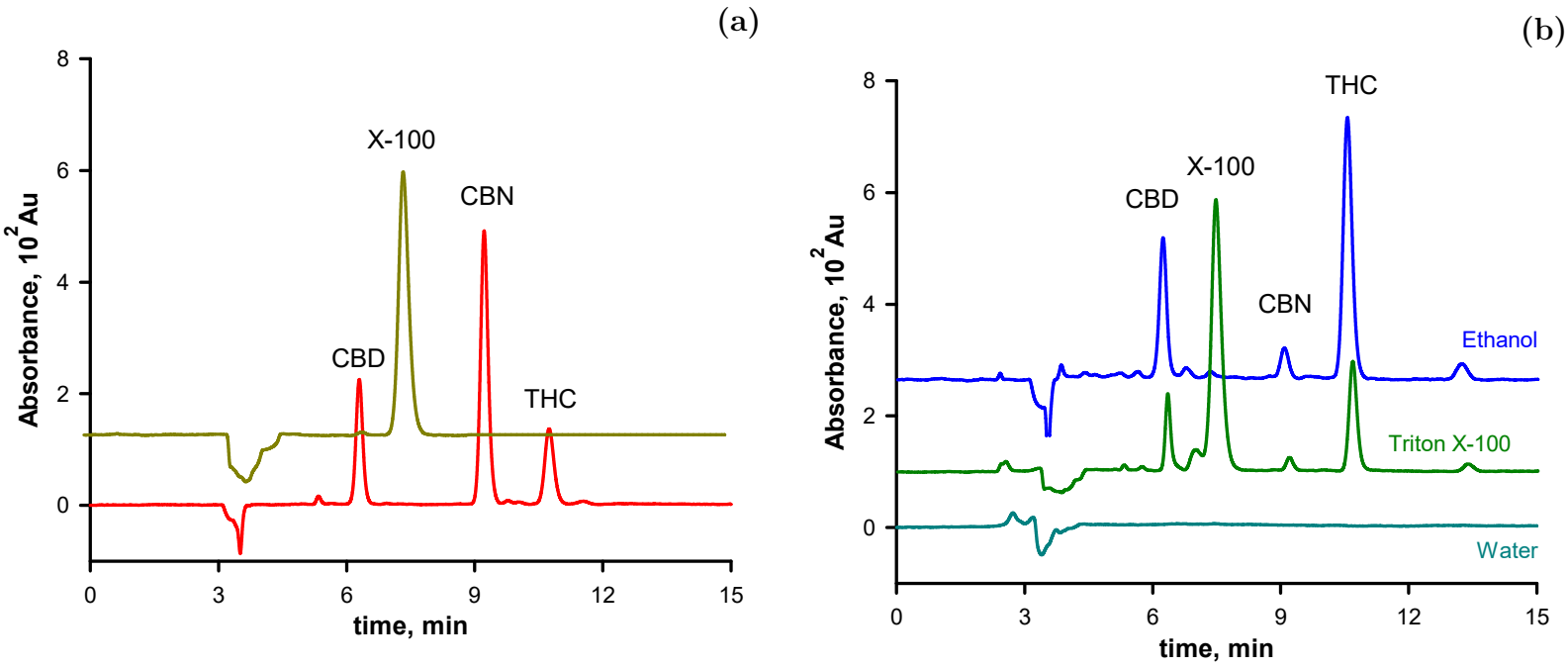

Figure B.4 Chromatograph of **(a)** pure analytical standards and **(b)** extracts in various solvents. Time dependance of adsorbance were obtained at 235 nm by eluting CH3-OH:H2O:CH3-COOH (volume ratios of 85:14.2:0.8) at a flow rate of 0.8 mL min^{-1} in a C18 column heat to 28 °C. Absorption of the carrier solvent is responsible for the trough at 3 minutes. Clear separation between the four compounds of interest can be observed.

APPENDIX C FOLIN-CIOCALTEU METHOD

Method development

The initial Folin-Ciocalteu method we employed was adapted from Bindes et al. [104] . However, surfactants in the extract caused the formation of yellow precipiate upon addition of alkaline Na_2CO_3 (figure C.1a). Dulley and Grieve [142] observed similar precipitation during Lowry assay for protein determination. X100 concentration above 0.15 wt.% caused significant reduction in absorbance. The interference was resolved by adding anionic surfactant to the mixture. This provided negative charge to the surfactant aggregates which renders them more soluble at high pH, yielding a translucent sample after color development. Hence, in our revised FC method, anionic sodium dodecylsulfate (SDS) was incorporated prior to Na_2CO_3 which prevented the precipitation (figure C.1b).

(a) (b)

Figure C.1 FC samples after 1 h of color development following methods by **(a)** Bindes' and **(b)** the one develop by us.

Table C.1 Folin-Ciocalteu method validation

	Without SDS		With SDS		
	H2O	EtOH Extract	H2O	EtOH Extract	X-100 1 wt.%
Absorbance, Au	0.031	0.106	0.031	0.108	0.033
Standard deviation, Au	0.000	0.004	0.000	0.003	0.002

To validate the new FC method, we compared it with the method were no SDS was added by replacing the 50 µL sample with H_2O and EtOH extracts. The absorbance of each sample

was measured twice (table C.1). The latter of which did not show signs of precipitation with or without SDS. Both methods were within experimental errors, demonstrating that the added anionic surfactant remained. Performing the same test at 1 wt.% X-100 resulted in an absorbance of 0.033 ± 0.002 Au, similar to the 0.031 AU of the blanks. This further demonstrates that the solubilized X-100 did not cause a response shift in absorbance.

Protocol

In a 4 mL vial, samples where added in the following order.

Bindes' method

1. 50 µL of tested sample
2. 250 µL FC reagent
3. 1000 µL Na_2CO_3 10 % by weight
4. 2700 µL distilled water

Method developed by us

1. 50 µL of tested sample
2. 1000 µL SDS 5000 ppm
3. 250 µL FC reagent
4. 1000 µL Na_2CO_3 10 % by weight
5. 1700 µL distilled water

Following 1 h of color development shielded from light, a spectrophotometer acquired the absorbance at λ=620 nm. TPC calculations were identical to those of THC and CBD one concentration was obtained (appendix B).

Calibration curve

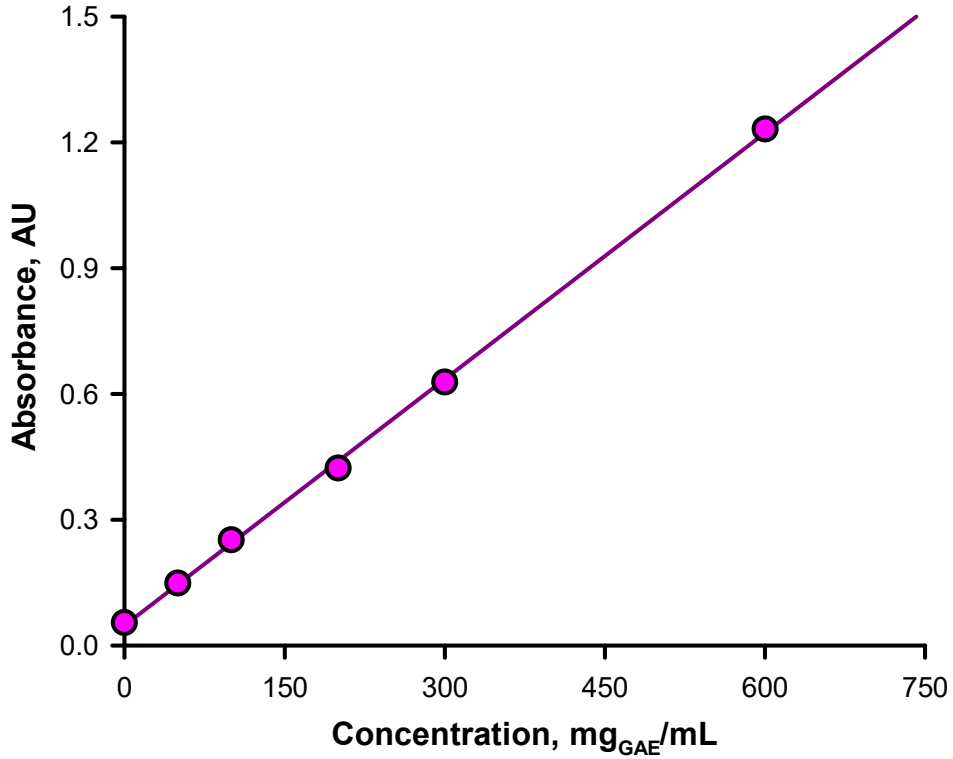

Figure C.2 FC sample calibration graph obtained at 760 nm from 0 mg_{GAE}/mL to 600 mg_{GAE}/mL

APPENDIX D KARL-FISHER METHOD

Calculation example

Table D.1 Karl-Fisher sample calculation data

m^{md}	$0.8864\,\mathrm{g}$
m^{co}	$0.0944\,\mathrm{g}$
$w_{H_2O}^{co'}$	0.0598
$w_{H_2O}^{md}$	0.007 ± 1

From **??**:

$$w_{H_2O}^{co} = \frac{(m^{co} + m^{md}) \times w_{H_2O}^{co'} - m^{md}\, w_{H_2O}^{md}}{m^{co}} \tag{D.1}$$

$$w_{H_2O}^{co} = \frac{(0.0944 + 0.8864) \times 0.0598 - 0.8864 \times 0.007}{0.0944} \tag{D.2}$$

$$w_{H_2O}^{co} = 0.503 = 50.3\,\% \tag{D.3}$$

APPENDIX E CLOUD POINT SEPARATION: ADDITIONAL INFORMATION

Assumptions

The following hypotheses are made for quantification of the species within the extract. Due to its dilute nature, specific mass, $\rho_{ext}^{21\,^{\circ}\mathrm{C}}$, were assumed equal to that of the initial solvents used at 21 °C. Slight deviations from this hypothesis do not affect data interpretation given a sufficiently large variation in the response.

Detailed procedure

The CPS of 14 mL extract samples generated coacervate of less than 1 mL. In order to accurately quantify THC, CBD, TPC and water content, calculations were paired with a rather complex series of manipulation. Here, we detail the procedure in greater detail in order to provide clarity and better understanding of the examples in the following section.

Due to practical limitations, we maintained centrifugation temperature and speed at 95 °C and 4000 rpm, promoting a clear and defined interface between water and surfactant. Below these conditions, accurately separating the two phases, either by pouring or using a syringe as suggested by [87], becomes considerably more difficult. Specifically, it resulted in non-homogeneous and water-high coacervate which, due to its reduced viscosity, inclined to mix into the supernatant upon disturbances to the centrifuge tube. Combined with the small sample volumes this contributed to increased data errors. As such, we restrained the study of the effect of the electrolyte by varying concentration was studied in this section.

1. We pre-weighted 15 mL empty centrifuge tubes (m^t) and added varying masses of extract (m^{ext}) and sodium sulfate to yield approximately 14 g of mixtures (m^{mix}) with salt weight fraction ranging from 1 % to 4 %. A vortex homogenized the content of the tube until the sodium sulfate completely dissolved. We then submitted the centrifuge tube to the CPS procedure described in section 4.4.2).

2. Following centrifugation, we placed the tubes in an ice-bath for 10 min, cooling it to approximately 5 °C. This increases the viscosity of the coacervate and the water phase was easily removed by pouring. We then carefully wiped-off excess water from the outer walls of the centrifugal tube and measured the combined weight of the coacervate and the tube ($m^{tube+co}$) .

3. To homogenize the content of the tube, we stirred the content of the tube using the tips of a volumetric micro-dispenser (Drummond, United States). The same micro-dispenser then removed 100 µL of the surfactant phase which was set aside for Karl-Fisher analysis. We weighted then once again obtained the combined weight of the remaining coacervate and the tube ($m^{tube+co\prime}$) .

4. Using the graduations on the centrifugal tube, we brought its liquid volume to approximately 10 mL by addition of distilled water. The tube was homogenized to ensure the dissolution of the surfactant phase and weighted ($m^{tube+co\prime\prime}$).

The dilution of step item 4 was necessary due to the viscosity from the high viscosity of surfactants, which could not be fully recovered by other methods. Full recovery was necessary for mass balance. Additionally, due to the small volume of coacervate, no available method enabled density measurements. We further benefit from a dilute solution as it reasonably allow to assume that the density mixture equals that of water at room temperature ($\rho^{t+co\prime\prime}(21\,°\mathrm{C}) = \rho_{H2O}(21\,°\mathrm{C}) = 0.998\,\mathrm{g\,mL^{-1}}$). Consequently to the protocol described, we expressed the content of each phase as a mass fraction (w_j^i in $\mathrm{mg\,g^{-1}}$) and the concentration factor (Fmc_j) as the ratio of the mass fraction in the coacervate over that in the mix (**??**). It is worth pointing out that, in published literature, it is standard practice to express these values on a volumetric basis.

$w^{ext}_{Na_2CO_4}$, %	$\bar{X}^{co}_{THC}$, %	$\bar{X}^{co}_{CBD}$, %	$\bar{X}^{co}_{X100}$, %	$\bar{X}^{co}_{TPC}$, %
0	98.3 ± 0.3	96.7 ± 0.3	95.79 ± 0.04	78 ± 1
1	95.3 ± 0.4	94.7 ± 0.5	93.23 ± 0.25	76.30 ± 0.01
2	96.8 ± 1.4	95.3 ± 1.3	93.97 ± 1.22	79 ± 2
3	91.8 ± 1.4	91.4 ± 1.6	89.81 ± 1.23	72 ± 1
4	76.6 ± 0.3	77.3 ± 0.9	76.21 ± 0.48	61.8 ± 0.4
$w^{ext}_{Na_2CO_4}$, %	$\bar{Fmc}^{co}_{THC}$	$\bar{Fmc}^{co}_{CBD}$	$\bar{Fmc}^{co}_{X-100}$	$\bar{Fmc}^{co}_{TPC}$
0	25.0 ± 0.4	24.6 ± 0.3	24.4 ± 0.3	16.4 ± 0.4
1	29.3 ± 0.3	29.06 ± 0.06	28.6 ± 0.1	19.286 ± 0.004
2	30.6 ± 0.6	30.1 ± 0.6	29.7 ± 0.5	20.3 ± 0.4
3	31.2 ± 0.8	31.1 ± 0.8	30.5 ± 0.7	19.8 ± 0.3
4	30.7 ± 0.9	31.0 ± 0.6	30.5 ± 0.8	19.9 ± 0.6

Table E.1 Average recovery and mass concentration factor of CPS at different weight fractions of Na_2SO_4 (n=2)

$w^{ext}_{Na_2CO_4}$, %	$\bar{w}^{co}_{THC}$, mg g^{-1}	$\bar{w}^{co}_{CBD}$, mg g^{-1}	$\bar{w}^{co}_{X100}$, mg g^{-1}	$\bar{w}^{co}_{TPC}$, mg g^{-1}	$\bar{w}^{co}_{H_2O}$, %
0	16.5 ± 0.3	2.45 ± 0.03	507 ± 7	5.1 ± 0.1	61 ± 3
1	19.1 ± 0.2	2.867 ± 0.006	589 ± 3	5.906 ± 0.001	50.7 ± 0.7
2	19.8 ± 0.4	2.95 ± 0.06	606 ± 10	6.2 ± 0.1	48.2 ± 0.6
3	20.0 ± 0.5	3.01 ± 0.08	620 ± 10	5.96 ± 0.08	47.8 ± 0.8
4	19.4 ± 0.6	2.97 ± 0.06	610 ± 20	5.9 ± 0.2	49 ± 1

Table E.2 Average composition of the extract at different weight fractions of Na_2SO_4 (n=2)

Results

Calculation example

Calculations examples are provided for THC content during experiment CP3. Weight fractions, recovery and mass concentration factors were similarly obtained for CBD, X100 and TPC.

Initial raw extract contents We first obtain the total mass of each compound within the initial mixture. As only Na_2SO_4 is added, the mass balance gives : $m_j^{mix} = m_j^{ext}$. Therefore, from the initial concentrations and the extract's weight:

$$m_j^{mix} = m_j^{ext} = \gamma_j^{mix} * \frac{m^{mix}}{\rho_{\mathrm{H_2O}}^{21}} \tag{E.1}$$

$$m_{THC}^{mix} = 0.6578\,\mathrm{mg\,mL^{-1}} * \frac{14.2035\,\mathrm{g}}{0.997\,992\,\mathrm{g\,mL^{-1}}} = 9.36\,\mathrm{mg} \tag{E.2}$$

Coacervate content We then compute total mass of each compound within the coacervate. As a fraction of the coacervate was removed for water content quantification using Karl-Fisher titration, a mass balance must be performed to account for lost fraction.

To obtain the mass of the coacervate samples, we subtract the mass of the centrifugal tube m^t to that of the weighted mass of the combined tube and coacervate $m^{tube+co}$.

$$m^{co} = m^{tube+co} - m^t = 7.2584\,\mathrm{g} - 6.6841\,\mathrm{g} = 0.5743\,\mathrm{g} \tag{E.3}$$

The same calculation is repeated after removing the sample of Karl-Fisher titration and after diluting in water.

$$m^{co\prime} = m^{tube+co\prime} - m^t = 0.4707 \pm 0.0001\,\mathrm{g} \tag{E.4}$$

Compound	Concentration
γ_{THC}^{ext}	$0.6578 \pm 0.0003\,\mathrm{mg\,mL^{-1}}$
γ_{CBD}^{ext}	$0.0995 \pm 0.0005\,\mathrm{mg\,mL^{-1}}$
C_{X100}^{ext}	$20.74 \pm 0.08\,\mathrm{mg\,mL^{-1}}$
γ_{TPC}^{ext}	$0.31 \pm 0.01\,\mathrm{mg_{GAE}\,mL^{-1}}$

Table E.3 Raw extract composition

$$m^{co\prime\prime} = m^{tube+co\prime\prime} - m^t = 9.9624 \pm 0.0001\,\mathrm{g} \tag{E.5}$$

During step 3, assuming homogeneity in the coacervate before a fraction was removed for Karl-Fisher titration, the mass fraction of each compound remains the same. Hence, for each species non-water j we have:

$$w_j^{co\prime} = w_j^{co} \tag{E.6}$$

$$\frac{w_j^{co\prime}}{m^{co\prime}} = \frac{w_j^{co}}{m^{co}} \tag{E.7}$$

$$w_j^{co} = w_j^{co\prime} * \frac{m^{co\prime}}{m^{co}} \tag{E.8}$$

Additonally, during step 4, only water is added. The mass balance on individual species i gives:

$$w_j^{co\prime} = w_j^{co\prime\prime} = c_j^{co\prime\prime} * \frac{m^{co\prime\prime}}{\rho^{21}_{\mathrm{H_2O}}} \tag{E.9}$$

Hence, combining equation (E.8) and equation (E.9):

$$w_j^{co} = c_j^{co\prime\prime} * \frac{m^{co\prime\prime}}{\rho^{21}_{\mathrm{H_2O}}} * \frac{m^{co\prime}}{m^{co}} \tag{E.10}$$

For sample CP3 and THC,

$$m^{co}_{THC} = \frac{0.4707\,\mathrm{g} * 0.5743\,\mathrm{g} * 0.997\,992\,\mathrm{g\,mL^{-1}}}{0.729\,\mathrm{mg\,mL^{-1}} * 9.9624\,\mathrm{g}} = 8.88\,\mathrm{mg} \tag{E.11}$$

Recovery, weight fraction and mass concentration factor Knowing the mass of each compound within the mixed extract (m_j^{mix}) and the coacervate (w_j^{co}), the percentage mass recovery is obtained with:

$$X_j = \frac{w_j^{co}}{m_j^{mix}} * 100\,\% \tag{E.12}$$

The mass fraction in the coacervate is obtained as follow:

$$w_j^{co} = \frac{w_j^{co}}{m^{co}} \tag{E.13}$$

The concentration factor is herein expressed as the ratio of weight fractions. We first estimate the weight fraction of each species in the initial mixture.

$$w_j^{mix} = \frac{m_j^{mix}}{m^{mix}} \tag{E.14}$$

The concentration factor is then given by:

$$Fmc_j = \frac{w_j^{co}}{w_j^{mix}} \tag{E.15}$$

For THC in sample CP3,

$$X_{THC}^{co} = \frac{8.88\,\mathrm{mg}}{9.36\,\mathrm{mg}} * 100\,\% = 94.9\,\% \tag{E.16}$$

$$w_{THC}^{co} = \frac{8.88\,\mathrm{mg}}{0.5743\,\mathrm{g}} = 18.9\,\mathrm{mg\,g^{-1}} \tag{E.17}$$

$$w_{THC}^{mix} = \frac{9.36\,\mathrm{mg}}{13.6637\,\mathrm{g}} = 0.653\,\mathrm{mg\,g^{-1}} \tag{E.18}$$

$$Fmc_{THC} = \frac{18.9\,\mathrm{mg\,g^{-1}}}{0.653\,\mathrm{mg\,g^{-1}}} = 28.9 \tag{E.19}$$

Mass balance validation

In order to validate our method, we performed mass balance calculation (table E.7) before and after CPS.

Raw data

Sample	$w^{ext}_{Na_2CO_4}$, %	m^{ext}, g	$m_{\mathrm{Na_2SO_4}}$, g	m^{mix}, g
CP1	0	14.2807	0.0000	14.2807
CP2	0	14.0796	0.0000	14.0796
CP3	1	14.2035	0.1407	14.3442
CP4	1	14.2160	0.1411	14.3571
CP5	2	14.1129	0.2829	14.3958
CP6	2	14.5601	0.2825	14.8426
CP7	3	13.9936	0.4230	14.4166
CP8	3	13.9352	0.4204	14.3556
CP9	4	13.7666	0.5636	14.3302
CP10	4	13.6686	0.5611	14.2297

Table E.4 Sodium sulfate and starting mass of mixtures

Sample	$m^{tube+co}$, g	$m^{tube+co\prime}$, g	$m^{tube+co\prime\prime}$, g	$\gamma^{co\prime\prime}_{THC}$, mg mL^{-1}	$\gamma^{co\prime\prime}_{CBD}$, mg mL^{-1}	$\gamma^{co\prime\prime}_{X100}$, mg mL^{-1}	$\gamma^{co\prime\prime}_{TPC}$, mg$_{\mathrm{GAE}}$ mL^{-1}
CP1	7.3469	7.2277	16.5815	0.770	0.114	23.6	0.291
CP2	7.3467	7.2318	16.5791	0.761	0.114	23.4	0.280
CP3	7.2584	7.1548	16.6465	0.729	0.111	22.7	0.278
CP4	7.292	7.1816	16.6184	0.730	0.109	22.4	0.276
CP5	7.2857	7.1772	16.6653	0.720	0.107	22.1	0.278
CP6	7.2245	7.0967	16.7393	0.730	0.109	22.3	0.290
CP7	7.1874	7.0775	16.6287	0.663	0.100	20.5	0.252
CP8	7.1792	7.0594	16.601	0.667	0.101	20.5	0.253
CP9	7.1558	7.0492	16.6772	0.540	0.083	17.0	0.211
CP10	7.1165	7.0101	16.7463	0.520	0.079	16.3	0.207

Table E.5 Coacervate measured weights and composition

Sample	X^{co}_{THC} %	X^{co}_{CBD} %	X^{co}_{X100} %	X^{co}_{TPC} %	w^{co}_{THC} mg g^{-1}	w^{co}_{CBD} mg g^{-1}	w^{co}_{X-100} mg g^{-1}	w^{co}_{TPC} mg g^{-1}	$Fmc^{mc,co}_{THC}$	$Fmc^{mc,co}_{CBD}$	$Fmc^{mc,co}_{X-100}$	$Fmc^{mc,co}_{TPC}$
CP1	98.7	96.3	95.8	79.4	16.8	2.48	513	5.23	25.5	24.9	24.7	16.9
CP2	98.0	97.0	95.8	76.7	16.2	2.42	500	4.95	24.6	24.3	24.0	16.0
CP3	94.9	95.1	93.5	77.0	18.9	2.86	586	5.91	28.9	29.0	28.5	19.3
CP4	95.7	94.2	93.0	77.1	19.3	2.87	592	5.91	29.6	29.1	28.8	19.3
CP5	95.4	94.0	92.8	78.3	19.4	2.89	594	6.05	30.0	29.6	29.2	20.0
CP6	98.2	96.6	95.2	82.9	20.2	3.00	617	6.29	31.2	30.7	30.3	20.7
CP7	90.4	89.8	88.6	72.9	19.5	2.93	602	5.88	30.4	30.2	29.8	19.6
CP8	93.2	93.1	91.0	75.3	20.4	3.09	630	6.04	31.9	31.9	31.2	20.1
CP9	76.9	78.2	76.7	64.0	18.9	2.90	594	5.73	29.8	30.3	29.8	19.3
CP10	76.3	76.4	75.7	64.8	20.0	3.03	626	6.09	31.6	31.6	31.3	20.5

Table E.6 Recovery, weight fraction and concentration factor of species in the coacervate

Sample	$\frac{\Delta m_{THC}}{m_{THC}}$, %	$\frac{\Delta m_{CBD}}{m_{CBD}}$, %	$\frac{\Delta m_{X100}}{m_{X100}}$, %	$\frac{\Delta m_{TPC}}{m_{TPC}}$, %
CP1	0.92	-0.76	-1.06	-0.98
CP2	0.14	-0.34	-1.22	0.07
CP3	-0.68	0.19	-1.44	-2.32
CP4	0.17	-0.78	-1.92	-2.77
CP5	0.84	0.05	-1.43	-1.78
CP6	3.28	2.26	0.72	-4.93
CP7	0.34	e -0.02	-1.86	1.34
CP8	3.04	3.09	0.53	-1.69
CP9	0.41	-1.02	-4.46	4.08
CP10	1.07	-2.42	-4.47	1.03

Table E.7 Relative loss in the mass balance of each species

APPENDIX F STARTING MATERIAL CHARACTERIZATION

Quantification of cannabinoids in the starting material

Table F.1 Starting material properties

Sample	w_{THC}^{pm}, mg g^{-1}	w_{CBD}^{pm}, mg g^{-1}	w_{CBN}^{pm}, mg g^{-1}	D_p, µm	σ_p µm	Description
PM00	-	-	-	-	-	Raw material obtained from the SQDC
PM01	85 ± 2	-	4.31 ± 0.06	700	300	Decarboxylated at 140 for 105 min and ground to 700 µm
PM01-500	85 ± 2	-	4.31 ± 0.06	500	300	PM01 with particle size reduced 500 µm by grinding
PM01-300	85 ± 2	-	4.31 ± 0.06	600	300	PM01 with particle size reduced 300 µm by grinding
PM02	96 ± 6	45 ± 3	-	700	400	Decarboxylated at 140 for 105 min and ground
PM03	105 ± 1	63.5 ± 0.3	1.5 ± 0.2	700	500	Decarboxylated at 120 for 105 min and ground
PM04	-	-	-	-	-	Decarboxylated at 140 for 105 min and ground

Content in cannabinoids j (THC, CBD or CBN) is expressed as the weight ratio of cannabinoids in respect to the starting material, w_j^{pm}, in mg g^{-1}. The same plant material was extracted up to $k = 3$ times in fresh ethanol at room temperature.

$$w_j^{pm} = \frac{\sum_k m_j^k}{m^{pm}} \tag{F.1}$$

Effect of sieving of the cannabis ground

Study of particle size in extraction procedure usually involves sieves of plant powder to obtained the desired range. Such method was not employed herein. Anecdotal evidence suggest that sieving induce breakage of the more brittle trichomes which, due to their diameter of 40 µm to 150 µm, could contribute to higher amounts traveling to the bottom of the sieve and thereby fractionate cannabinoid content in the original sample.

To assess the validity of this hypothesis, we sieved 5.6 g of PM02 over 500 µm mesh. A Rotap model-E sieve shaker (W.S. Tyler, United States) sifted the powder on the coarse analysis setting for 3 min. Once the time elapsed, we carefully collected the two fractions and quantified THC content by performing three successive ethanol extractions on 0.3 g of the same sample of plant material, each with a duration of 120 minutes. Each series of three extractions were duplicated for particles above 500 µm and below 500 µm (table F.2). Extractions were performed in triplicates.

Table F.2 Sieve test results

	$D_p > 500\,\mu m$	$D_p < 500\,\mu m$
w_{THC}^{pm}, mg g^{-1}	120 ± 10	95 ± 3

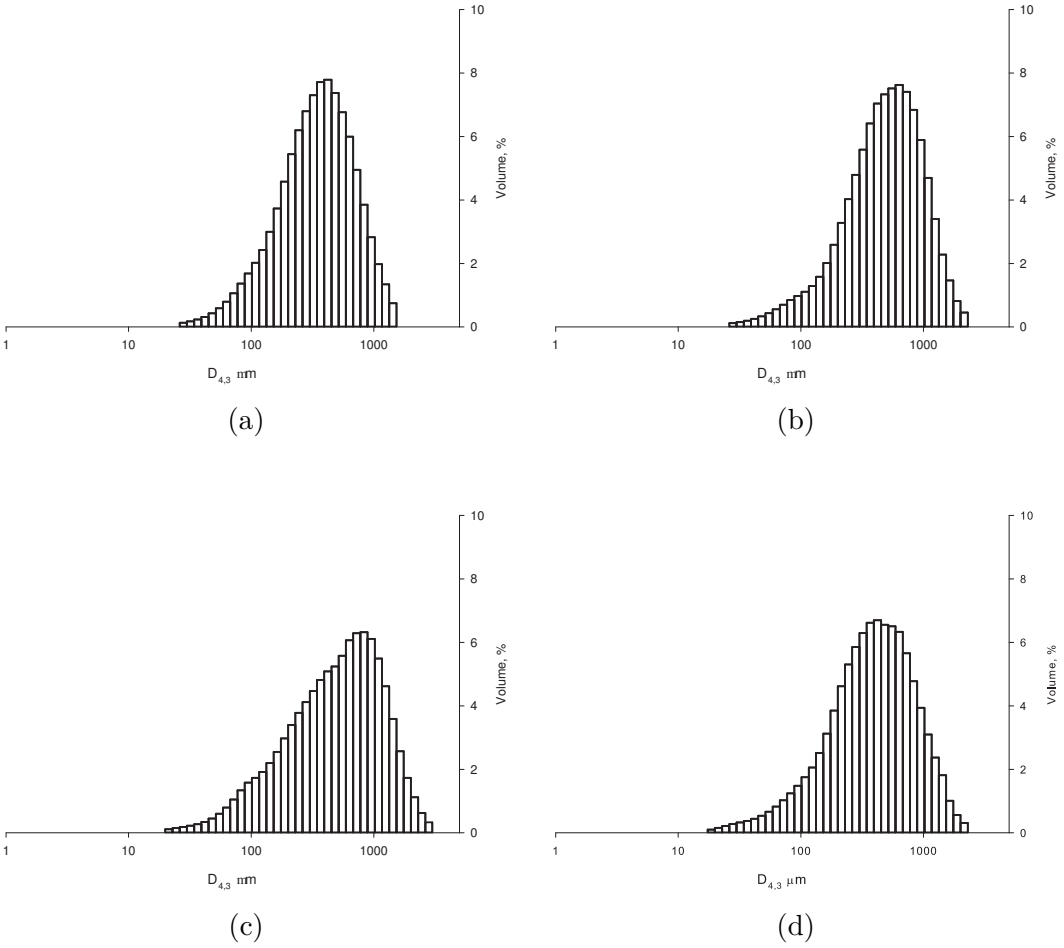

Figure F.1 Particle size distribution obtained by laser diffraction for **(a)** PM01, **(b)** PM02, **(c)** PM03 and **(d)** PM04